

Supporting information

Exploring the Versatility of the Covalent Thiol-Alkyne Reaction with Substituted Propargyl Warheads – A Deciding Role for the Cysteine Protease

Elma Mons,^a Robbert Q. Kim,^a Bjorn R. van Doodewaerd,^a Peter A. van Veelen,^b
Monique P. C. Mulder^{a,*} and Huib Ovaa.^{a,†}

^a Department of Cell and Chemical Biology, Oncode Institute, Leiden University Medical Center,
2300 RC Leiden, The Netherlands

^b Center for Proteomics and Metabolomics, Leiden University Medical Center,
2333 ZA Leiden, The Netherlands

* *e-mail*: m.p.c.mulder@lumc.nl

Table of Contents

Supplemental Figures, Schemes and Tables

Figure S1. Design and chemical synthesis of Rho-Ub-ABPs	SI-3
Figure S2. Lysate incubation with Rho-Ub-ABPs	SI-4
Figure S3. Coomassie recombinant DUBs	SI-5
Figure S4. Selectivity and reactivity of electron-deficient alkyne 18 as warhead	SI-6
Scheme S1. Chemical synthesis of amine [D ₂]-Prg	SI-7
Scheme S2. Chemical synthesis of amine 18	SI-7
Table S1. Crystal structures in PDB	SI-8
Table S2. Recombinant purified DUBs used in this work	SI-9

Materials and Methods; *Biochemistry*

Recombinant protein expression and purification	SI-10
Lysate preparation	SI-11
Gel-based activity-based probe (ABP) reactivity	SI-11
<i>Incubation of whole lysate</i>	SI-12
<i>Incubation of recombinant DUBs</i>	SI-12
<i>Incubation of recombinant USP16CD^{WT} (+/- NEM) and USP16CD^{C205A}</i>	SI-12
<i>Kinetic analysis of adduct formation with recombinant USP16CD^{WT}</i>	SI-13
Fluorescence polarization (FP) binding assay of Rho-Ub-ABPs with USP16CD ^{C205S}	SI-13
Mass spectrometry of intact covalent USP16-ABP adducts	SI-13
Bottom-up mass spectrometric analysis of (deuterated) DUB adducts	SI-14
Thiol reactivity assay	SI-15

Supporting Data; *Biochemistry*

Gel analysis unbound Rho-Ub-ABPs	SI-16
Incubation of whole lysates	SI-17
Incubation of recombinant DUBs	SI-20
Gel analysis of adducts with recombinant USP16CD ^{WT} (+/- NEM) and USP16CD ^{C205A}	SI-22
Gel analysis of recombinant USP16CD ^{WT} and USP16CD ^{C205A} with Rho-Ub- 18	SI-23
Time-dependent covalent USP16-ABP adducts	SI-23
Kinetic analysis of covalent USP16 occupancy	SI-25
Fluorescence polarization (FP) binding assay of Rho-Ub-ABPs with USP16CD ^{C205S}	SI-27
Mass Spectrometry of intact covalent USP16-ABP adducts	SI-29
Bottom-up mass spectrometric analysis of (deuterated) DUB adducts	SI-41
<i>HRMS of unbound Rho-Ub-Prg and Rho-Ub-[D₂]-Prg</i>	SI-41
<i>Expected and detected peptides for Rho-Ub-Prg and Rho-Ub-[D₂]-Prg adducts</i>	SI-42
Thiol reactivity assay with GSH	SI-45

Materials and Methods; *ABP Synthesis*

General	SI-49
Synthesis of Rho-Ub-ABPs	SI-51

Supporting Data; *ABP Synthesis*

Step I. Synthesis of NH ₂ -Ub(PG)-resin	SI-53
Step II + III. Synthesis of (Boc) ₂ Rho-Ub(PG)-OH	SI-55
Step IV + V. Synthesis of Rho-Ub-ABP	SI-56
LC-MS spectra of Rho-Ub-ABPs	SI-57

Materials and Methods; *Chemical Synthesis*

Synthesis of amine [D ₂]-Prg	SI-70
Synthesis of amine 18	SI-72
¹ H/ ¹³ C NMR spectra	SI-73

References

SI-81

Supplemental Figures, Schemes and Tables

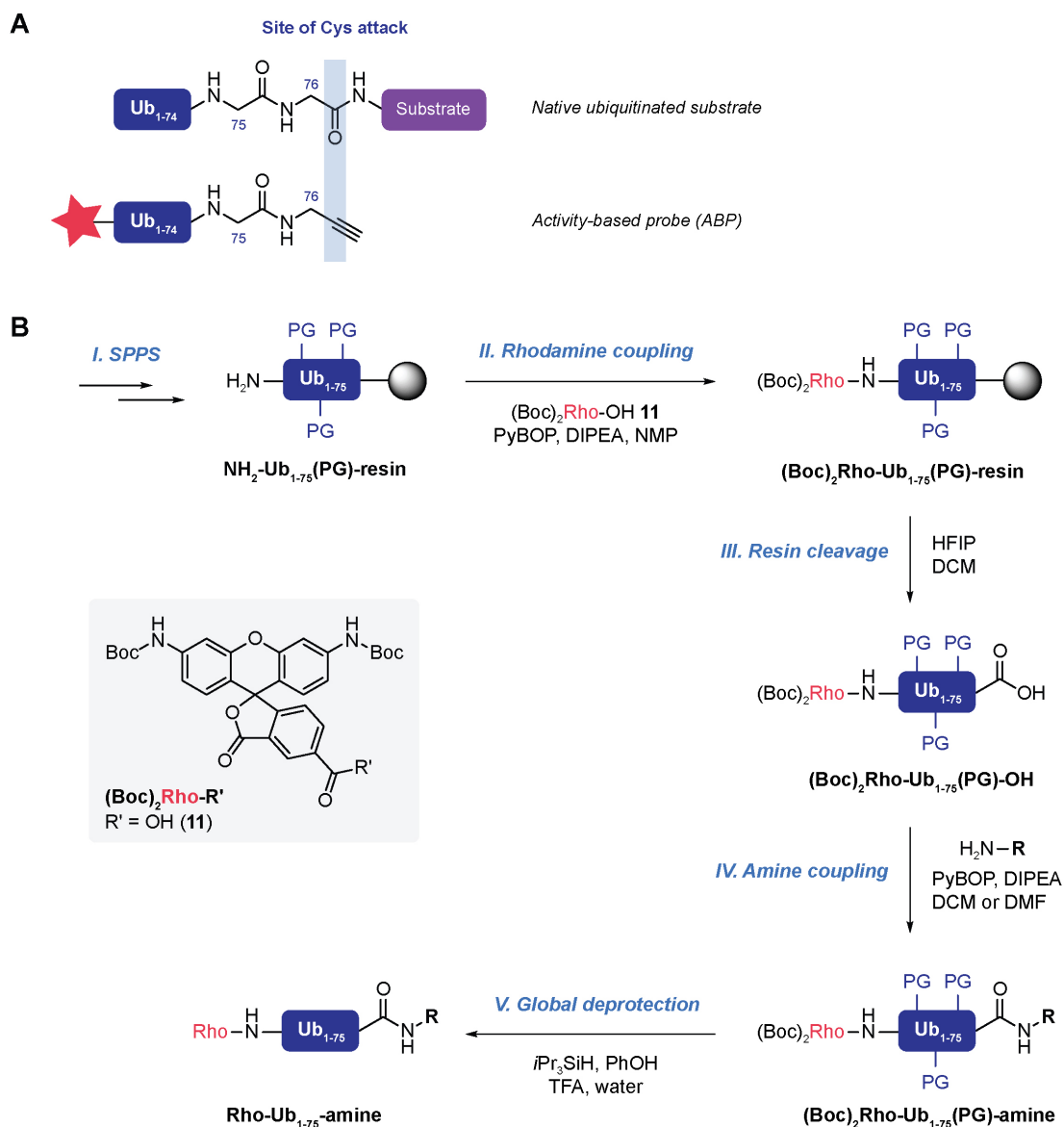


Figure S1. Design and chemical synthesis of Rho-Ub-ABPs. **A)** Alignment of warhead with native isopeptide bond. Top; nucleophilic attack of catalytic Cys on isopeptide carbonyl between C-terminal Gly76 in Ub and Lys residue in substrate or distal Ub. Bottom; nucleophilic attack of catalytic Cys on reactive carbon C2 in alkyne warhead. **B)** Synthetic scheme for cysteine DUB ABPs with N-terminal 5-carboxy-Rhodamine110 as fluorescent reporter and C-terminal alkyne derivatives as warheads. *Step I.* Linear chemical synthesis of protected Ubiquitin ΔG (Ub_{1-75}) on Trt resin via solid phase synthesis (SPPS) as described before.¹ *Step II.* Coupling of $(\text{Boc})_2\text{Rho}-\text{OH 11}$ to the N-terminus. *Step III.* Cleavage from resin while retaining side chain protecting groups. *Step IV.* Coupling of propargylamine (**Pr**g) or derivatives (**2-10**) to C-terminus. *Step V.* TFA-mediated global deprotection to remove all protecting groups, followed by purification by RP-HPLC to obtain pure $\text{Rho}-\text{Ub}_{1-75}\text{-ABPs}$. PG = acid-labile protecting group. Rho = 5-carboxy-Rhodamine110. DIPEA = N,N-diisopropylethylamine. NMP = N-Methylpyrrolidone. HFIP = hexafluoroisopropanol. DCM = dichloromethane. DMF = dimethylformamide. TFA = trifluoroacetic acid. Sequence $\text{Rho}-\text{Ub}_{1-75}\text{-ABP}$;

$\text{Rho}-(\text{Nle})\text{QIFVKLTGKTITLEVEPSDTIENVKAKIQDKEGIPPDQQLIFAGKQLEDGRTLSDYNIQKESTLHLVLRRLG}\text{-amine}$

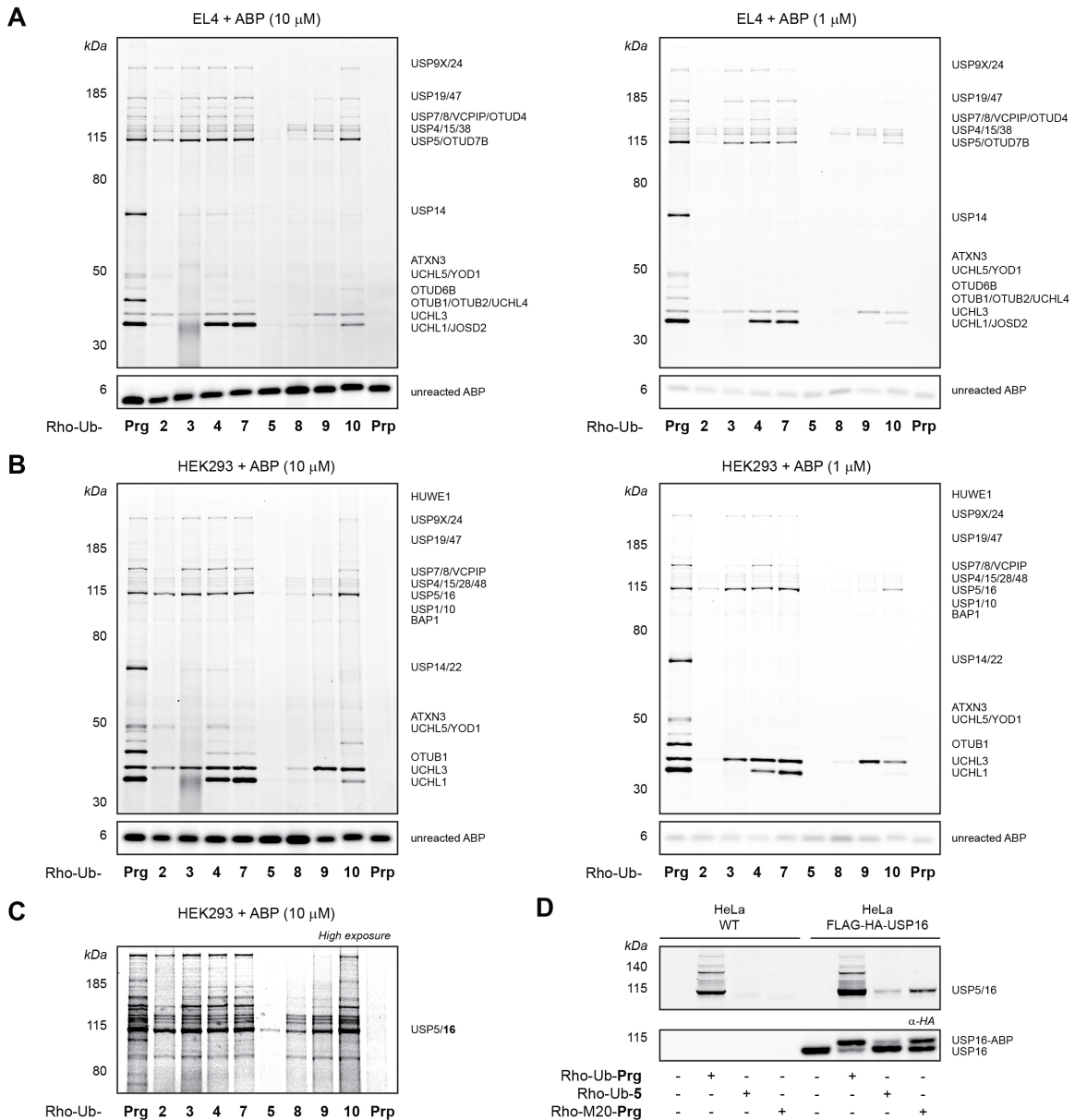


Figure S2. Lysate incubation with 1-10 μ M Rho-Ub-ABPs. Full gel scans and Coomassie stain are provided in Figure S6 and Figure S7 (SI-17/18). **A**) In-gel fluorescence scan of EL4 lysate incubated with 10 μ M (left) or 1 μ M (right) Rho-Ub-ABP. Assignment of labeled DUBs based on proteomic analysis with biotin-Ub-Prg by Ekkebus *et al.*² **B**) In-gel fluorescence scan of HEK293 lysate incubated with 10 μ M (left, also shown in Figure 2B) or 1 μ M Rho-Ub-ABP (right). Assignment of labeled DUBs based on proteomic analysis by Altun *et al.*³ Lysates were incubated with a higher ABP concentration (10 μ M instead of the standard 1 μ M) to allow slower covalent adduct formation caused by the introduction of bulky and electron-donating substituents, but adduct formation with substituted alkynes is also observed upon incubation with 1 μ M ABP. Cell lysates of the mouse lymphoma cell line (EL4) are commonly used as benchmark cell line for DUB activity,⁴ but do not express (detectable levels of) endogenous USP16.² **C**) Alternative image processing (increased exposure, contrast and adjusted levels) of Figure S2B to visualize adduct formation between 10 μ M Rho-Ub-5 and endogenous USP16 in HEK293 lysate. Endogenous USP16 levels in HEK293 lysate are low, and adduct formation with Rho-Ub-5 is relatively slow (as illustrated in Figure 5C and Figure S2D). **D**) Incubation of HeLa cell lysate expressing endogenous levels of USP16 (left) or expressing HA-FLAG-USP16 (right) with Rho-Ub-Prg, Rho-Ub-5 or USP16-selective ABP Rho-M20-Prg.⁵ Adduct formation of Rho-Ub-5 with overexpressed HA-FLAG-USP16 can be observed with in-gel fluorescence (top), and western blotting for HA (bottom).

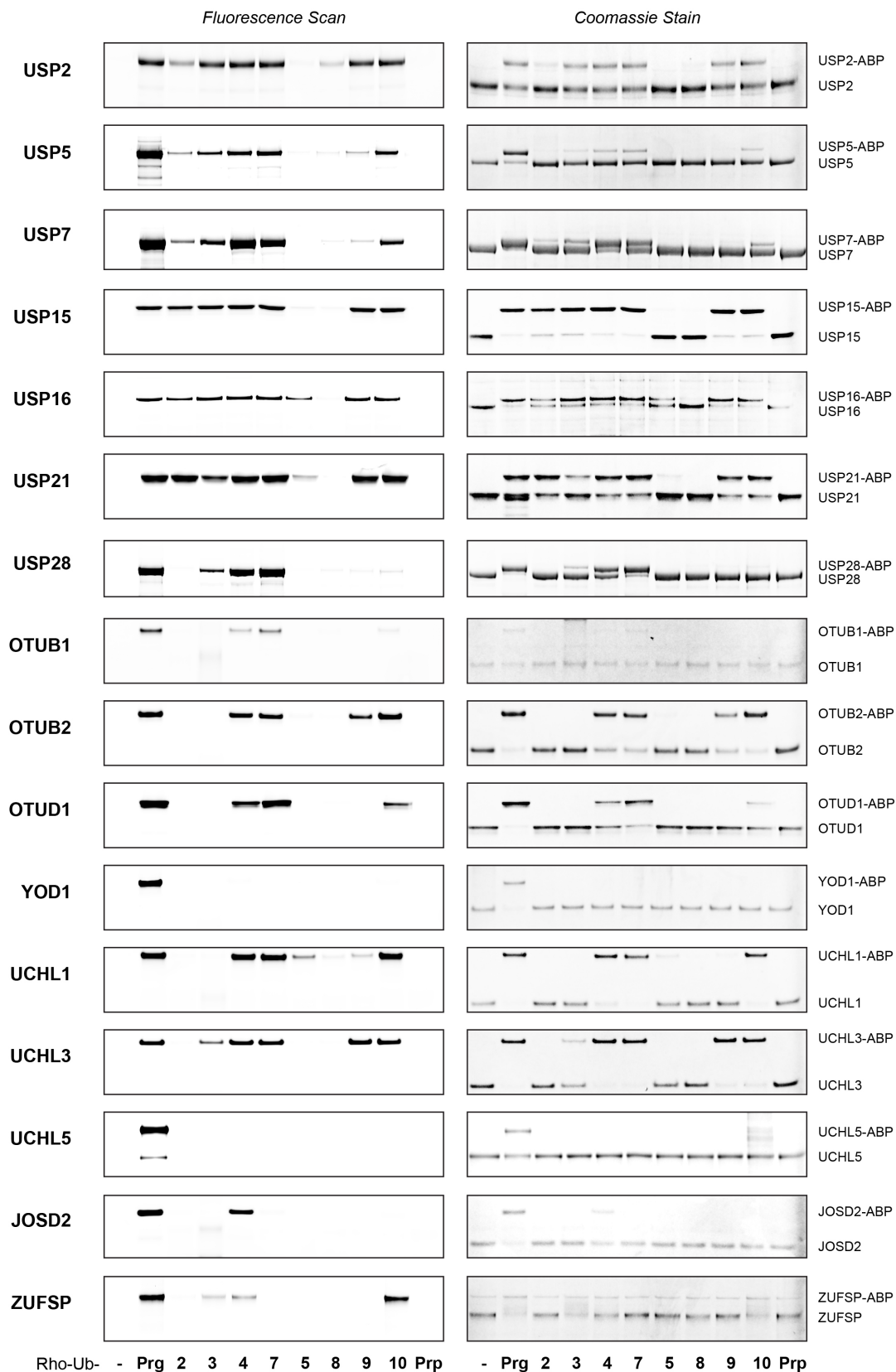


Figure S3. Covalent adduct formation between recombinant cysteine DUBs and Rho-Ub-ABPs. Unbound DUBs and covalent DUB-ABP complex are resolved by SDS-PAGE electrophoresis. Left; in-gel fluorescence ($\lambda_{ex} = 473$ nm, $\lambda_{em} = 530 \pm 10$ nm). Right; Coomassie protein stain. Sources of recombinant DUBs are listed in Table S2. Full gel scans are provided in Figure S9 and Figure S10 (SI-20/21).

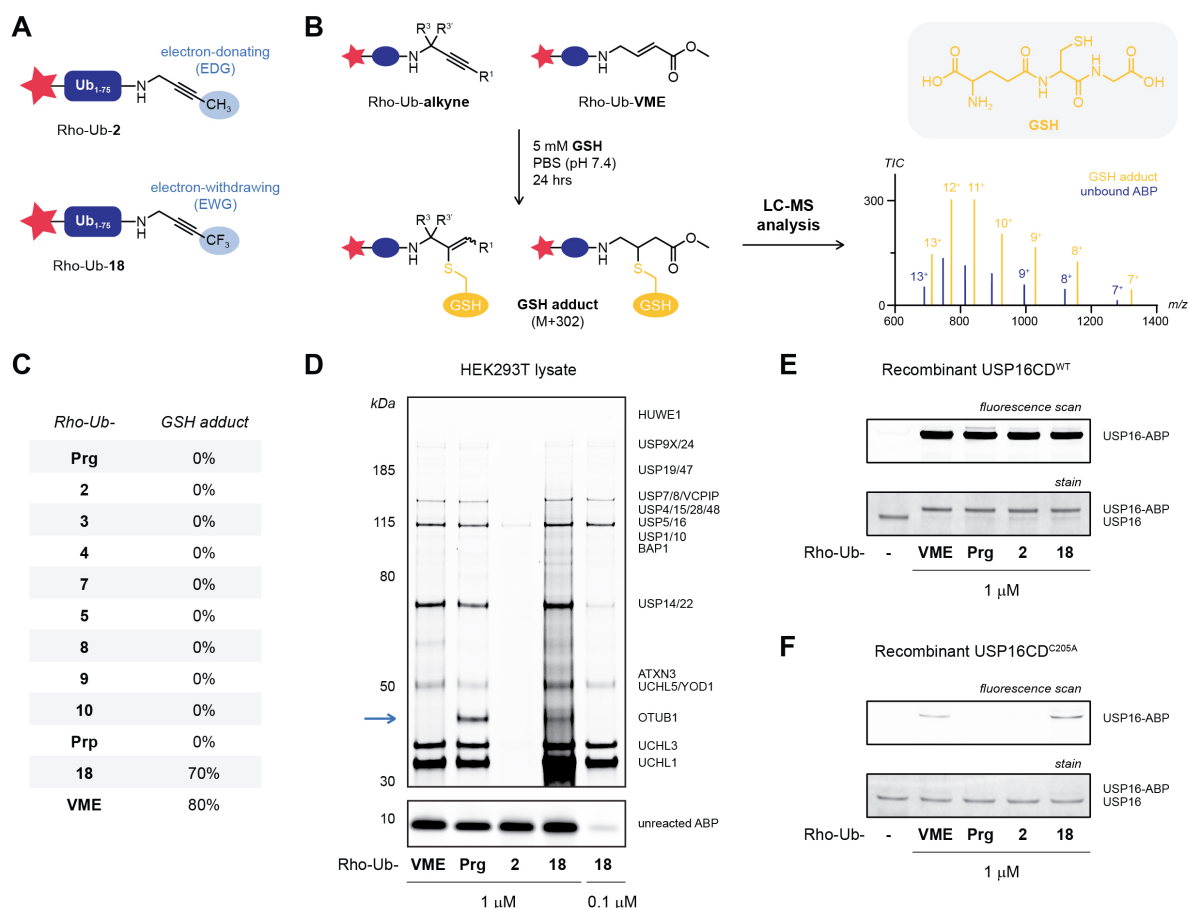
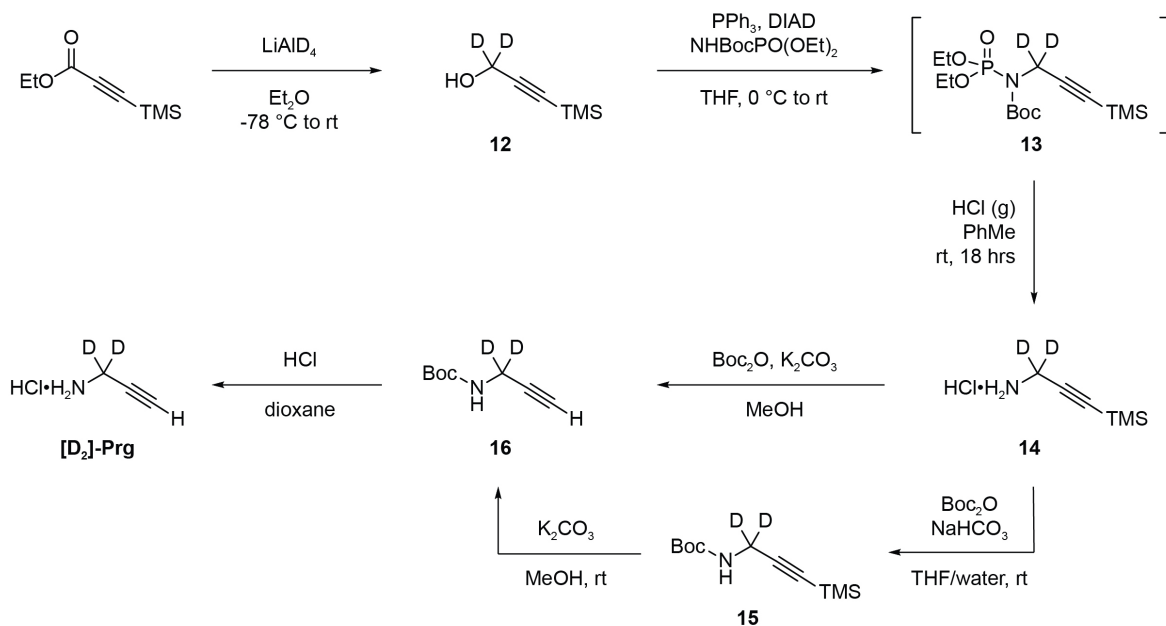
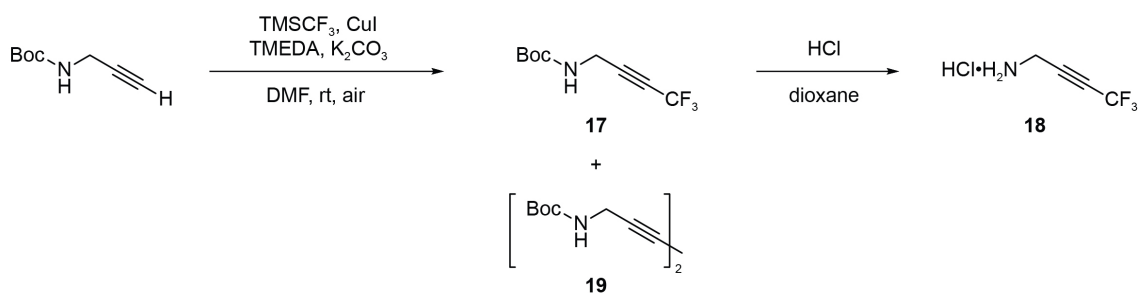


Figure S4. Selectivity and reactivity of electron-deficient alkyne **18** as warhead in Rho-Ub-ABPs. **A**) Electron-donating methyl group on terminal C1 position of alkyne **2** and electron-withdrawing trifluoromethyl group on terminal C1 position of alkyne **18**. Details on trifluoromethylation of terminal alkynes to obtain alkyne **18** are provided in Scheme S2.⁶ Our design is based on the assumption that the terminal trifluoromethyl ($-\text{CF}_3$) in alkyne **18** is sterically similar to the terminal methyl ($-\text{CH}_3$) in alkyne **2**, while having the opposite electronic property. Here, the trifluoromethyl group is strongly electron-withdrawing, whereas the methyl group is mildly electron-donating. **B**) Schematic overview of methodology for indiscriminate thiol reactivity. Rho-Ub-ABPs are incubated with 5 mM glutathione (GSH) in phosphate-buffered saline (PBS) for 24 hours, after which the reaction mixture was submitted to LC-MS analysis. GSH adduct and unreacted ABP are quantified from the total ion count (TIC). **C**) GSH adduct formed upon incubation with 5 mM GSH for 24 hours as percentage of total. Charge states and TIC intensities used for quantification are provided in Table S7 and Table S8. Thiol addition to electron-deficient alkyne **18** can also occur in absence of enzyme. Adduct formation with GSH does not necessarily equal complete loss of selectivity; as illustrated by the established DUB-selective ABP Ub-VME.⁷ **D**) Fluorescence scan of HEK293T lysate incubated with Rho-Ub-ABPs reveals the importance of both steric and electronic effects of alkyne substituents; most but not all DUBs that are unreactive with Rho-Ub-**2** do form covalent adducts with Rho-Ub-**18**, indicating an electronic rather than steric component driving the lack of reactivity with Rho-Ub-**2**. The blue arrow marks a DUB adduct previously identified as OTUB1,³ which is unreactive towards electrophilic ABPs Rho-Ub-VME and Rho-Ub-**18**, suggesting that lack of reactivity for this specific DUB could be driven by the available space at the active site to accommodate bulky substituents at the C1 position (disfavored steric interactions) rather than electronic effects. Full gel scans are provided in Figure S8. **E**) In-gel fluorescence (top) and Coomassie protein stain (bottom) for adduct formation with recombinant USP16CD^{WT} upon incubation with Rho-Ub-ABPs for 1 hr. Full gel scans are provided in Figure S12. **F**) In-gel fluorescence (top) and Coomassie protein stain (bottom) for adduct formation with recombinant USP16CD^{C205A} upon incubation with Rho-Ub-ABPs for 1 hr. Faint labeling can be observed for Rho-Ub-VME and Rho-Ub-**18** in the fluorescence scan, indicating that these ABPs are reactive towards non-catalytic cysteines, but selectivity is retained as adduct formation with the catalytic cysteine residue is much faster than reaction with non-targeted thiols. Full gel scans are provided in Figure S12.



Scheme S1. Chemical synthesis of deuterated propargylamine **[D₂]-Prg**. **[D₂]-propargyl alcohol 12** was formed by reduction of ethyl propiolate with lithium aluminum deuteride, and subsequently converted into protected amine **13** under Mitsunobu conditions.⁸ Acid-mediated deprotection generated hydrochloride **[D₂]-propargylamine 14** bearing an acid-stable terminal TMS protecting group. Base-mediated TMS removal had to be performed after or simultaneous with Boc protection, as the free amine **[D₂]-propargylamine** is very volatile and cannot be separated from reagents and solvents without loss of the product. The resulting Boc-**[D₂]-Prg 16** is soluble in organic solvents and can be isolated by simple extraction. Stepwise Boc-protection and TMS-deprotection was performed to generate intermediates Boc-1-TMS-**[D₂]-Prg 15** and Boc-**[D₂]-Prg 16** as reference compounds for reaction progress detection by TLC. Finally, hydrochloride salt of deuterated propargylamine **[D₂]-Prg** could be obtained after acid-mediated Boc-deprotection.



Scheme S2. Chemical synthesis of electron-deficient propargylamine derivative **18**. Direct trifluoromethylation of Boc-propargylamine with Ruppert–Prakash reagent (TMSCF₃)⁶ gave desired trifluoromethylated acetylene **17**, which could be separated by FCC from homocoupling product **19** (an undesired side product generated by the copper-catalyzed Glaser–Hay dimerization). Hydrochloride salt of amine **18** was obtained by treatment of Boc-protected alkyne **17** with hydrochloric acid.

Table S1. Crystal structures in PDB of covalent thiovinyl bond between catalytic cysteine and alkyne.

Protease	Alkyne	PDB	Reference
USP12 + UAF1	Ub-Prg	5L8W	[Dharadhar, 2016] ⁹
USP28	Ub-Prg	6HEK	[Gersch, 2019] ¹⁰
USP28 (insertion deleted)	Ub-Prg	6HEI	
USP28CD ^{E593D}	Ub-Prg	6H4H	[Sauer, 2019] ¹¹
USP30	Ub-Prg	5OHK	[Gersch, 2017] ¹²
	Ub-Prg	5OHN	
UCHL5 + INO80G	Ub-Prg	4UF6	[Sahtoe, 2015] ¹³
UCHL5 + RPN13 DEUBAD	Ub-Prg	4UEL	
A20 OTU	Ub-Prg	5LRX	[Mevissen, 2016] ¹⁴
ZUFSP (232-578)	Ub-Prg	6EI1	[Hermanns, 2018] ¹⁵
ZUFSP	Ub-Prg	6FGE	[Kwasna, 2018] ¹⁶
MINDY-1	Ub-Prg	5JQS	[Abdul Rehman, 2016] ¹⁷
mUSP18	mISG15-Prg	5CHV	[Basters, 2017] ¹⁸
CCHFV vOTU	Ub-Prg	3ZNH	[Ekkebus, 2013] ²
SARS CoV PL ^{pro}	K48 diUb-Prg	5E6J	[Békés, 2016] ¹⁹
SARS CoV PL ^{pro}	hISG15(ct)-Prg mISG15(ct)-Prg	5TL6 5TL7	[Daczkowski, 2017] ²⁰
MERS CoV PL ^{pro}	hISG15(ct)-Prg hISG15(ct)-Prg	5W8U 5W8T	[Daczkowski, 2017] ²¹
MERS CoV PL ^{pro}	ISG15-Prg	6BI8	[Clasman, 2020] ²²
SARS CoV-2 PL ^{pro}	Ub-Prg ISG15(ct)-Prg	6XAA 6XA9	[Klemm, 2020] ²³
KUPEV OTU	sheepISG15(ct)-Prg	6OAR	[Dzimianski, 2019] ²⁴
GANV OTU	sheepISG15(ct)-Prg	6OAT	
FMDV LB ^{pro}	ISG15-Prg	6FFA	[Swatek, 2018] ²⁵
ERVV OTU	mISG15(ct)-Prg	5JZE	[Deaton, 2016] ²⁶
HAZV OTU	Ub-Prg	7JMS	[Dzimianski, 2020] ²⁷
<i>Xanthomonas</i> XopD	Ub-Prg tomatoSUMO-Prg	5JP3 5JP1	[Pruneda, 2016] ²⁸
<i>L. pneumophila</i> Lem27 (1-417)	Ub-Prg	7BU0	[Liu, 2020] ²⁹
ChlaDUB1	Ub-Prg	6FDK	[Ramirez, 2018] ³⁰
ChlaDUB1	Ub-Prg	6GZS	[Pruneda, 2018] ³¹
ChlaDUB2 (93–339)	Ub-Prg	6OAM	[Hausman, 2020] ³²
hCatK	7 (Inhibitor-Prg)	6QBS	[Mons, 2019] ³³

PDB = Protein Data Bank. h = human. m = mouse. Prg = propargylamide warhead. Ub = ubiquitin. ct = C-terminus. PL^{pro} = papain-like protease. CCHFV = Crimean Congo Hemorrhagic fever virus. SARS CoV = Severe acute respiratory syndrome coronavirus. MERS CoV = Middle East respiratory syndrome coronavirus. KUPEV = Kupe virus. GANV = Ganjam virus. FMDV = Foot-and-mouth disease virus. ERVV = Erve virus. HAZV = Hazara virus. Chla = Chlamydia trachomatis. CatK = cathepsin K.

Table S2. Purified recombinant DUBs used in this work.

DUB	Tag	Domain	Source or reference
USP2	GST	FL (isoform 4)	Ubiquigent. #64-0014-050
USP5	6His	FL	Ubiquigent. #64-0002-050
USP7	-	FL	<i>In-house</i> . This work
USP15	His	D1D2	<i>In-house</i> . This work
USP16	His-3C	FL (isoform 3) CD ^{WT} (196-823) CD ^{C205A} (196-823) CD ^{C205S} (196-823)	<i>In-house</i> . This work
USP21	GST	CD (196-565)	Ubiquigent. #64-0037-050
USP28	6His	FL	<i>In-house</i> . This work
OTUB1	-	FL (1-271)	<i>In-house</i> . [Wang, 2009] ³⁴
OTUB2	-	FL	<i>In-house</i> . [Nanao, 2004] ³⁵
OTUD1	GST- <i>Thrombin</i>	CD + UIM (290-481)	<i>In-house</i> . [Mevisen, 2013] ³⁶
YOD1	-	FL	Gift from David Komander [Mevisen, 2013] ³⁶
UCHL1	-	FL	<i>In-house</i> . [Larsen, 1996] ³⁷
UCHL3	-	FL	<i>In-house</i> . [Larsen, 1996] ³⁷
UCHL5	-	FL	Novus biochemicals. #NBP1-72315
JOSD2	His	FL	Ubiquigent. #64-0032-050
ZUFSP	-	FL	Gift from Kay Hofmann [Hermanns, 2018] ¹⁵

Materials and Methods; *Biochemistry*

Recombinant protein expression and purification

Protein expression constructs. Expression constructs for USP7FL, USP15(D1D2) and OTUB1FL were kind gifts from Titia K. Sixma, Ingrid Dreveny and Frank Sicheri, respectively. Full-length USP16 (UniProtID: Q9Y5T5; isoform 3, Q141H, EY480DN) and USP16CD (residues 196-823; canonical numbering) were cloned into in-house baculovirus expression vector pCPF2.13 harboring an N-terminal His-tag and 3C protease site, using IVA cloning.³⁸ Point mutations C205A and C205S were introduced using overlapping primer mutagenesis.³⁹ USP28FL was cloned into pFastNKI-his3C-LIC using ligase-independent cloning.⁴⁰ OTUD1(CD+UIM) (residues 290-481) was cloned into pGEX-4T-1 with BamHI and HindIII. All expression constructs were sequence-verified.

Expression of USP16 (variants) and USP28FL. USP28FL and all USP16 constructs were expressed using baculovirus expression in *Spodoptera frugiperda* (Sf9) using an adapted Bac-to-Bac system (Invitrogen). Bacmids were generated using EmBacY cells (Geneva Biotech) or DH10Bac (USP28) and isolated using isopropanol precipitation. 10 µg was transfected into $0.8 \cdot 10^6$ sedentary Sf9 cells using CellFectin (Invitrogen) in SFM-II medium (Gibco) in a 6-well plate at 28 °C. After 72 hours cells were checked for fluorescence and the medium was harvested (P0) for infection of P1 cultures; 50 mL of $1 \cdot 10^6$ cells mL⁻¹ in Insect-Express medium (Lonza). P1 cultures were incubated at 28 °C whilst shaking for 72 hours and then harvested by spinning down at 500 G for 5 minutes. The supernatant was used to infect P2 cultures (like P1, but now 500 mL), whilst the pellet was used to check for expression and purification optimization. P2 cultures were infected with low MOI and harvested after 72 hours shaking at 28 °C.

Purification of USP16 (variants). Insect cells from P2 expressing USP16 variants were resuspended in lysis buffer (50 mM HEPES pH7.4, 500 mM NaCl, 20 mM imidazole and 5% glycerol), sonicated and centrifuged at 21,000 G at 4 °C to isolate the soluble fraction. The supernatant was applied to charged Ni-NTA beads, which were washed twice extensively with lysis buffer with 20 mM and 50 mM imidazole respectively. The protein was eluted using elution buffer (50 mM HEPES pH7.4, 100 mM NaCl, 200 mM imidazole, 1 mM DTT) and subsequently applied to a HiTrap MonoQ column (GE Healthcare). Protein was eluted using a salt gradient (20 mM HEPES pH7.4, 1 mM DTT, 50 to 1000 mM NaCl) and protein-containing fractions were pooled, concentrated and aliquoted before being flash frozen.

Purification of USP28FL. P2 expression cells were lysed using sonication in lysis buffer (20 mM Tris pH8.0, 500 mM NaCl, 5 mM BME, 10 mM imidazole and protease inhibitor cocktail). The lysates were centrifuged at 20,000 rpm for 30 minutes at 4 °C. The supernatants were incubated with washed Talon metal affinity resin (Clontech Inc., Palo Alto, CA) for 20 minutes at 4 °C and the beads were then washed with lysis buffer. Protein was eluted with lysis buffer supplemented 250 mM imidazole. Proteins were dialyzed to remove imidazole and purified over a Superdex200 gel filtration column. USP28(FL) was concentrated, aliquoted and flash-frozen for storage at -80 °C. Purified protein was confirmed via immunoblotting using anti-USP28 antibody (GeneTex, #EPR42492).

Expression and purification of USP7FL. USP7FL was expressed in BL21 (DE3) Rosetta2 bacteria using overnight induction with 0.2 mM IPTG in Terrific Broth medium at 18 °C. Cells were spun down and resuspended in GST buffer (50 mM HEPES pH7.5, 250 mM NaCl, 1 mM EDTA, 1 mM DTT) before being lysed using sonication. After high-speed centrifugation at 21,000 G at 4 °C, the supernatant was applied to Glutathione Sepharose 4B beads (GE Healthcare), which were washed extensively using GST buffer before eluting the protein using GST buffer supplemented with 15 mM GSH. The eluted protein was dialyzed overnight against PorosXQ buffer (20 mM HEPES pH7.5, 50 mM NaCl, 1 mM DTT) after the addition of 3C protease to remove the GST tag. To remove breakdown products and cleaved GST, the sample was purified on a PorosXQ column, eluting the protein using a gradient of buffer B (20 mM HEPES pH7.5, 1 M NaCl, 1 mM DTT). Appropriate fractions were concentrated and applied to a

Superdex200 gel filtration column (GE Healthcare) using GF buffer (20 mM HEPES pH7.5, 100 mM NaCl, 1 mM DTT). The peak fractions were pooled, concentrated to ~1 mg/mL and flash frozen using LN₂.⁴¹

Expression and purification of USP15(D1D2). USP15(D1D2) was expressed in BL21 (DE3) Rosetta2 cells, grown in 2xYT medium. Cells were induced overnight at 25 °C using 0.5 mM IPTG and harvested the next day in His-buffer (50 mM Tris pH7.5, 300 mM NaCl, 20 mM imidazole, 1% glycerol). Cells were lysed using sonication and the insoluble fraction was removed by centrifugation at 21,000 G at 4 °C for 30 minutes. Supernatant was applied to Ni-charged NTA beads and beads were washed extensively with His-buffer. USP15(D1D2) was eluted with the same buffer supplemented with 200 mM imidazole before being concentrated and applied to a Superdex200 gel filtration column in SEC buffer (20 mM Tris pH7.5, 150 mM NaCl, 1% glycerol). Appropriate fractions were concentrated to ~20 mg/mL, aliquoted and frozen in liquid nitrogen.⁴²

Lysate preparation

Cell culturing. HEK293 cells (ATCC, Manassas, VA), HeLa cells and HEK293T cells were cultured in Dulbecco's Modified Eagle's medium (DMEM) supplemented with 8-10% FCS/FBS. EL4 cells were cultured in Gibco RPMI 1640 medium (Life technologies) supplemented with 10% FCS. Cells were maintained in a humidified atmosphere of 5% CO₂ at 37 °C and regularly tested for the absence of mycoplasma. Transfection of HeLa cells with FLAG-HA-USP16 (Addgene, #22595) as reported previously.⁵

Harvesting and cell lysis. Cells were harvested by washing with PBS, trypsinization to dissociate adherent cells from surface, and centrifuged. Fresh cell pellets were resuspended in two pellet volumes of cold lysis buffer, sonicated (5 cycles, high. 30 sec on, 30 sec off) on a Bioruptor Pico (Diagenode), and solute was separated from insoluble fraction by centrifuge (10 minutes, 13,200 rpm, 4 °C). Supernatant was transferred to clean tube and protein concentration was determined on Nanodrop One spectrophotometer (Isogen Life Science). Subsequently, volume was adjusted by addition of lysis buffer to a protein concentration of 2 mg/mL. Harvesting and cell lysis of HeLa cells as reported previously.⁵

General methods for gel-based activity-based probe (ABP) reactivity

General. Purified Rho-Ub-ABPs are stored at -20 °C as powder or as 500 μM stock solution in DMSO. The concentration of stock solutions is calculated from the molecular mass and the added amount of dry powder. Rho-Ub-ABPs are added to whole lysate or recombinant DUBs as 2-5X solutions, prepared by careful addition of DMSO stock to reaction buffer. Dithiothreitol (DTT) in single-use 1 M aliquots stored at -20 °C, and surfactants are added freshly prior to reaction initiation to prepare lysis buffer (50 mM Tris-HCl pH7.4, 5 mM MgCl₂, 250 mM sucrose, 2 mM DTT), HEPES reaction buffer (50 mM HEPES pH7.4, 150 mM NaCl, 5 mM DTT, 0.005% Tween20) or Tris reaction buffer (50 mM Tris pH7.5, 100 mM NaCl, 5 mM DTT). Final DUB or ABP concentrations listed correspond to the concentration during incubation (before addition of sample buffer). For time-dependent/kinetic measurements Rho-Ub-**Prg**, Rho-Ub-**2** and Rho-Ub-**5** solutions were prepared from single-use aliquots of 500 μM stock solutions in DMSO. Incubation with Rho-Ub-ABPs is conducted under gentle agitation (300 rpm) with strict restriction of light.

General Method: Quench and SDS-PAGE gel electrophoresis. After indicated incubation time, the reaction was quenched by addition of 3X reducing sample buffer (150 μL 4X LDS-PAGE loading buffer (NuPAGE, Invitrogen) supplemented with 35 μL water and 15 μL β-mercaptoethanol (BME)) and boiling the samples for 10 minutes at 94 °C to abolish noncovalent interactions (denaturing conditions). Multiple timepoints; samples were stored on ice until the experiment was completed. Samples were loaded on precast Bis-Tris gels (Invitrogen) and resolved by SDS-PAGE gel electrophoresis with MES (NuPAGE MES SDS running buffer 20X, Novex by Life Technologies) or MOPS (NuPAGE MOPS SDS running buffer 20X, Novex by Life Technologies) as running buffer. Reference

protein standard/ladder; PageRuler™ Plus Prestained Protein Ladder (Thermo Fisher Scientific Inc., #26619), PageRuler™ Prestained Protein Ladder (Thermo Fisher Scientific Inc., #26616) or SeeBlue™ Plus2 Pre-stained Protein Standard (Invitrogen, LC5925). Covalent enzyme-ABP adducts were visualized by in-gel fluorescence using Typhoon FLA 9500 imaging system (GE Healthcare Life Sciences) with blue LD laser and BPB1 emission filter ($\lambda_{ex} = 473 \text{ nm}$, $\lambda_{em} = 530 \pm 10 \text{ nm}$), and protein marker was visualized with red LD laser and LPR emission filter ($\lambda_{ex} = 635 \text{ nm}$, $\lambda_{em} = 665 \text{ nm}$). Subsequently, covalent DUB-ABP adduct and unbound DUB were visualized by InstantBlue™ Ultrafast Protein Stain (Expedeon Protein Solutions, #ISB1L), and scanning stained gels using an Amersham Imager 600 (Trans-illumination).

Compound	Abbreviation	CAS#	Source or reference
1,4-Dithio-DL-threitol	DTT	3483-12-3	Chem-Impex, #00127
N-Ethylmaleimide	NEM	128-53-0	Sigma-Aldrich, #E3876
β -Mercaptoethanol	BME	60-24-2	Sigma-Aldrich, #M6250
Tween20	Tween20	9005-64-5	Sigma-Aldrich, #P1379
Glutathione (reduced)	GSH	70-18-8	Chem-Impex, #00159
Rho-M20-Prg	Rho-M20-Prg	-	<i>In-house</i> synthesis, [Gjonaj, 2019] ⁵

Incubation of whole lysate

EL4/HEK293/HEK293T. 20 μL lysate (final conc. 2 mg/mL) was incubated with 5 μL Rho-Ub-ABP (final conc. 1-10 μM) for 1 hour at 37 °C. Reaction was quenched as described in the general method above, and samples (10-15 μL) were loaded on 4-12% Bis-Tris gels (Invitrogen) and resolved by SDS-PAGE gel electrophoresis with MES as running buffer. Unreacted ABPs (loading control) were visualized by loading sample (3 μL) on 10% Bis-Tris gels (Invitrogen) and resolved by SDS-PAGE gel electrophoresis with MES as running buffer.

HeLa. 19 μL lysate (WT or overexpressing FLAG-HA-USP16) was incubated with 1 μL Rho-Ub-ABP for 1 hour at 37 °C. Reaction was quenched as described in the general method above, and samples (10 μL) were loaded on 4-12% Bis-Tris gels (Invitrogen) and resolved by SDS-PAGE gel electrophoresis with MOPS as running buffer. Gels were transferred to nitrocellulose membrane using a Trans-Blot Turbo Transfer System (Biorad) and subjected to standard Western Blotting protocols. Antibodies: mouse anti-HA (1:1000, Covance #MMS-101R) and goat anti-mouse HRP (1:5000, Dako #P0447). Blots with HRP secondary antibody were incubated with SuperSignal™ West Dura Extended Duration Substrate (Thermo Scientific, 34076) according to manufacturer protocols and scanned on an Amersham Imager 600.

Incubation of recombinant DUBs

Recombinant purified cysteine DUB (final conc. 1 μM) was incubated with Rho-Ub-ABP (final conc. 10 μM) for 1 hour at 37 °C. Reaction was quenched as described in the general method above. Bis-Tris gels and running buffer were adjusted to optimize separation of unbound enzyme and covalent ABP-enzyme adduct.

Incubation of recombinant USP16CD^{WT} (+/- NEM) and USP16CD^{C205A}

Recombinant purified USP16CD^{WT} or USP16CD^{C205A} mutant (final conc. 0.1 μM) was incubated with Rho-Ub-ABP (final conc. 10 μM) for 1 hour at 37 °C. Preincubation of USP16CD^{WT} with N-ethylmaleimide (10 mM) for 30 minutes at 37 °C was performed prior to incubation with ABPs to alkylate/block cysteine thiols. The reaction was quenched and resolved as described in the general method above.

Kinetic analysis of adduct formation with recombinant USP16CD^{WT}

Time-dependent covalent USP16-ABP adducts. USP16CD^{WT} (final conc. 0.25 μ M) was incubated with Rho-Ub-ABP (final conc. 10 μ M) at 37 °C. Samples were removed after indicated incubation time (0.5-4 h), and adduct formation was quenched and resolved as described in the general method above.

Kinetic analysis of covalent USP16 occupancy. USP16CD^{WT} (final conc. 0.1 μ M) was incubated with Rho-Ub-**Prg**, Rho-Ub-**2** or Rho-Ub-**5** (final conc. 1-10 μ M) at 21 °C. Samples were removed after indicated incubation time (5-30 minutes), and adduct formation was quenched and resolved as described in the general method above. Intensity of signals corresponding to unbound USP16 and covalent USP16-ABP adduct were quantified with ImageJ v1.52a.⁴³⁻⁴⁵ Incubation time-dependent covalent occupancy (%) was calculated for each incubation time from background-corrected intensity of bands corresponding to unbound USP16 and covalent adduct; (covalent occupancy = 100%*(adduct/(adduct+unbound))). Time-dependent covalent occupancy (triplicate measurement, n = 3) was then plotted against incubation time and fitted to one-phase exponential association (GraphPad Prism 8.1.1, Exponential - One-phase association) with fixed value of $Y_0 = 0$ (covalent occupancy at reaction initiation) and globally shared value for Plateau (maximum covalent occupancy) to obtain the rate of covalent bond formation k_{obs} (min^{-1}) and reaction half-life $t_{1/2}$ for each ABP concentration. Reaction completion (covalent occupancy = 97% of max) was calculated; reaction completion = $5t_{1/2}$. Details on equations and pseudo-first order reaction conditions are provided on SI-25.

Fluorescence polarization (FP) binding assay of Rho-Ub-ABPs with USP16CD^{C205S}

Binding assays between ABP and catalytically inactive USP16 mutant were performed in triplicate using HEPES reaction buffer (50 mM HEPES pH7.4, 150 mM NaCl, 2 mM DTT) supplemented with 0.005% Tween20. Rho-Ub-ABPs (20 nL of 5 μ M dilution in 1% DMSO, final conc. 5 nM) were dispensed using an ECHO 550 Liquid Handler (Labcyte Inc.) acoustic dispenser, followed by manual addition of serially diluted purified recombinant USP16CD^{C205S} (20 μ L, final conc. 0-64 μ M). Fluorescence polarization (FP) of the Rhodamine fluorophore was measured every 3 minutes for 120 minutes on a Pherastar plate reader (BMG LABTECH GmbH, Germany) with 485-520-520 FP module (λ_{ex} = 485 nm with detection of polarization at λ_{em} = 520 nm). Change in fluorescence polarization (in mP) upon USP16 interaction was calculated using MARS data analysis software (BMG LABTECH GmbH, Germany). Fluorescence polarization after sufficient incubation to reach equilibrium (60 minutes) was plotted against USP16CD^{C205S} concentration for each Rho-Ub-ABP and fitted using non-linear regression (Graphpad Prism 8.4.2, Binding – Saturation, One site – Total) with globally shared values for non-specific binding (NS), background and B_{max} to obtain the non-covalent dissociation constant K_D for each Rho-Ub-ABP. Details on fitting are provided on SI-27.

Mass spectrometry of intact covalent USP16-ABP adducts

Recombinant USP16CD^{WT} or USP16CD^{C205A} (1 μ M) in HEPES reaction buffer (20 μ L) was incubated with Rho-Ub-**Prg**, Rho-Ub-**2** or Rho-Ub-**5** (10 μ M) or buffer at 21 °C for at least 2 hours prior to analysis. Chromatographic separation and MS analysis was carried out on a Waters ACQUITY UPLC-MS system equipped with a Waters ACQUITY Quaternary Solvent Manager (QSM), Waters ACQUITY FTN AutoSampler, Waters ACQUITY UPLC Protein BEH C4 Column (300 Å, 1.7 μ m, 2.1 x 50 mm) and XEVO-G2 XS QTOF Mass Spectrometer (m/z = 200-2500) in ES+ mode. Samples were run with a 7 minute gradient (run time 15 min) using 0.1% FA in MeCN and 0.1% FA in water as mobile phases (flow rate 0.6-0.8 mL/min). The first 4 minutes the flow was diverted to the waste to avoid contamination of the MS with high concentrations of buffer components. After 4 minutes, the elution flow was ionized with an electrospray ionization (ESI) source in positive ion mode. The data was analyzed using Waters MassLynx Mass Spectrometry Software V4.2. The total mass of the covalent USP16-ABP adducts was obtained by deconvolution of electrospray ionization mass spectrum envelope (average isotopes) with the MaxEnt1 function. More details on SI-29.

Time (min)	0.1% FA in water (%)	0.1% FA in MeCN (%)	Flow rate (mL/min)
0.00	98.0	2.0	0.6
0.10	98.0	2.0	0.8
3.00	98.0	2.0	0.8
3.60	98.0	2.0	0.6
4.00	98.0	2.0	0.6
4.50	82.0	18.0	0.6
9.50	68.0	32.0	0.6
11.00	50.0	50.0	0.6
11.50	2.0	98.0	0.6
13.40	2.0	98.0	0.6
13.50	98.0	2.0	0.6
15.00	98.0	2.0	0.6

Bottom-up mass spectrometric analysis of deuterated adduct with Rho-Ub-[D₂]-Prg

HRMS of unbound ABPs. Stock solutions of Rho-Ub-Prg and Rho-Ub-[D₂]-Prg in DMSO (500 μM) were diluted 500-fold in 2% MeCN in water (0.1% FA). MS analysis was carried out on a Waters ACQUITY UPLC-MS system in Resolution Mode, equipped with a Waters ACQUITY Quaternary Solvent Manager (QSM), Waters ACQUITY FTN AutoSampler, Waters ACQUITY UPLC Protein BEH C4 Column (300 Å, 1.7 μm, 2.1 x 50 mm) and XEVO-G2 XS QTOF Mass Spectrometer (m/z = 500-2000). Samples were run with a 1.6 minute gradient (run time 3 min) using 0.1% FA in MeCN and 0.1% FA in water as mobile phases (flow rate 0.6 mL/min). The elution flow was ionized with an electrospray ionization (ESI) source in positive ion mode. Data processing was performed using Waters MassLynx Mass Spectrometry Software 4.2. Theoretical mass was calculated with the isotope modelling function; Tools – Isotope model – Create charge state series.

Time (min)	0.1% FA in water (%)	0.1% FA in MeCN (%)	Flow rate (mL/min)
0.00	98.0	2.0	0.6
0.15	98.0	2.0	0.8
1.85	0.0	100.0	0.8
2.05	0.0	100.0	0.6
2.10	98.0	2.0	0.6
3.00	98.0	2.0	0.6

Adduct formation with DUB. Recombinant purified USP16CD^{WT} (2.4 μM) or UCHL3FL^{WT} (7 μM) in HEPES reaction buffer was incubated with Rho-Ub-Prg or Rho-Ub-[D₂]-Prg (final conc. 10 μM) for 1 hour at 37 °C. Reaction was quenched as described in the general method above. Samples (21 μL, corresponding to 2.5 μgr protein/lane) were run on a 10% Bis-Tris gel, and stained with InstantBlue™ Ultrafast Protein Stain.

Sample preparation and bottom-up mass spectrometric analysis. The DUB-ABP adduct band was cut out, and the proteins subjected to reduction with DTT, alkylation with iodoacetamide and in-gel trypsin digestion using Proteineer DP digestion robot (Bruker). Tryptic peptides were extracted from the gel slices, lyophilized, dissolved in 95/3/0.1 v/v/v water/acetonitrile/formic acid and subsequently analyzed by on-line C18 nanoHPLC MS/MS with a system consisting of an Easy nLC 1200 gradient HPLC system (Thermo, Bremen, Germany), and a LUMOS mass spectrometer (Thermo). Digests were injected onto a homemade precolumn (100 μm × 15 mm; Reprosil-Pur C18-AQ 3 μm, Dr. Maisch, Ammerbuch, Germany) and eluted via a homemade analytical nano-HPLC column (15 cm × 75 μm; Reprosil-Pur C18-AQ 3 μm). The gradient was run from 0% to 50% solvent B (20/80/0.1 water/acetonitrile/formic acid (FA) v/v/v) in 20 min. The nano-HPLC column was drawn to a tip of ~5

μm and acted as the electrospray needle of the MS source. The LUMOS mass spectrometer was operated in data-dependent MS/MS (top-10 mode) with collision energy at 32 V and recording of the MS2 spectrum in the orbitrap. In the master scan (MS1) the resolution was 120,000, the scan range 400-1500, at an AGC target of 400,000 @maximum fill time of 50 ms. Dynamic exclusion after $n=1$ with exclusion duration of 10 s. Charge states 2-5 were included. For MS2 precursors were isolated with the quadrupole with an isolation width of 1.2 Da. HCD collision energy was set to 32 V. The MS2 scan resolution was 30,000 with an AGC target of 50,000 @maximum fill time of 60 ms. In a post-analysis process, raw data were first converted to peak lists using Proteome Discoverer version 2.4 (Thermo Electron), and then submitted to the Homo sapiens database (71591 entries), using Mascot v. 2.2.07 (www.matrixscience.com) for protein identification. Mascot searches were with 10 ppm and 0.02 Da deviation for precursor and fragment mass, respectively, and trypsin as enzyme. Up to two missed cleavages were allowed. Methionine oxidation, carbamidomethyl on cysteine, and the Gly-Prg modification (also in mono and dideuterated form) on cysteine were set as a variable modification. More details on SI-42.

Thiol reactivity assay

Stock solutions of Rho-Ub-ABPs in DMSO (500 μM) were diluted in PBS (10 mM phosphate buffer pH7.45, 140 mM NaCl, 2.7 mM KCl, Gibco PBS tablets) freshly supplemented with GSH (Chem-Impex, #00159) to a final concentration of 5 μM Rho-Ub-ABP and 5 mM GSH. Immediately a 30 μL sample was removed, quenched by 2-fold dilution in 0.1% formic acid in water and submitted to LC-MS analysis. The remaining material was incubated at 37 °C under gentle agitation (600 rpm) for 24 hrs, after which the reaction was quenched by 2-fold dilution in 0.1% formic acid in water, and submitted to LC-MS analysis. LC-MS analysis was performed on a Waters ACQUITY UPLC H-class System equipped with Waters ACQUITY Quaternary Solvent Manager (QSM), Waters ACQUITY UPLC Photodiode Array (PDA) e λ Detector ($\lambda = 210\text{-}800$ nm), Waters ACQUITY UPLC Protein BEH C4 Column (300 Å, 1.7 μm , 2.1 x 50 mm) and LCT Premier Orthogonal Acceleration Time of Flight Mass Spectrometer ($m/z = 100\text{-}1600$) in ES+ mode. Samples were run with a 7 minute gradient (run time 10 min) using three mobile phases detailed below (flow rate = 0.5 mL/min). Data processing was performed using Waters MassLynx Mass Spectrometry Software V4.2. Adduct formation was quantified from the total ion count (TIC) detected for GSH adduct, remaining unreacted ABP or hydrolysis product; the intensity of the naturally most abundant isotope peak in seven charge states ($z = 7\text{-}13$) of the ionization envelope was combined to calculate the ratio of GSH adduct over total ABP content for each sample. More details on SI-47.

Time (min)	Water (%)	MeCN (%)	2.5% FA in water/MeCN (%)
0:00	94.0	2.0	4.0
0.50	94.0	2.0	4.0
7.50	0.0	96.0	4.0
8.00	0.0	96.0	4.0
8.10	94.0	2.0	4.0
10.00	94.0	2.0	4.0

Supporting Data; *Biochemistry*

Stock solution concentrations of Rho-Ub-ABPs

Stock solutions in DMSO (500 μ M) are prepared by adding the appropriate volume of DMSO to the lyophilized powder, as calculated from the weight and the molecular mass. Quantification of fluorescence intensity and stained gel with ImageJ⁴³⁻⁴⁵ confirmed that the concentration of unbound Rho-Ub-ABP stocks are in the same range; maximum 2-fold difference.

Method; To 30 μ L Rho-Ub-ABP (10 μ M) in HEPES reaction buffer was added 15 μ L sample buffer, samples were boiled, loaded on gel (5 μ L/lane) and separated by gel electrophoresis.

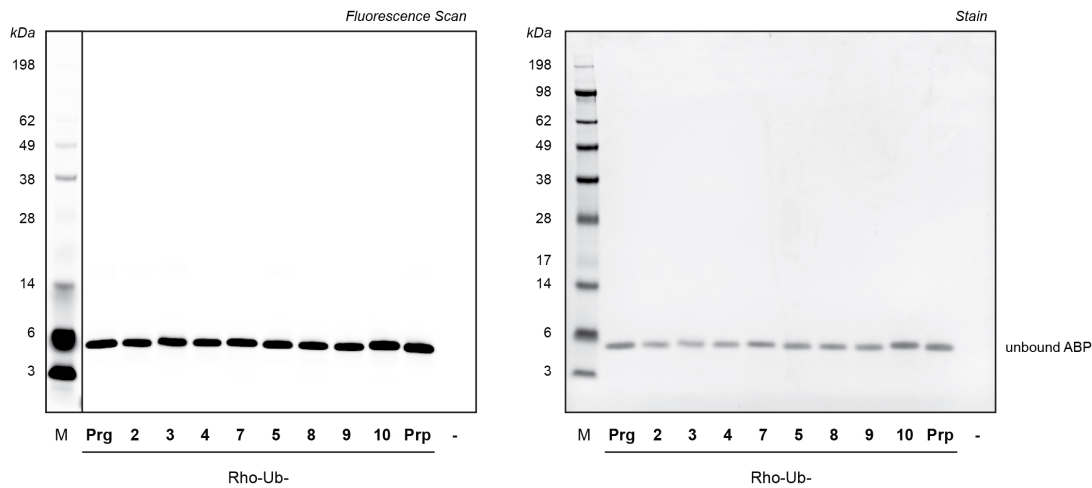


Figure S5. Unbound Rho-Ub-ABPs on 10% Bis-Tris gel. Left; In-gel fluorescence (Sample; $\lambda_{\text{ex}} = 473$ nm, $\lambda_{\text{em}} = 530 \pm 10$ nm. Marker; $\lambda_{\text{ex}} = 635$ nm, $\lambda_{\text{em}} = 665$ nm). Right; Coomassie stain. Protein marker = SeeBlue™ Plus2 Pre-stained Protein Standard.

Incubation of HEK293/EL4 lysate with Rho-Ub-alkyne panel

Gels for incubation with 1 and 10 μ M ABP were scanned and processed simultaneously for direct comparison (same exposure/image processing). Electrophoresis conditions were optimized for DUB separation (4-12% Bis-Tris gels with as MES running buffer) or for visualization of excess unbound ABP (10% Bis-Tris gels with MES as running buffer). Stability/purity of 10 μ M Rho-Ub-3 results in a background signal around \sim 35 kDa.

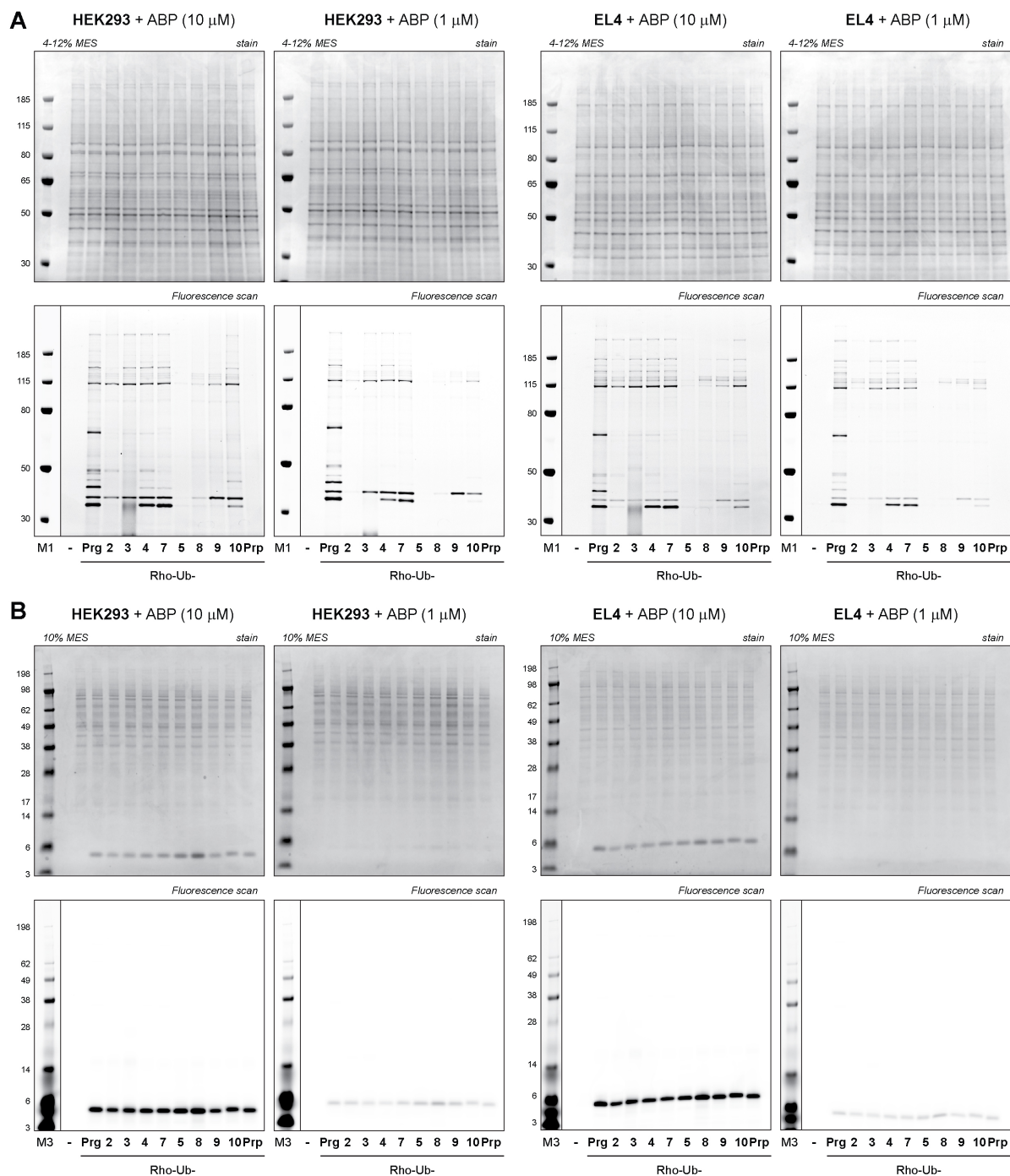


Figure S6. Full gel scans of EL4/HEK293 lysate incubation with Rho-Ub-ABPs related to Figure 2B and Figure S2A-C with gel electrophoresis conditions optimized for **A**) DUB separation or **B**) visualization of unbound ABP. Top; Coomassie stain (loading control). Bottom; in-gel fluorescence (Sample; λ_{ex} = 473 nm, λ_{em} = 530 ± 10 nm, Marker; λ_{ex} = 635 nm, λ_{em} = 665 nm). Protein marker M1 = PageRuler™ Plus Prestained Protein Ladder, M3 = SeeBlue™ Plus2 Pre-stained Protein Standard.

Incubation of HeLa lysate (WT or overexpressing FLAG-HA-USP16) with alkyne 5

Labeling of FLAG-HA-USP16 in HeLa lysate with Rho-Ub-5 was confirmed by fluorescence scan (observation of a faint band) and western blotting for the protein tag. Western blotting also confirms that labeling with Rho-Ub-**Prg** and Rho-M20-**Prg** is much faster; adduct formation of 10 μ M Rho-Ub-5 with FLAG-HA-USP16 is incomplete after incubation for one hour, which could explain the faint labeling observed with Rho-Ub-5 compared to positive control Rho-M20-**Prg**. Rho-M20-**Prg** is a USP16-selective ABP based on Ubiquitin mutant 20 developed in our group; synthesis and selectivity are reported by Gjonaj *et al.*⁵

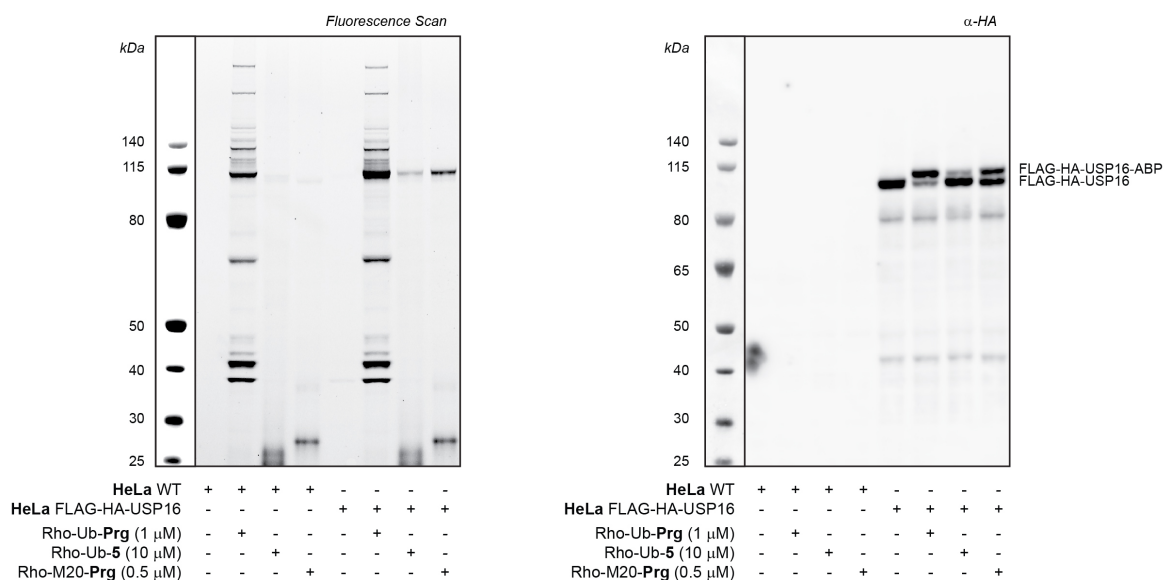


Figure S7. Full gel scans for incubation of HeLa lysate (WT or overexpressing FLAG-HA-USP16) with Rho-Ub-**Prg** (1 μ M), Rho-Ub-5 (10 μ M) or Rho-M20-**Prg** (0.5 μ M) related to Figure S2D. Left; In-gel fluorescence scan (Sample; λ_{ex} = 473 nm, λ_{em} = 530 \pm 10 nm, Marker; λ_{ex} = 635 nm, λ_{em} = 665 nm). Right; anti-HA western blot with HRP secondary antibody. Protein marker = PageRuler™ Prestained Protein Ladder.

Incubation of HEK293T lysate with electron-deficient alkyne **18**

Fresh HEK293T lysate was incubated with 1 μ M Rho-Ub-ABPs. Adduct formation with 1 μ M Rho-Ub-**2** is lower than with 10 μ M Rho-Ub-**2** (as shown in Figure S2B). Electrophoresis conditions were optimized for DUB separation (4-12% MES) or visualization of excess unbound ABP (10% MES).

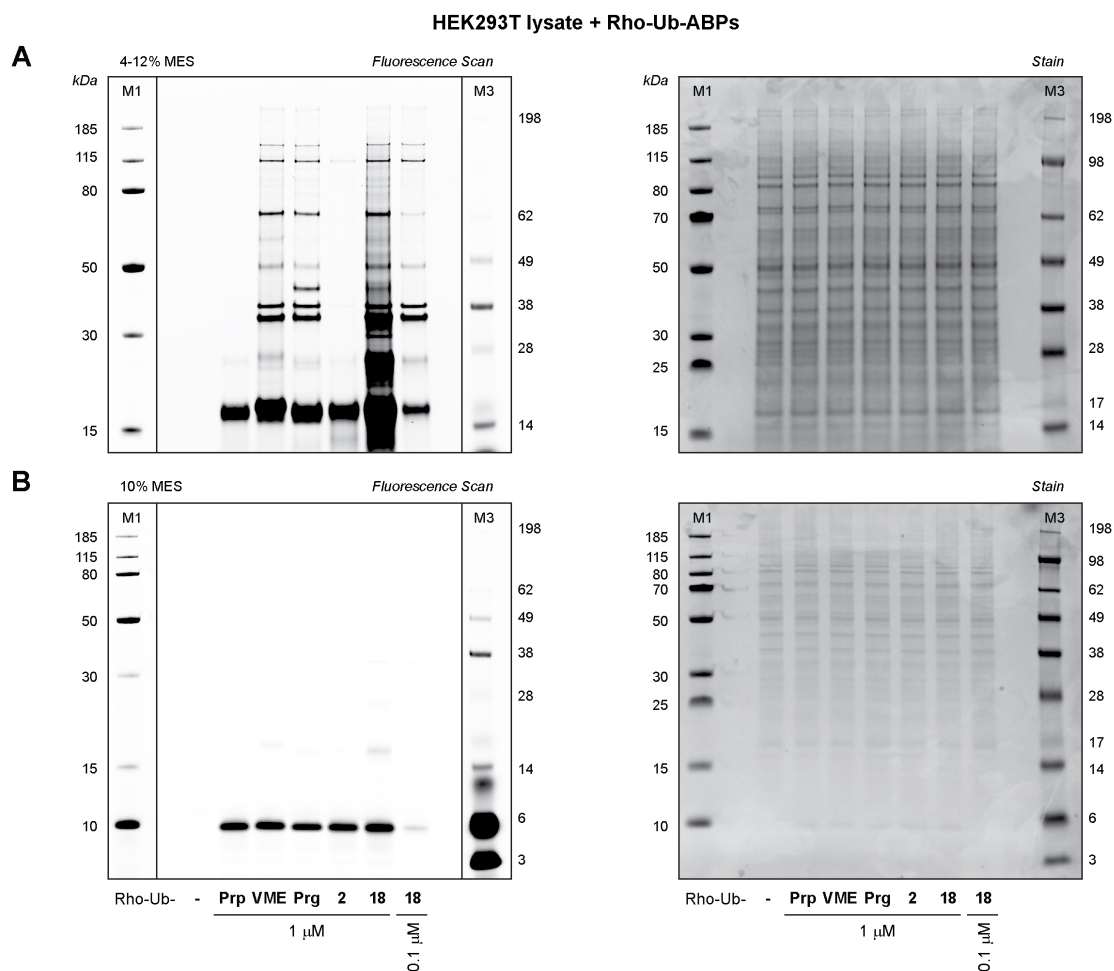


Figure S8. Full gels scans of HEK293T lysate incubation with Rho-Ub-Prp/VME/Prg/2/18 (1 μ M) or Rho-Ub-18 (0.1 μ M) related to Figure S4D with gel electrophoresis conditions optimized for **A**) DUB separation or **B**) visualization of unbound ABP. Left; in-gel fluorescence (Sample; λ_{ex} = 473 nm, λ_{em} = 530 \pm 10 nm, Marker; λ_{ex} = 635 nm, λ_{em} = 665 nm). Right; Coomassie stain (loading control). Protein marker M1 = PageRuler™ Plus Prestained Protein Ladder, M3 = SeeBlue™ Plus2 Pre-stained Protein Standard.

Incubation of recombinant DUBs

Recombinant purified DUBs were obtained from commercial sources, received as gift, or expressed and purified according to reported procedures (details provided in Table S2). Full gel scans of in-gel fluorescence and Coomassie stain are shown in Figure S9 and Figure S10. Bis-Tris gel percentage and running buffer were adjusted to optimize separation of unbound enzyme and covalent ABP-enzyme adduct.

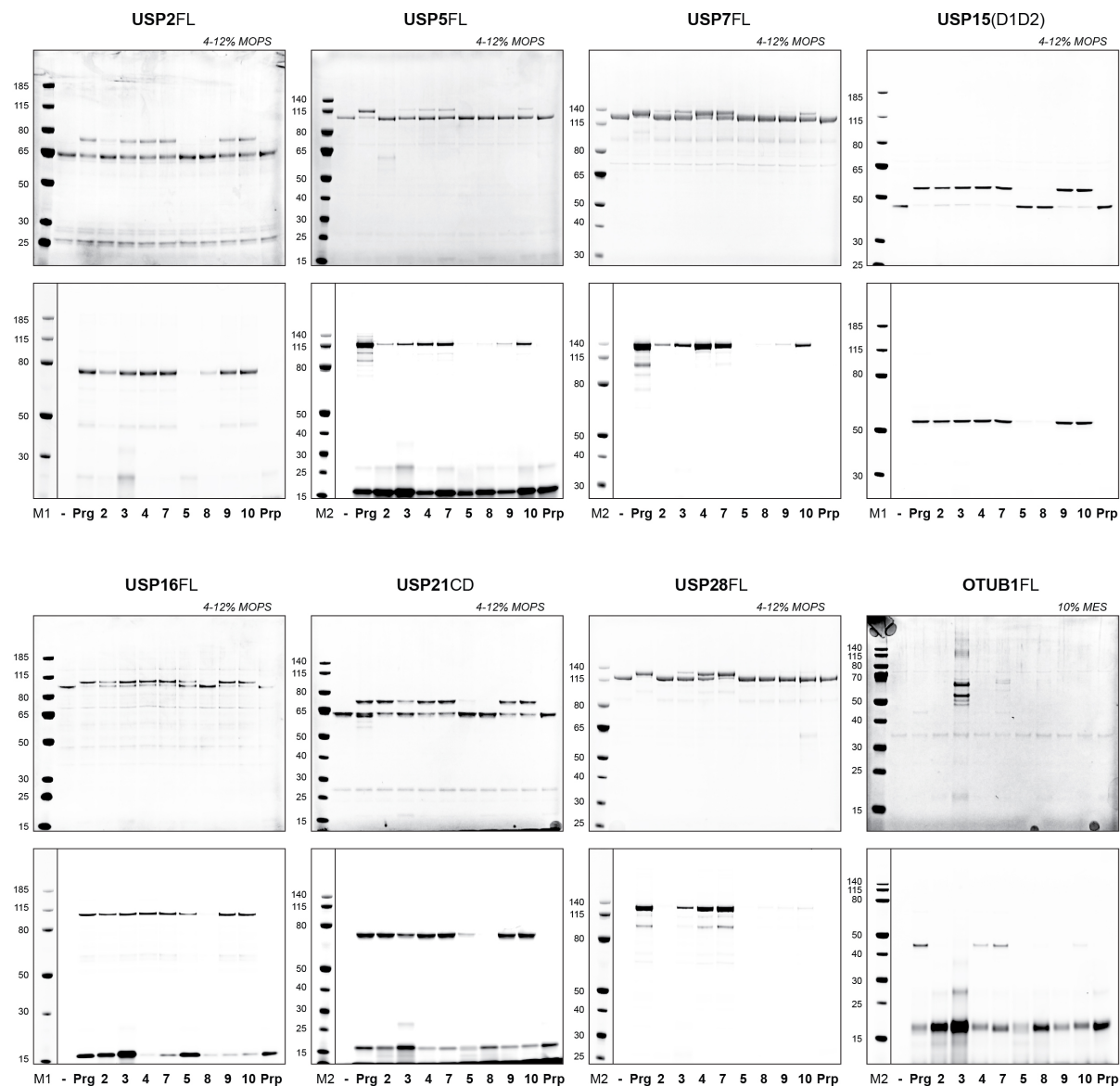


Figure S9. Full gel scans of recombinant cysteine DUB labeling with 10 μ M Rho-Ub-ABPs related to Figure 2C and Figure S3. Top; Coomassie stain. Bottom; In-gel fluorescence scan (Samples: λ_{ex} = 473 nm, λ_{em} = 530 \pm 10 nm. Marker: λ_{ex} = 635 nm, λ_{em} = 665 nm). Unbound cysteine DUB and covalent ABP-enzyme adduct were resolved by SDS-PAGE electrophoresis on 4-12% or 10% Bis-Tris gels with MOPS or MES as running buffer. Protein marker = PageRuler™ Plus Prestained Protein Ladder (M1) or PageRuler™ Prestained Protein Ladder (M2).

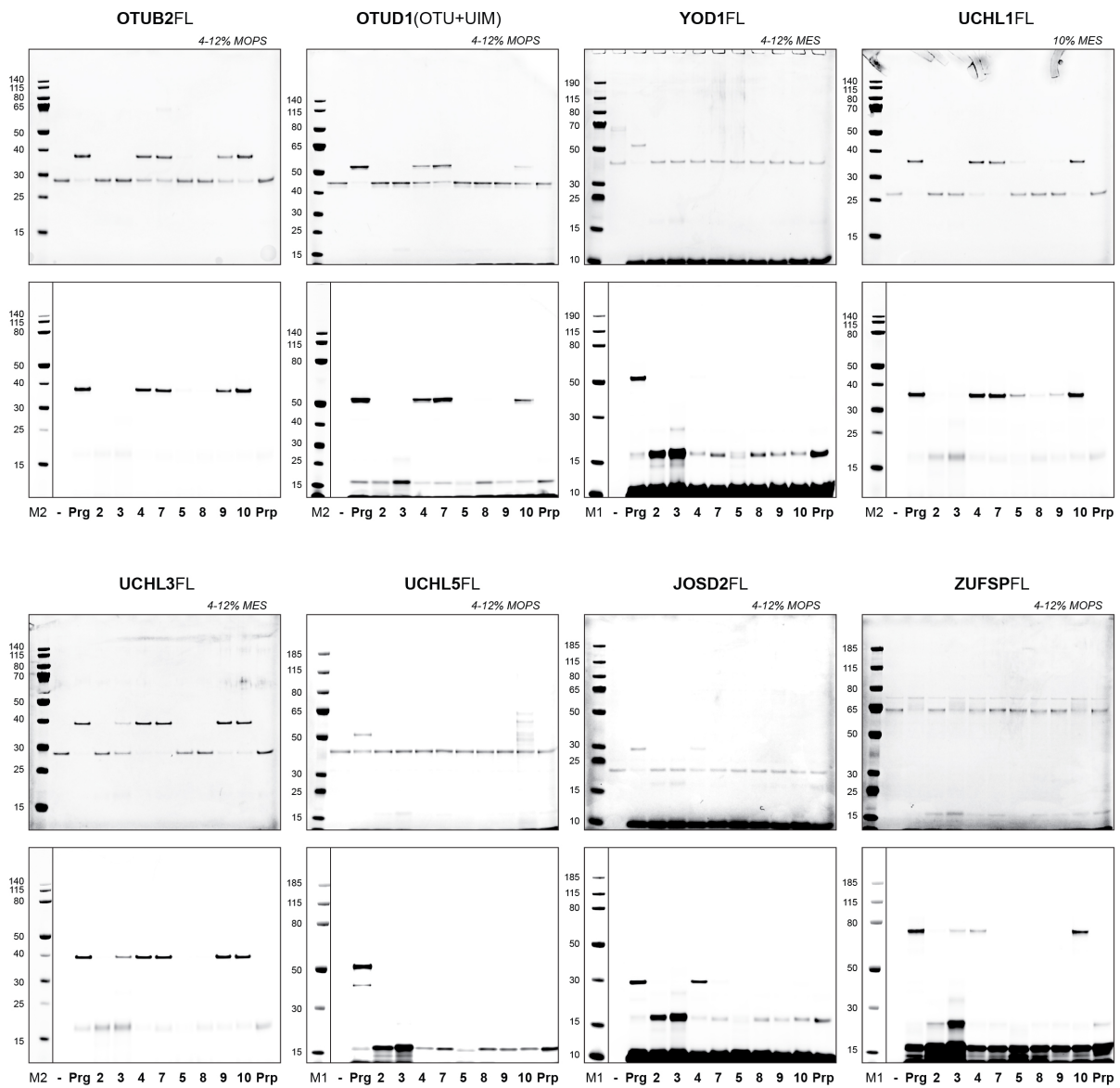


Figure S10. Full gel scans of recombinant cysteine DUB labeling with 10 μ M Rho-Ub-ABPs related to Figure 2C and Figure S3. Top; Coomassie stain. Bottom; In-gel fluorescence scan (Samples: $\lambda_{\text{ex}} = 473$ nm, $\lambda_{\text{em}} = 530 \pm 10$ nm. Marker: $\lambda_{\text{ex}} = 635$ nm, $\lambda_{\text{em}} = 665$ nm). Unbound cysteine DUB and covalent ABP-enzyme adduct were resolved by SDS-PAGE electrophoresis on 4-12% or 10% Bis-Tris gels with MOPS or MES as running buffer. Protein marker = PageRuler™ Plus Prestained Protein Ladder (M1) or PageRuler™ Prestained Protein Ladder (M2).

Gel analysis of adducts with recombinant USP16CD^{WT} (+/- NEM) and USP16CD^{C205A}

USP16CD^{WT} was preincubated with thiol-alkylating reagent *N*-ethylmaleimide (NEM) prior to incubation with Rho-Ub-ABPs to alkylate cysteine thiols thus blocking them from covalent adduct formation with Rho-Ub-ABPs. As a control, USP16CD^{WT} was preincubated in absence of NEM to ensure loss of adduct formation is due to thiol-alkylation rather than spontaneous loss of USP16 reactivity during preincubation. Fluorescence scans for resolved gels with USP16CD^{WT} and USP16CD^{C205A} were obtained with the same settings/sensitivity (PMT = 500), and images were processed simultaneously to ensure observed (lack of) fluorescent covalent adduct is independent of settings. Fluorescent background signals for Rho-Ub-ABP around 14-17 kDa are artifacts commonly observed at high exposure, especially when ABP is present in very large excess relative to enzyme.

Detailed procedure USP16CD^{WT} incubation. 25 μ L USP16CD^{WT} (concentration during preincubation; 0.2 μ M) was preincubated with 25 μ L NEM (concentration during preincubation; 10 mM) or 25 μ L buffer for 30 minutes at 37 °C in HEPES reaction buffer (supplemented with 0.005% Tween20). Then 10 μ L USP16CD^{WT} +/- NEM (final USP16 conc. 0.1 μ M) was incubated with 10 μ L Rho-Ub-ABP (final conc. 10 μ M) for 1 hour at 37 °C. The reaction was quenched by addition of 10 μ L reducing sample buffer and boiling. Of each sample 24 μ L was loaded on 10% Bis-Tris gels, and covalent complex was resolved by SDS-PAGE gel electrophoresis with MES as running buffer.

Detailed procedure USP16CD^{C205A} incubation. 10 μ L USP16CD^{C205A} mutant (final USP16 conc. 0.1 μ M) was incubated with 10 μ L Rho-Ub-ABP (final conc. 10 μ M) for 1 hour at 37 °C in HEPES reaction buffer (supplemented with 0.005% Tween20). The reaction was quenched by addition of 10 μ L reducing sample buffer and boiling. Of each sample 24 μ L was loaded on 10% Bis-Tris gels, and covalent complex was resolved by SDS-PAGE gel electrophoresis with MES as running buffer.

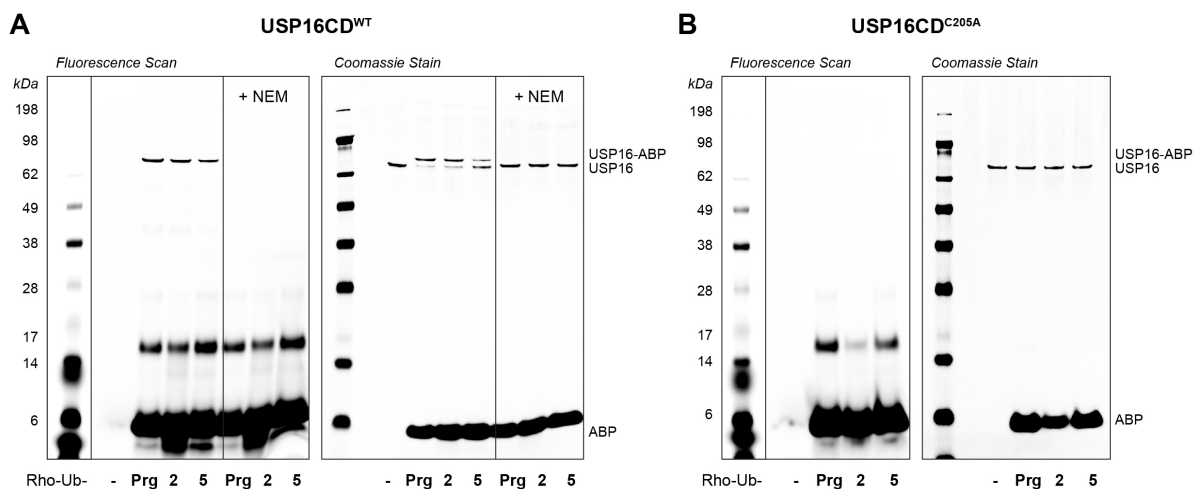


Figure S11. Full gel scans of incubation with 10 μ M Rho-Ub-ABPs related to Figure 3A for **A**) USP16CD^{WT} after preincubation in absence/presence of NEM, or **B**) USP16CD^{C205A}. Left; In-gel fluorescence (Samples: λ_{ex} = 473 nm, λ_{em} = 530 \pm 10 nm. Marker: λ_{ex} = 635 nm, λ_{em} = 665 nm). Right; Coomassie stain. Protein marker = SeeBlue™ Plus2 Pre-stained Protein Standard.

Adduct formation of recombinant USP16CD^{WT} and USP16CD^{C205A} with Rho-Ub-18

Fluorescence scans for resolved gels with USP16CD^{WT} and USP16CD^{C205A} were obtained with the same settings/sensitivity (PMT = 800), and images were processed simultaneously to ensure observed (lack of) fluorescent covalent adduct is independent of settings. Rho-Ub-ABPs with electrophilic warheads (**VME** or electron-deficient alkyne **18**) show some labeling of the catalytic dead USP16CD^{C205A} mutant, indicative of residual reactivity with non-catalytic cysteines. Adduct formation with catalytic cysteine residue is much faster.

Detailed procedure. 20 μ L USP16CD^{WT} (final conc. 0.2 μ M) or USP16CD^{C205A} mutant (final conc. 0.1 μ M) was incubated with 20 μ L Rho-Ub-ABP (final conc. 1 μ M) for 1 hour at 37 °C in HEPES reaction buffer (supplemented with 0.005% Tween20). The reaction was quenched by addition of 20 μ L reducing sample buffer and boiling. Of each sample 10 μ L (USP16CD^{WT}) or 20 μ L (USP16CD^{C205A}) was loaded on 10% Bis-Tris gels, and covalent complex was resolved by SDS-PAGE gel electrophoresis with MES as running buffer.

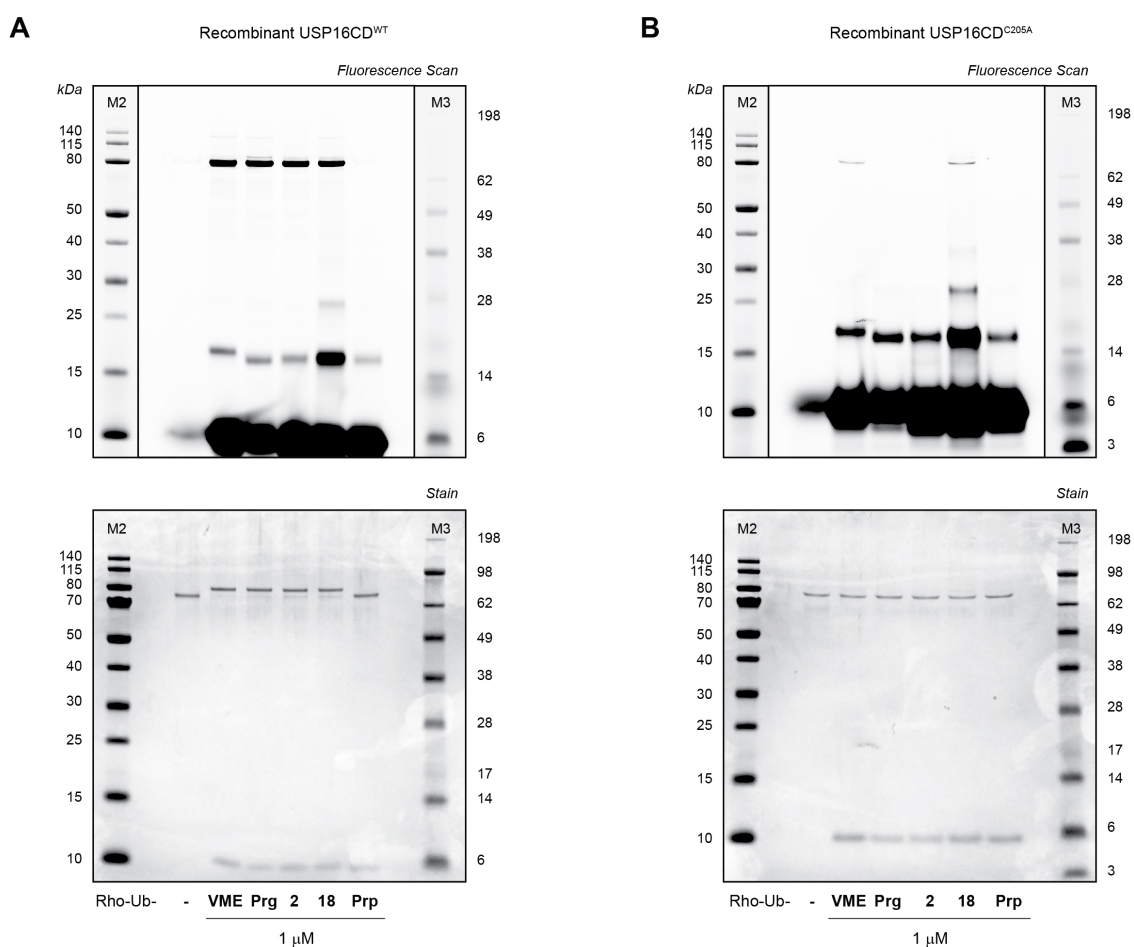


Figure S12. Full gel scans related to Figure S4E/F for incubation with Rho-Ub-ABPs for **A**) USP16CD^{WT} or **B**) USP16CD^{C205A}. Top; In-gel fluorescence (Samples: λ_{ex} = 473 nm, λ_{em} = 530 \pm 10 nm. Marker: λ_{ex} = 635 nm, λ_{em} = 665 nm). Bottom; Coomassie stain. Protein marker; PageRuler™ Prestained Protein Ladder (M2) or SeeBlue™ Plus2 Pre-stained Protein Standard (M3).

Time-dependent covalent USP16-ABP adducts

Incubation was performed in Protein Lobind Tubes (Eppendorf, #022431018) to minimize (time-dependent) loss of enzyme due to precipitation/aggregation. Maximum adduct formation with Rho-Ub-Prg was reached within 15 minutes, but time-dependent increase of covalent adduct could be observed for Rho-Ub-2 and Rho-Ub-5. Conditions for gel electrophoresis were optimized for separation of unbound USP16 and USP16-ABP adduct while ensuring unbound ABP does not run off the gel.

Detailed procedure. 25 μL USP16CD^{WT} (final conc. 0.25 μM) was incubated with 25 μL Rho-Ub-Prg, Rho-Ub-2 or Rho-Ub-5 (final conc. 10 μM) at 37 °C in HEPES reaction buffer (supplemented with 0.005% Tween20). Samples (8 μL) were removed after indicated incubation time (0.5-4 h), and adduct formation was quenched. All samples (10 $\mu\text{L}/\text{lane}$) were loaded on 10% Bis-Tris gels (Invitrogen) and resolved by SDS-PAGE gel electrophoresis with MES as running buffer. Fluorescence scans for resolved gels were obtained and processed simultaneously (one scan) to ensure observed increase in fluorescent covalent adduct is independent of scanner settings.

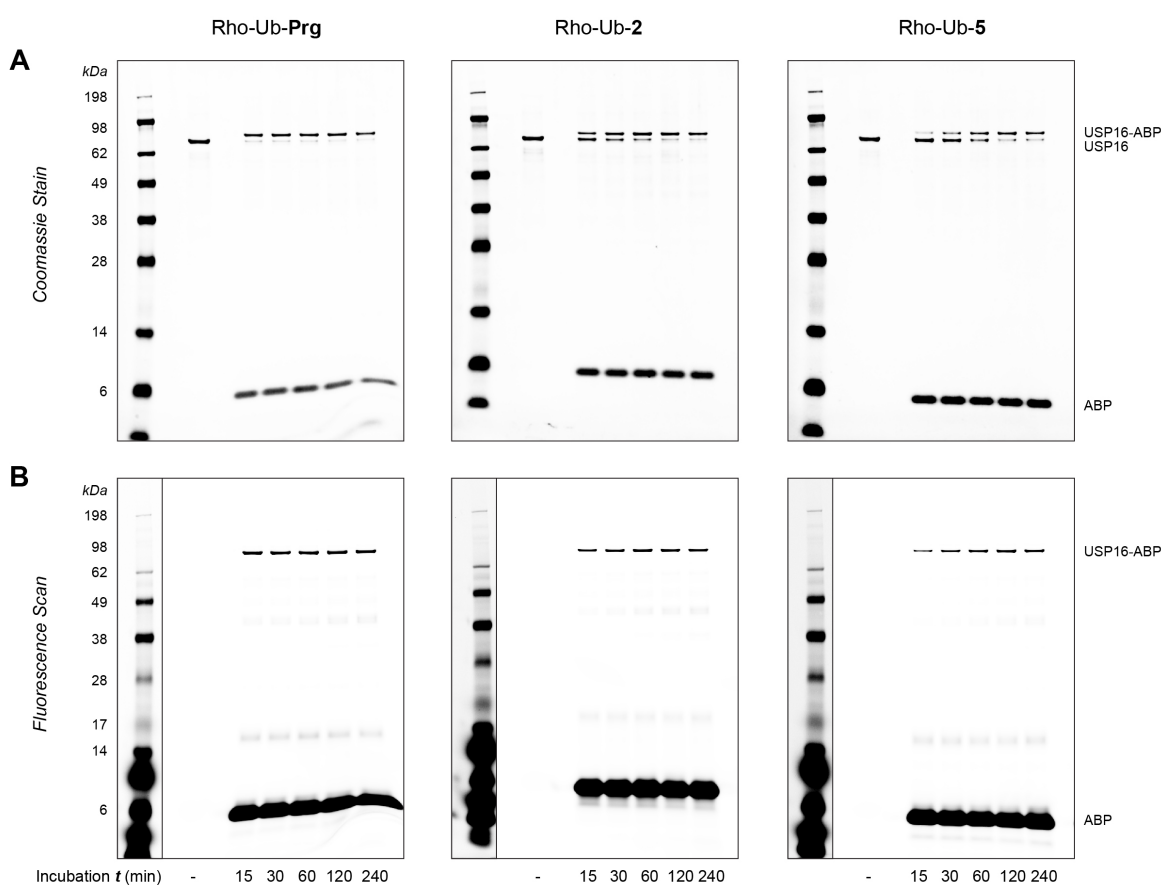


Figure S13. Full gel scans of USP16CD^{WT} incubation with 10 μM Rho-Ub-Prg (left), Rho-Ub-2 (middle) or Rho-Ub-5 (right) related to Figure 5A. **A)** Coomassie stain. **B)** In-gel fluorescence (Samples: $\lambda_{\text{ex}} = 473 \text{ nm}$, $\lambda_{\text{em}} = 530 \pm 10 \text{ nm}$. Marker: $\lambda_{\text{ex}} = 635 \text{ nm}$, $\lambda_{\text{em}} = 665 \text{ nm}$). Protein marker = SeeBlue™ Plus2 Pre-stained Protein Standard.

Kinetic analysis of covalent USP16 occupancy

Incubation was performed in Protein Lobind Tubes (Eppendorf, #022431018) to minimize (time-dependent) loss of enzyme due to precipitation/aggregation. Incubation temperature was lowered to 21 °C to reduce the reaction rate for Rho-Ub-Prg, but this was not sufficient; maximum adduct formation was still observed before the first timepoint. Fluorescence scans for resolved gels were obtained and processed simultaneously (one scan) to ensure observed increase in fluorescent covalent adduct is independent of settings. Representative full gel scans are shown in Figure S14.

Detailed experimental procedure. 49 μL USP16CD^{WT} (final conc. 0.1 μM) was incubated with 49 μL Rho-Ub-Prg, Rho-Ub-2 or Rho-Ub-5 (final conc. 1-10 μM) at 21 °C. Samples (18 μL) were removed after indicated incubation time (5-30 minutes), and adduct formation was quenched. All samples (24 μL) were loaded on 10% Bis-Tris gels (Invitrogen) and resolved by SDS-PAGE gel electrophoresis with MES as running buffer.

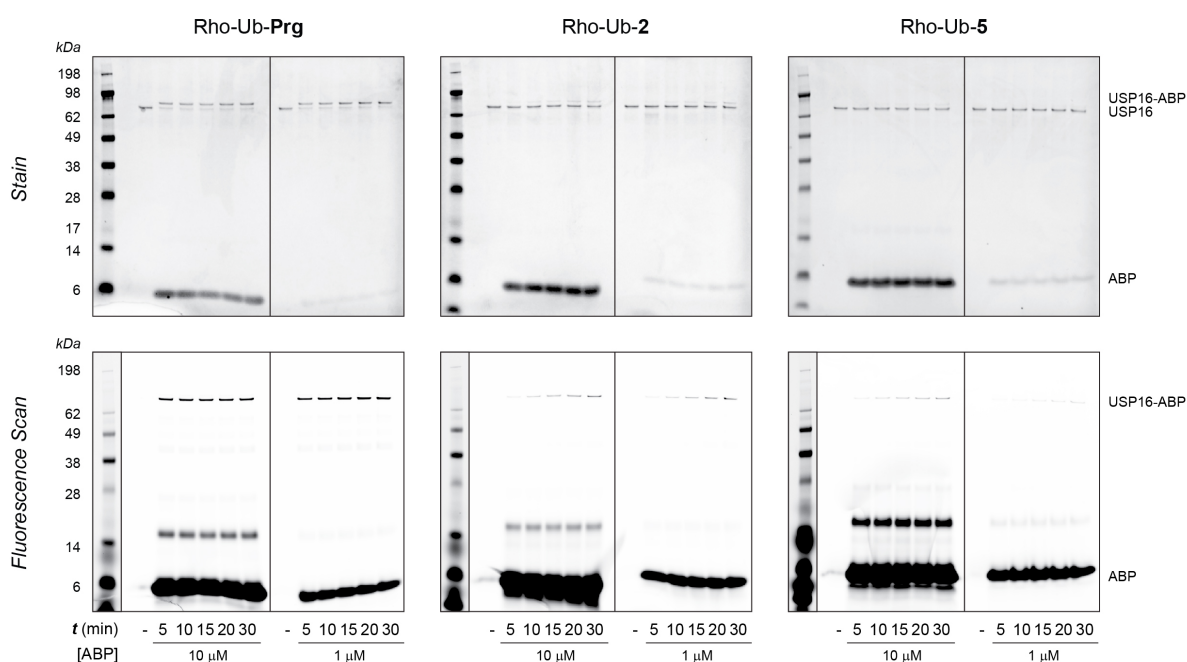


Figure S14. Representative full gel scans for kinetic covalent adduct formation of 1-10 μM Rho-Ub-ABPs with 0.1 μM recombinant USP16CD^{WT} related to Figure 5C. Top; In-gel fluorescence (Samples: $\lambda_{\text{ex}} = 473 \text{ nm}$, $\lambda_{\text{em}} = 530 \pm 10 \text{ nm}$. Marker: $\lambda_{\text{ex}} = 635 \text{ nm}$, $\lambda_{\text{em}} = 665 \text{ nm}$). Bottom; Coomassie stain. Protein marker = SeeBlue™ Plus2 Restained Protein Standard.

Detailed kinetic analysis. Quantification of unbound USP16 and USP16-ABP adduct was performed with ImageJ v1.52a,⁴³⁻⁴⁵ and the gel-specific background was subtracted to calculate the covalent occupancy for each sample with Equation I. Noncovalent USP16-ABP association complexes disintegrate into unbound USP16 and unbound ABP, since the gels are run under denaturing conditions. Each condition was repeated three times (triplicate, $n = 3$), thus there were three values for covalent occupancy for each ABP concentration/incubation time. Covalent occupancy was fitted to Equation II with GraphPad Prism 8.1.1 software, with a globally shared value for maximum covalent occupancy, and including 1-5 minute measurements with Rho-Ub-Prg ($n = 1$), that still showed reaction completion within the first minute. The standard deviation for Rho-Ub-Prg is thus very large. It is important to note here that kinetic analysis is performed under pseudo-first order reaction conditions ($[\text{ABP}]_0 \geq 10[\text{E}]_0$) to allow algebraic analysis, assuming the unbound ABP concentration does not decrease significantly upon binding to enzyme. It is essential not to violate this assumption to obtain reliable estimates for the rate of covalent adduct formation k_{obs} .

$$(\text{Covalent Occupancy})_t = 100\% \frac{(\text{adduct})_t}{(\text{adduct})_t + (\text{unbound})_t}$$

Equation I. **Covalent occupancy.** $(\text{Covalent occupancy})_t$ = incubation time-dependent occupancy (%). $(\text{adduct})_t$ = background-subtracted signal for covalent adduct after incubation t (%). $(\text{unbound})_t$ = background-subtracted signal for unbound enzyme after incubation t (%).

$$(\text{Covalent Occupancy})_t = Y_0 + (\text{Plateau} - Y_0)(1 - e^{-k_{\text{obs}}t}) = \text{Max}(1 - e^{-k_{\text{obs}}t})$$

Equation II. **Rate of covalent bond formation.** Fit to Covalent occupancy (triplicate) against incubation time. $(\text{Covalent occupancy})_t$ = incubation time-dependent occupancy (%). Y_0 = signal at reaction initiation = 0. $\text{Plateau} = \text{Max} = \text{Maximum covalent occupancy (\%)} = \text{shared value for all ABPs}$. k_{obs} = Rate of covalent bond formation (min^{-1}). t = Incubation time (min).

$$t_{1/2} = \frac{\ln 2}{k_{\text{obs}}}$$

Equation III. **Reaction half-life.** $t_{1/2}$ = Reaction half-life (min) = incubation time to reach 50% of maximum covalent occupancy. k_{obs} = Pseudo-first order rate of covalent bond formation (min^{-1}).

$$\text{Reaction completion} = 5t_{1/2}$$

Equation IV. **Reaction completion.** Reaction completion = time to reach covalent occupancy = 97% of max. $t_{1/2}$ = Reaction half-life (min) = incubation time to reach 50% of maximum covalent occupancy.

$$k_{\text{obs}} = \frac{k_{\text{inact}}[I]_0}{K_I + [I]_0}$$

Equation V. **Rate of covalent bond formation under pseudo-first order conditions.** k_{obs} = Rate of covalent bond formation (min^{-1}). $[I]_0$ = ABP concentration at reaction initiation (M). k_{inact} = Maximum rate of covalent bond formation at saturating ABP concentration (min^{-1}). K_I = ABP concentration where $k_{\text{obs}} = \frac{1}{2} k_{\text{inact}}$ (M). Assumption; $[I]_0 \gg [E]_0$ so that $[I]_t = [I]_0$ (concentration of unbound ABP does not change significantly upon enzyme-binding, and ABP is present in excess).

Background on kinetics of irreversible ligands; reaction order. Covalent adduct formation between ABP and enzyme is a two-step ligand binding reaction, and we normally assume that the non-covalent equilibrium is reached almost instantly (much faster than covalent adduct formation).⁴⁶ The rate of covalent adduct formation k_{obs} depends on both the concentration of enzyme and ABP if neither of these are present in large excess; the reaction slows down because the concentration of both ABP and enzyme decreases as the reaction progresses under second order reaction conditions. Reaction kinetics of (irreversible) ligand binding are normally studied under pseudo-first order reaction conditions;⁴⁷⁻⁴⁸ one of the reactants is present in at least 10-fold excess, so we can assume that the concentration of this reactant does not change significantly during the reaction (and this also ensures we also don't have to address tight-binding effects that shift the non-covalent equilibrium that require using Morrison quadratic equation, as this complicates the system beyond algebraic fitting). In our experiments we ensured that ABP is present in large excess at reaction initiation ($t = 0$); $[\text{ABP}]_0 \geq 10[\text{E}]_0$. Under pseudo-first order conditions, covalent adduct formation can be fitted to a one-phase exponential increase, with covalent occupancy increasing by 50% every half-life. After five half-lives 97% covalent adduct formation is reached, which generally is considered 'close enough' to reaction completion, since detection of changes beyond this point will be affected by error margins.

Fluorescence polarization (FP) binding assay of Rho-Ub-ABPs with USP16CD^{C205S}

Fluorescence polarization (FP) binding assays are based on excitation of a fluorescently labelled reporter/ligand with polarized light, and detection of the degree of polarization in the emitted light.⁴⁹ This technique is often used to detect peptide-protein binding because light emitted by the (small) unbound ligand is more depolarized than the emitted light by the ligand bound to the (large) protein, as a result of its higher rate of molecular rotation. The observed polarization is proportional to the fraction of bound ligand, and titration of protein to a fixed concentration of ligand can be used to generate a binding curve. FP Binding assays of catalytic inactive DUBs with fluorophore-labeled ubiquitin as ligand are commonly performed to determine the non-covalent affinity.^{41, 50}

FP binding assays of reporter/ligand Rho-Ub-ABPs (9 kDa) with catalytically inactive USP16CD^{C205S} mutant (73 kDa) were performed to determine K_D -values that are independent of electronic factors as covalent adduct formation with USP16CD^{C205S} does not occur. Catalytic inactive mutant USP16CD^{C205S} rather than USP16CD^{C205A} was used because active site alanine mutations in cysteine DUBs increase the affinity for ubiquitin.⁵¹ The concentration of Rho-Ub-ABP (5 nM) was kept constant and excess USP16 (>50 nM) was varied, as is common for FP binding assays to maximize the assay window.^{41, 49} Fluorescence polarization was measured every 3 minutes for 120 minutes (Figure S15A), and values after sufficient incubation (60 minutes) to reach equilibrium between unbound and non-covalent bound Rho-Ub-ABP were plotted against USP16 concentration (Figure S15B).

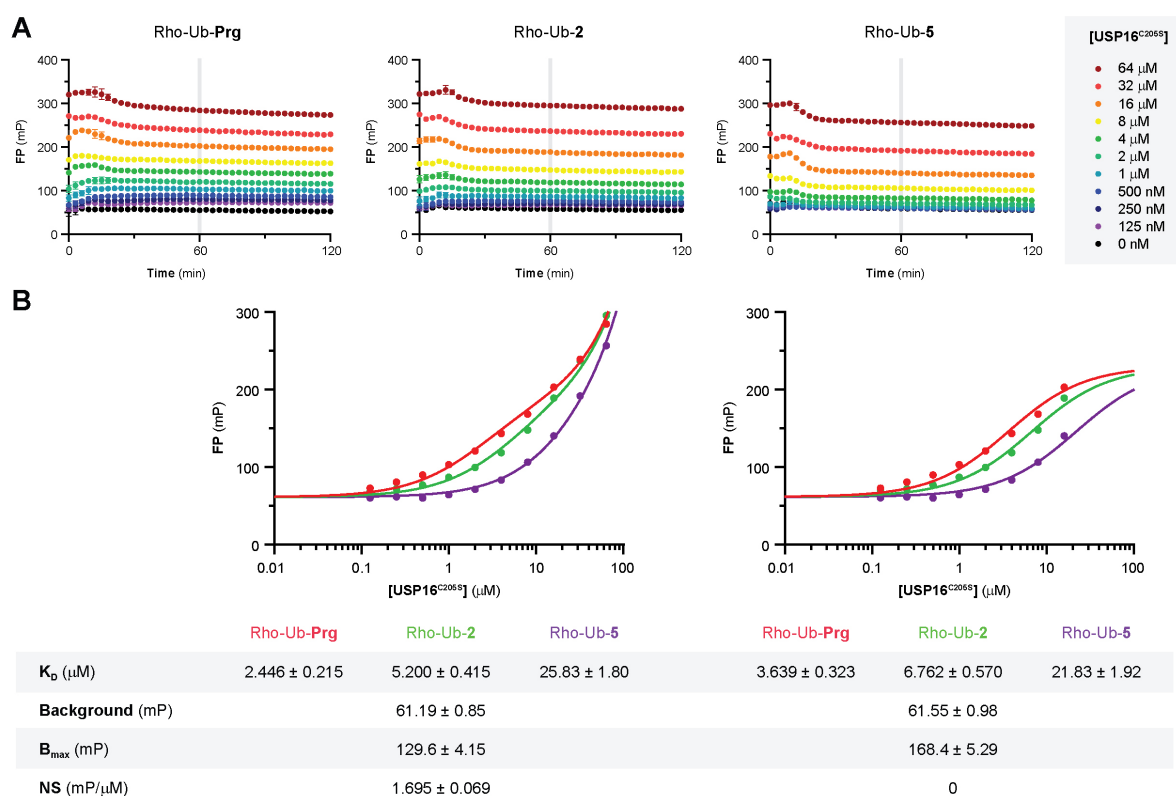


Figure S15. Fluorescence polarization (FP) binding assay related to Figure 5C. **A**) Progress curve for fluorescence polarization signal over time for Rho-Ub-ABPs (5 nM) with USP16CD^{C205S} (0-64 μM). Non-covalent equilibrium between ABP and enzyme is reached after ~30 minutes. **B**) Direct binding curve; fluorescence polarization after incubation for 60 minutes as a function of USP16CD^{C205S} concentration. Fitted to equation VI with shared values for NS, B_{max} and background to obtain K_D -value for each Rho-Ub-ABP. Left; All USP16 concentrations were fitted with a shared value for non-specific binding. Right; [USP16] < 20 μM was fitted with non-specific binding NS = 0. Graphical data represents the mean ± standard deviation for a single representative experiment.

K_D -values were obtained by fitting to Equation VI with shared background (minimum), B_{max} (maximum-background) and NS (non-specific binding) because the tested Rho-Ub-ABPs have the same size/mass. High protein concentrations are prone to exhibit non-specific binding due to hydrophobic interactions

and crowding effects, which was observable as the inability to reach a plateau despite supplementing the buffer with 0.005% Tween20 or additional 0.1 mg/mL bovine serum albumin (BSA, Chemcruz, sc-2323A).⁴⁹ We fitted all USP16 concentrations with a shared value for non-specific binding (NS > 0, Figure S15B, left) but also USP16 concentrations below 20 μ M without taking non-specific binding into account (NS = 0, Figure S15B right). These restraints affect the absolute K_D -values, but regardless of the settings we observe the same trend; K_D for **Prg** < **2** < **5**.

$$FP = \frac{B_{\max}[E]}{K_D + [E]} + NS \times [E] + \text{background}$$

Equation VI. **Binding curve for non-covalent binding affinity of enzyme E and fluorescent reporter/ligand ABP.**

FP = concentration-dependent fluorescent polarization value at equilibrium (mP). B_{\max} = maximum specific binding (mP). [E] = enzyme concentration (M). K_D = dissociation constant (M); enzyme concentration corresponding to 50% occupancy. NS = non-specific binding (mP/M). Background = minimum FP signal (mP), corresponds with FP in absence of enzyme. Assumptions; [E] = $[E]_0$ (no significant change in unbound enzyme concentration) because $[E]_0 \gg [ABP]_0$ (excess enzyme, first order conditions). Equilibrium between unbound E + ABP and bound E-ABP complex should be reached; sufficient incubation time prior to measurement.

Mass spectrometry of intact covalent USP16-ABP adducts

USP16CD^{WT} and USP16CD^{C205A} were incubated with Rho-Ub-ABP prior to MS measurement to allow sufficient adduct formation; incubation time of 2 hours was based on estimates for reaction completion obtained with the kinetic analysis of Rho-Ub-2 and Rho-Ub-5. HEPES reaction buffer did not contain surfactant because Tween20 is not compatible with mass spectrometry. Incubation was performed in Protein Lobind Tubes (Eppendorf, #022431018) to reduce (time-dependent) loss of enzyme due to precipitation/aggregation. Deconvoluted mass was obtained from convolution of spectrum ($m/z = 600-1600$ Da) with MaxEnt1 function in MassLynx V4.2.

Table S3. Calculated and deconvoluted mass of intact USP16CD^{WT} and USP16CD^{C205A} (adducts)^a

Enzyme	ABP	Mass (Da)		Covalent adduct
		<i>Calc.</i> ^b	<i>Found</i>	
-	Rho-Ub-Prg	8,883.12	8,884	N.A.
	Rho-Ub-2	8,897.21	8,898	N.A.
	Rho-Ub-5	8,911.24	8,912	N.A.
USP16CD ^{WT}	-	N.A.	73,344 + 73,426	N.A.
	Rho-Ub-Prg	82,228 + 82,310	82,229 + 82,309	YES
	Rho-Ub-2	82,243 + 82,324	82,242 + 82,324	YES
	Rho-Ub-5	82,258 + 82,339	82,256 + 82,338	YES
USP16CD ^{C205A}	-	N.A.	73,406 + 73,488	N.A.
	Rho-Ub-Prg	82,290 + 82,372	73,407 + 73,489	NO
	Rho-Ub-2	82,304 + 82,386	73,408 + 73,490	NO
	Rho-Ub-5	82,318 + 82,400	73,408 + 73,489	NO

^a Related to Figure 3B+C. ^b Mass of USP16-ABP adduct calculated based on deconvoluted mass of unbound ABP and unbound USP16.

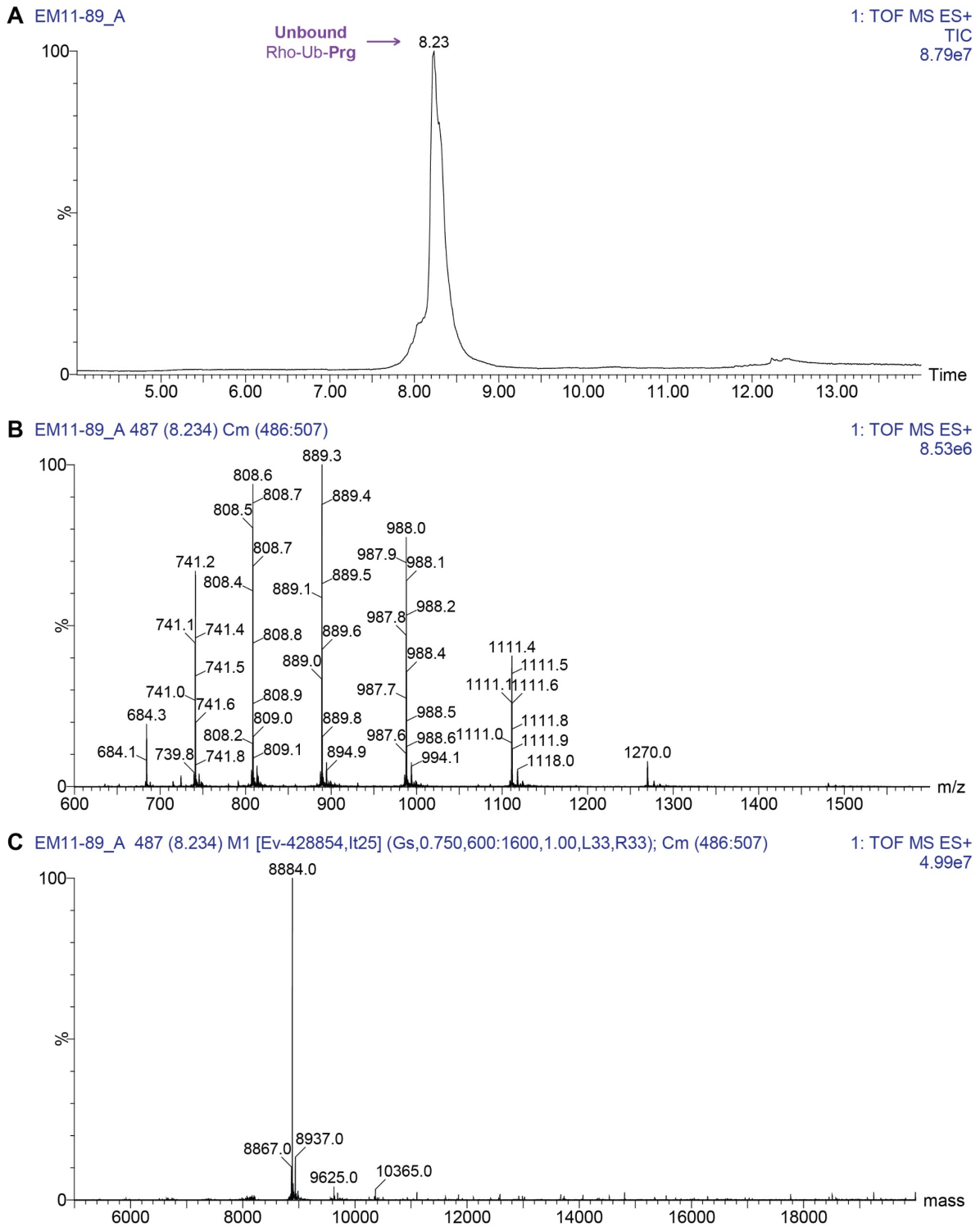


Figure S16. LC-MS data for intact unbound Rho-Ub-Prg related to Figure 3B+C. **A**) Chromatogram. TIC (m/z = 200-2500). **B**) Spectrum of unbound ABP. **C**) Deconvoluted mass: 8884 Da (Found)/8883.12 (Calc.).

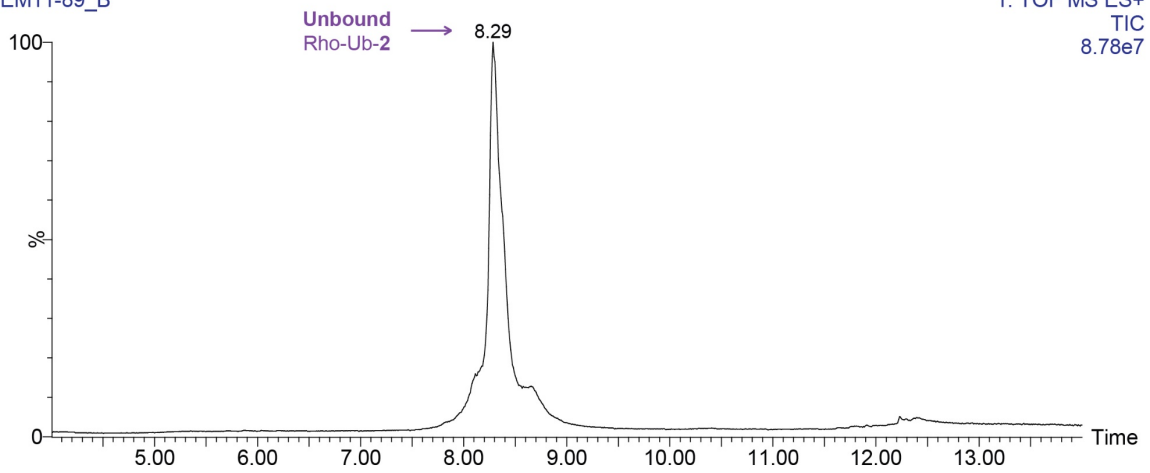
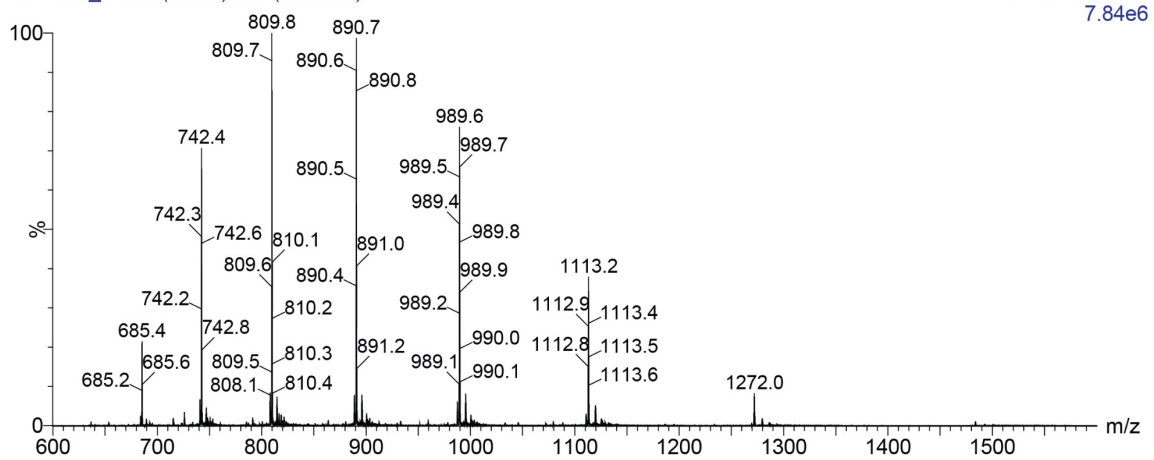
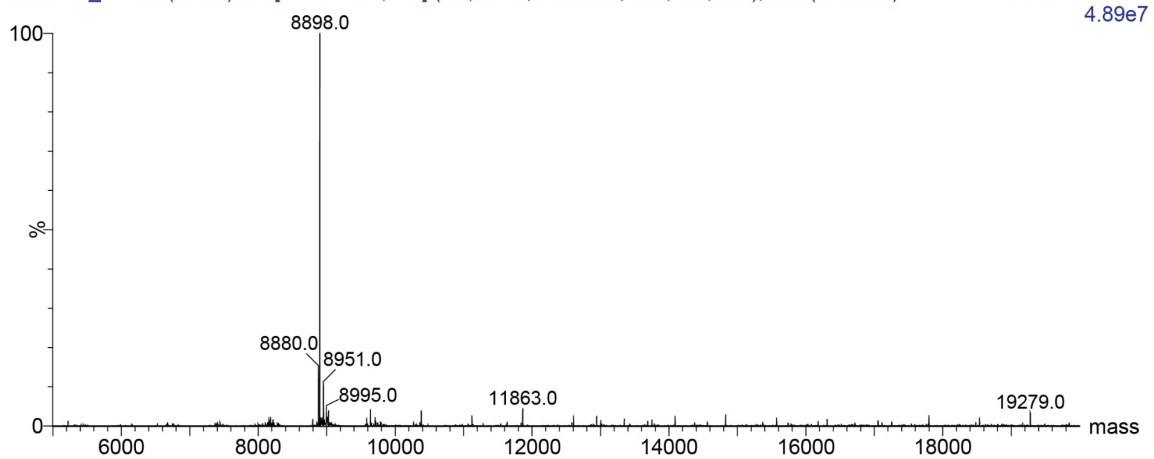
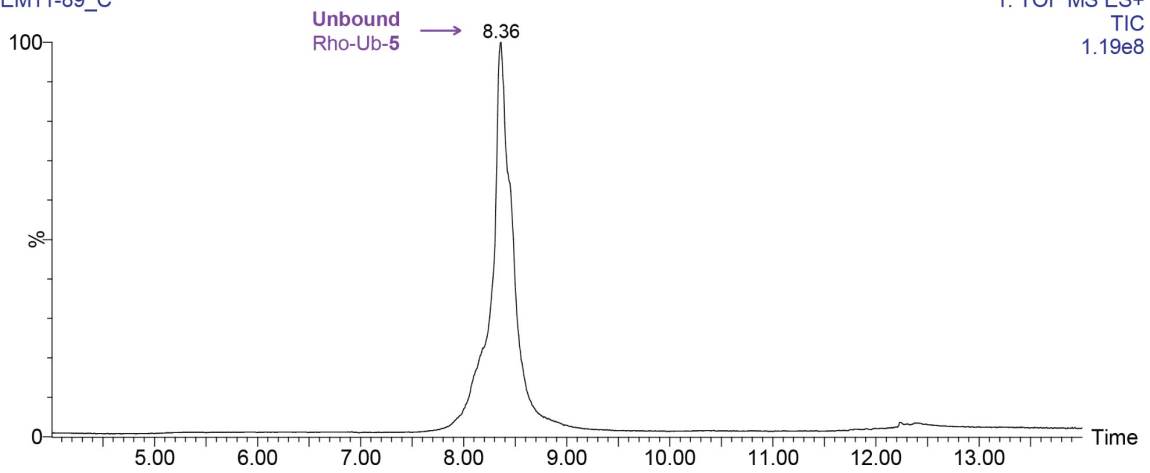
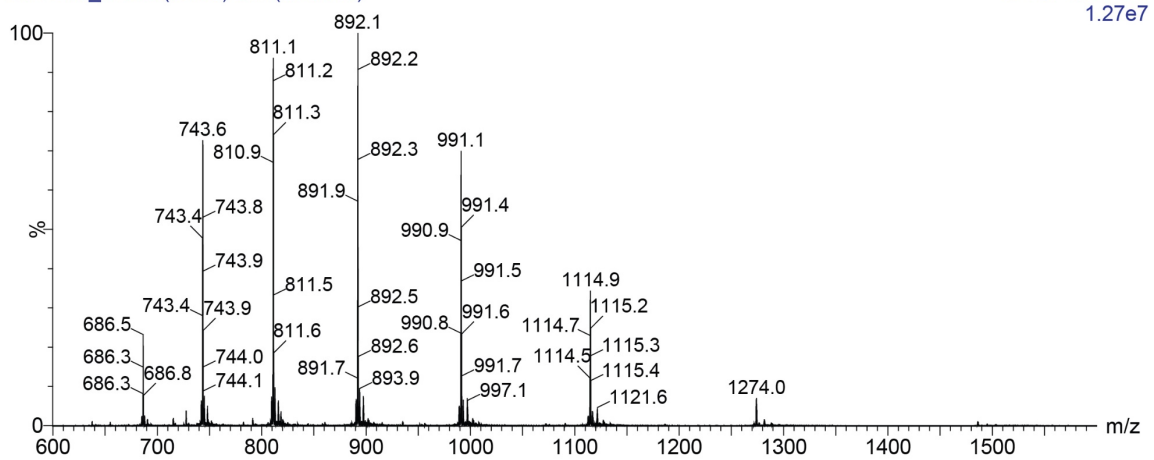
A EM11-89_B**B** EM11-89_B 493 (8.286) Cm (489:512)**C** EM11-89_B 493 (8.286) M1 [Ev-431849,t24] (Gs,0.750,600:1600,1.00,L33,R33); Cm (489:512)

Figure S17. LC-MS data for intact unbound Rho-Ub-2 related to Figure 3B+C. **A**) Chromatogram. TIC (m/z = 200-2500). **B**) Spectrum of unbound ABP. **C**) Deconvoluted mass: 8898 Da (Found)/8897.21 (Calc.).

A EM11-89_C



B EM11-89_C 502 (8.363) Cm (494:518)



C EM11-89_C 502 (8.363) M1 [Ev-445055,lt25] (Gs,0.750,600:1600,1.00,L33,R33); Cm (494:518)

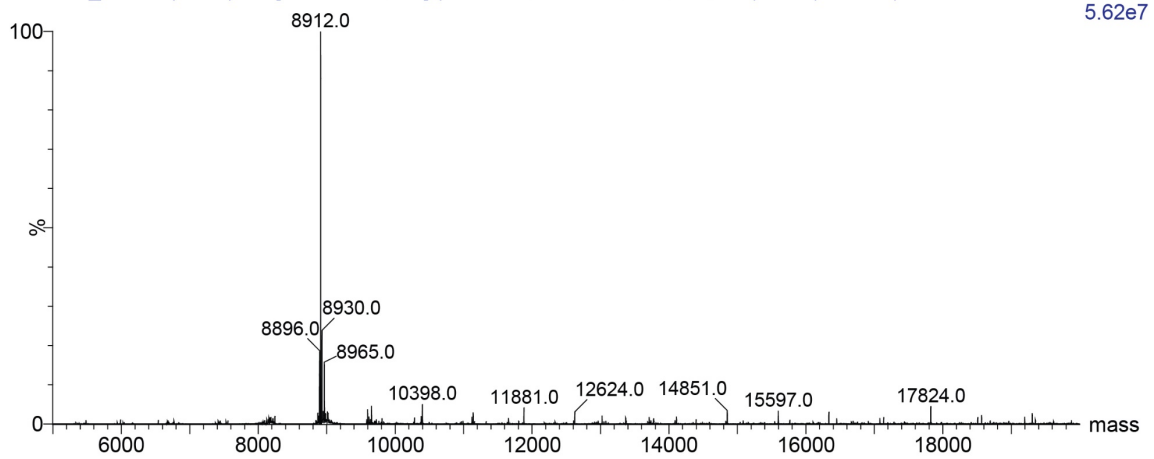


Figure S18. LC-MS data for intact unbound Rho-Ub-5 related to Figure 3B+C. **A**) Chromatogram. TIC ($m/z = 200-2500$). **B**) Spectrum of unbound ABP. **C**) Deconvoluted mass: 8912 Da (Found)/8911.24 (Calc.).

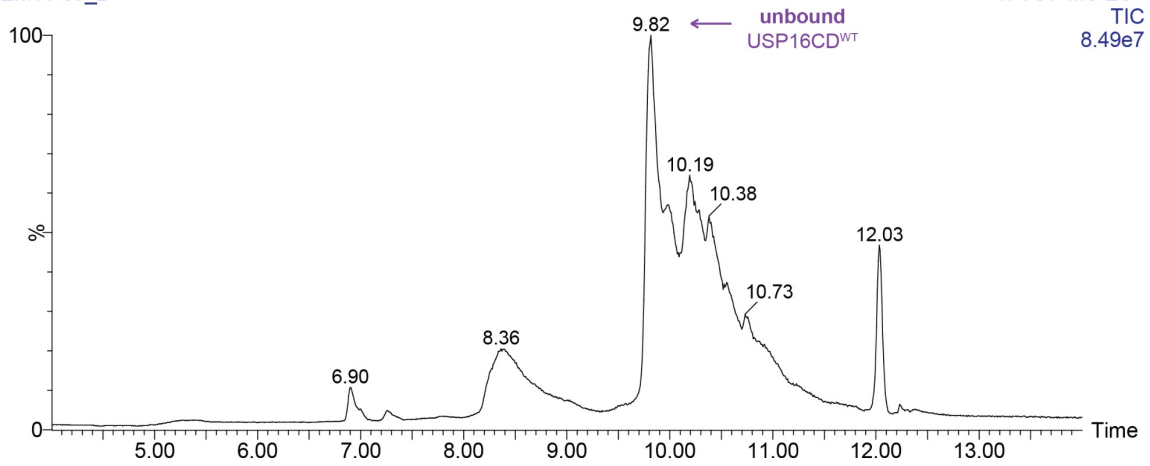
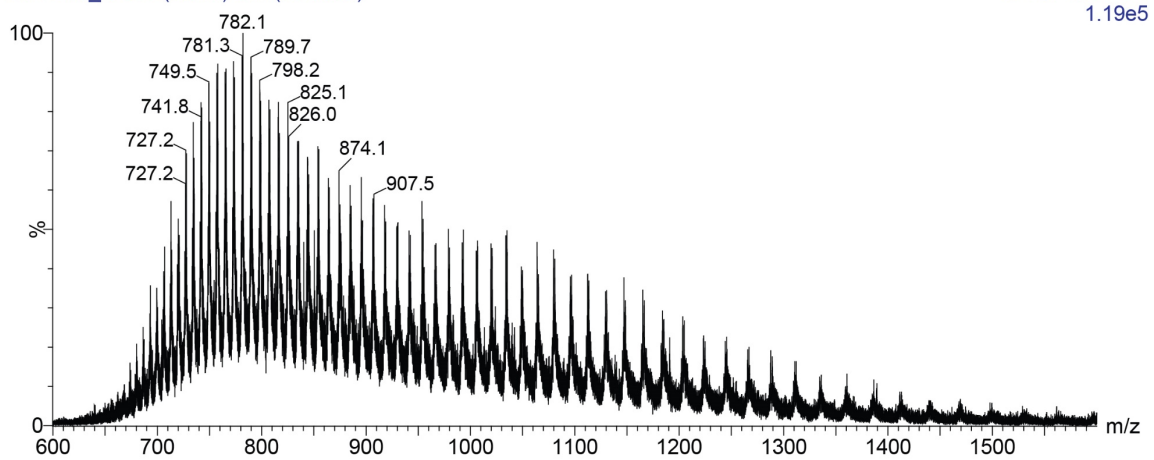
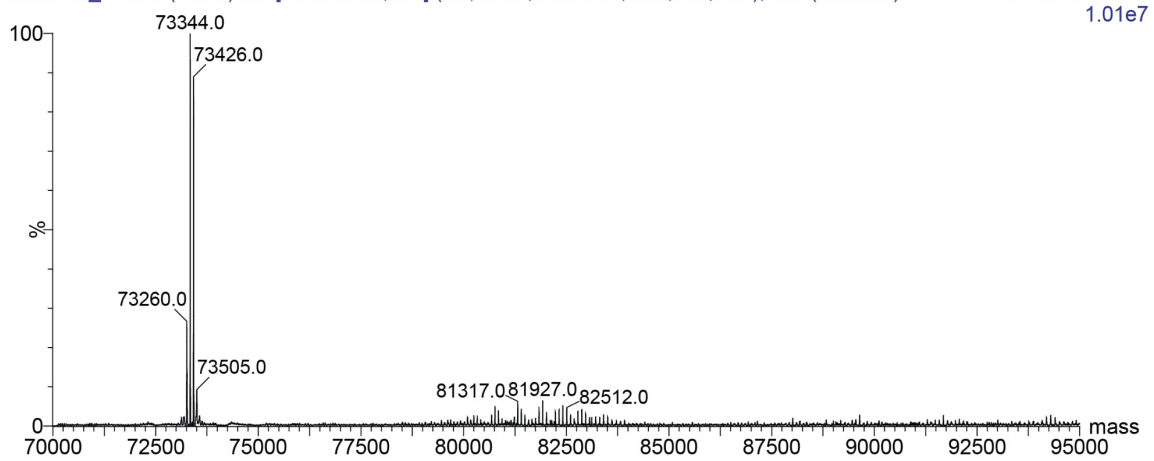
A EM11-89_D**B** EM11-89_D 669 (9.817) Cm (664:682)**C** EM11-89_D 669 (9.817) M1 [Ev-374500,lt34] (Gs,0.750,600:1600,1.00,L33,R33); Cm (664:682)

Figure S19. LC-MS data for intact unbound **USP16CD^{WT}** related to Figure 3B. **A**) Chromatogram. TIC (m/z = 200-2500). **B**) Spectrum of USP16(adduct). **C**) Deconvoluted mass: 73,344 + 73,426 Da (Found).

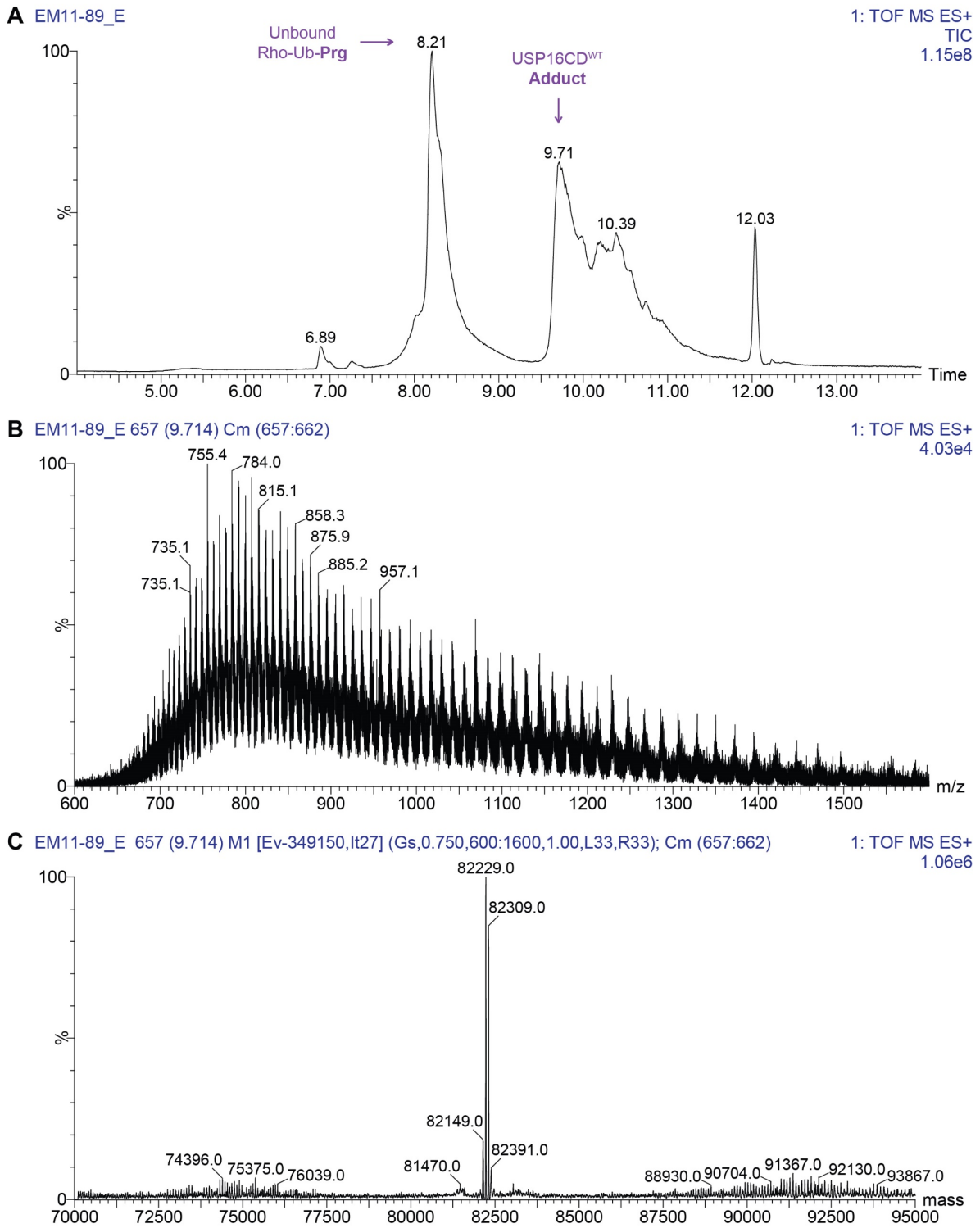


Figure S20. LC-MS data for intact **USP16CD^{WT}** + Rho-Ub-Prg related to Figure 3B. **A**) Chromatogram. TIC ($m/z = 200-2500$). **B**) Spectrum of USP16(adduct). **C**) Deconvoluted mass: $82,229 + 82,309$ Da (Found)/ $82,228 + 82,310$ Da (Calc.). Covalent USP16-ABP adduct is detected.

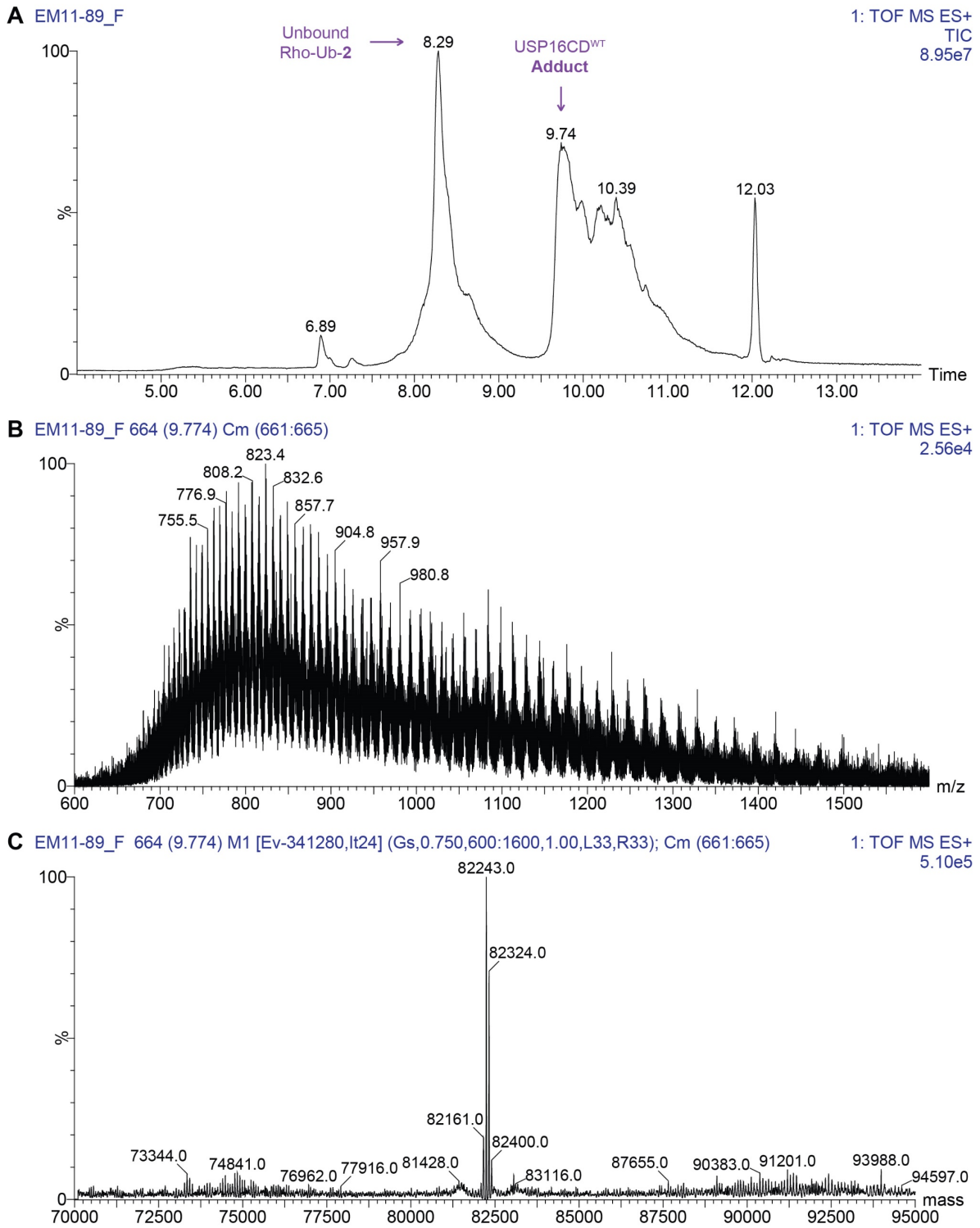


Figure S21. LC-MS data for intact **USP16CD^{WT}** + Rho-Ub-2 related to Figure 3B. **A**) Chromatogram. TIC ($m/z = 200-2500$). **B**) Spectrum of USP16(adduct). **C**) Deconvoluted mass: $82,243 + 82,324$ Da (Found)/ $82,242 + 82,324$ Da (Calc.). Covalent USP16-ABP adduct is detected.

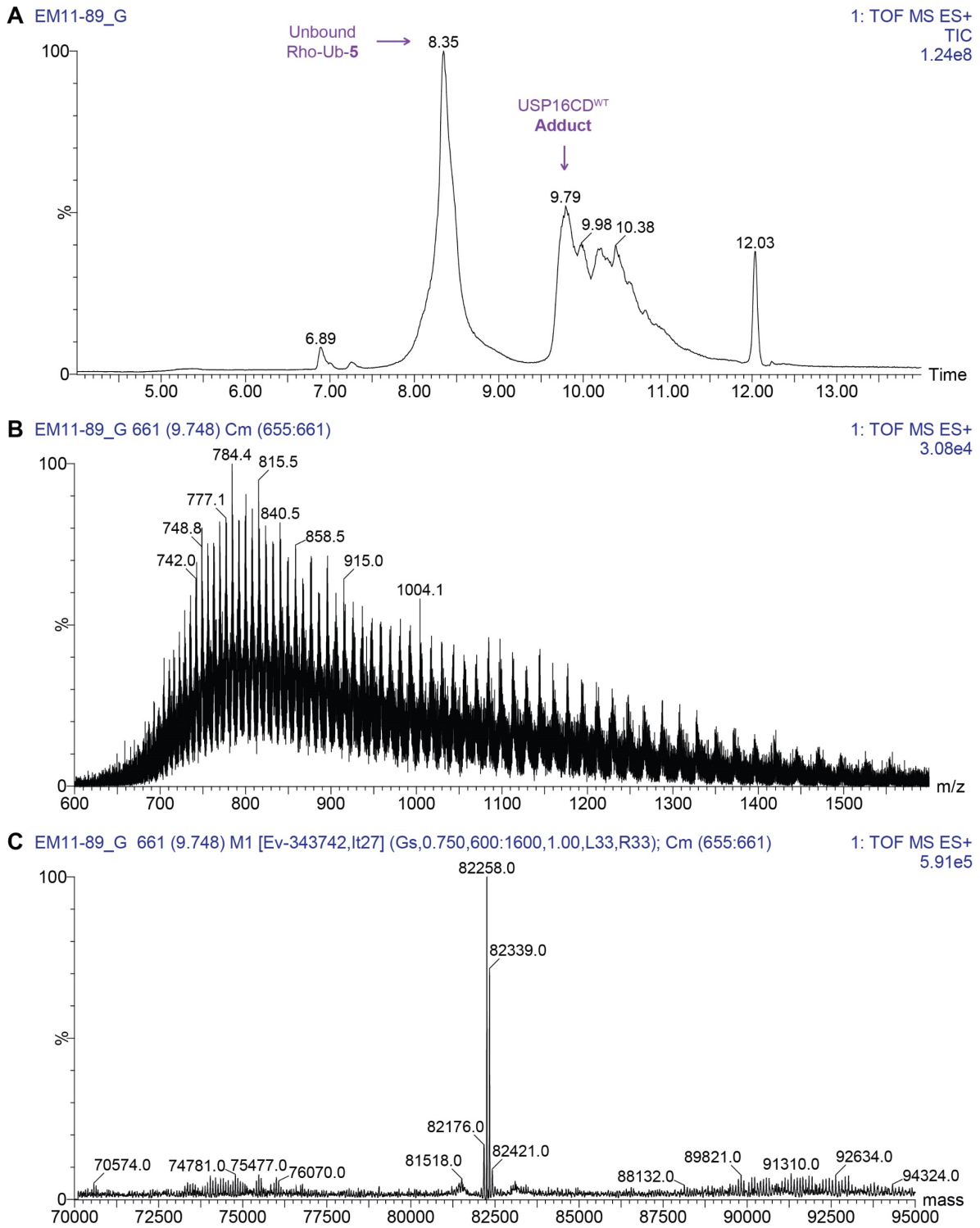
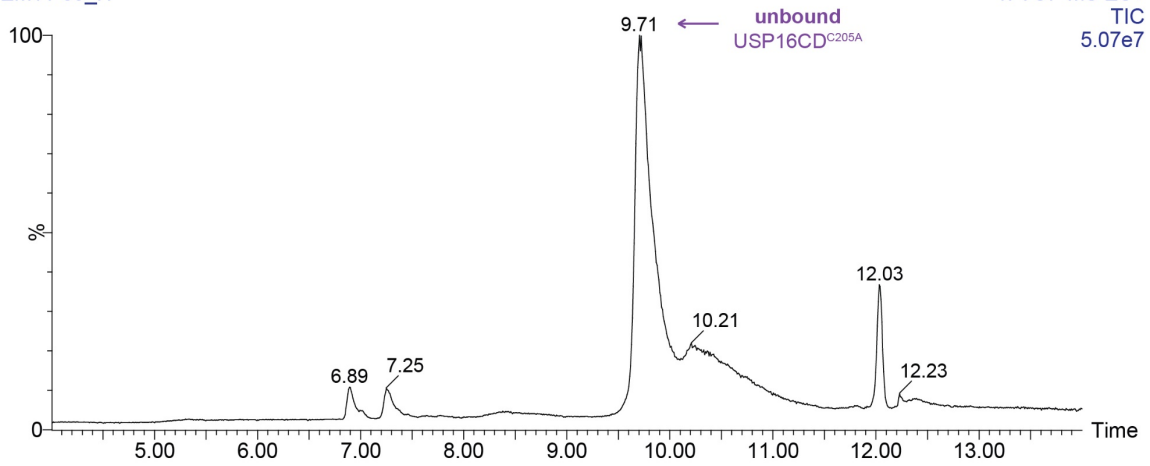
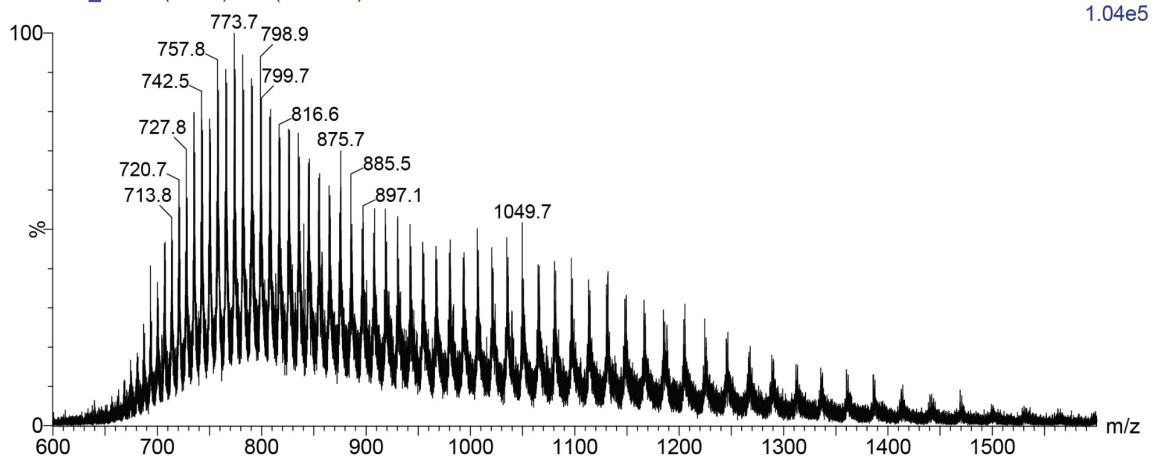


Figure S22. LC-MS data for intact **USP16CD^{WT}** + Rho-Ub-5 related to Figure 3B. **A**) Chromatogram. TIC (m/z = 200-2500). **B**) Spectrum of USP16(adduct). **C**) Deconvoluted mass: 82,258 + 82,339 Da (Found)/82,256 + 82,338 Da (Calc.). Covalent USP16-ABP adduct is detected.

A EM11-89_H



B EM11-89_H 656 (9.705) Cm (649:679)



C EM11-89_H 656 (9.705) M1 [Ev-370698,It31] (Gs,0.750,600:1600,1.00,L33,R33); Cm (649:679)

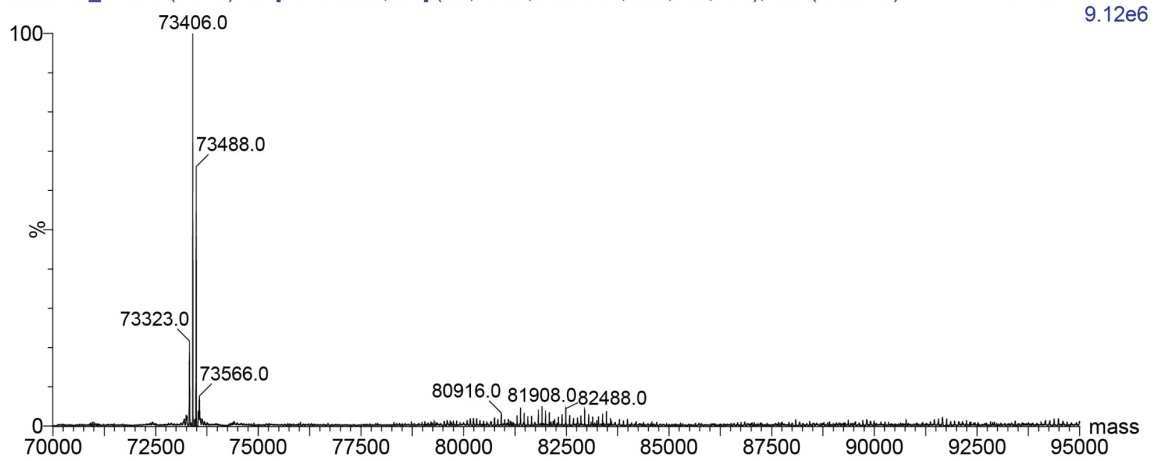


Figure S23. LC-MS data for intact unbound **USP16CD^{C205A}** related to Figure 3C. **A)** Chromatogram. TIC (m/z = 200-2500). **B)** Spectrum of USP16(adduct). **C)** Deconvoluted mass: 73,406 + 73,488 Da (Found).

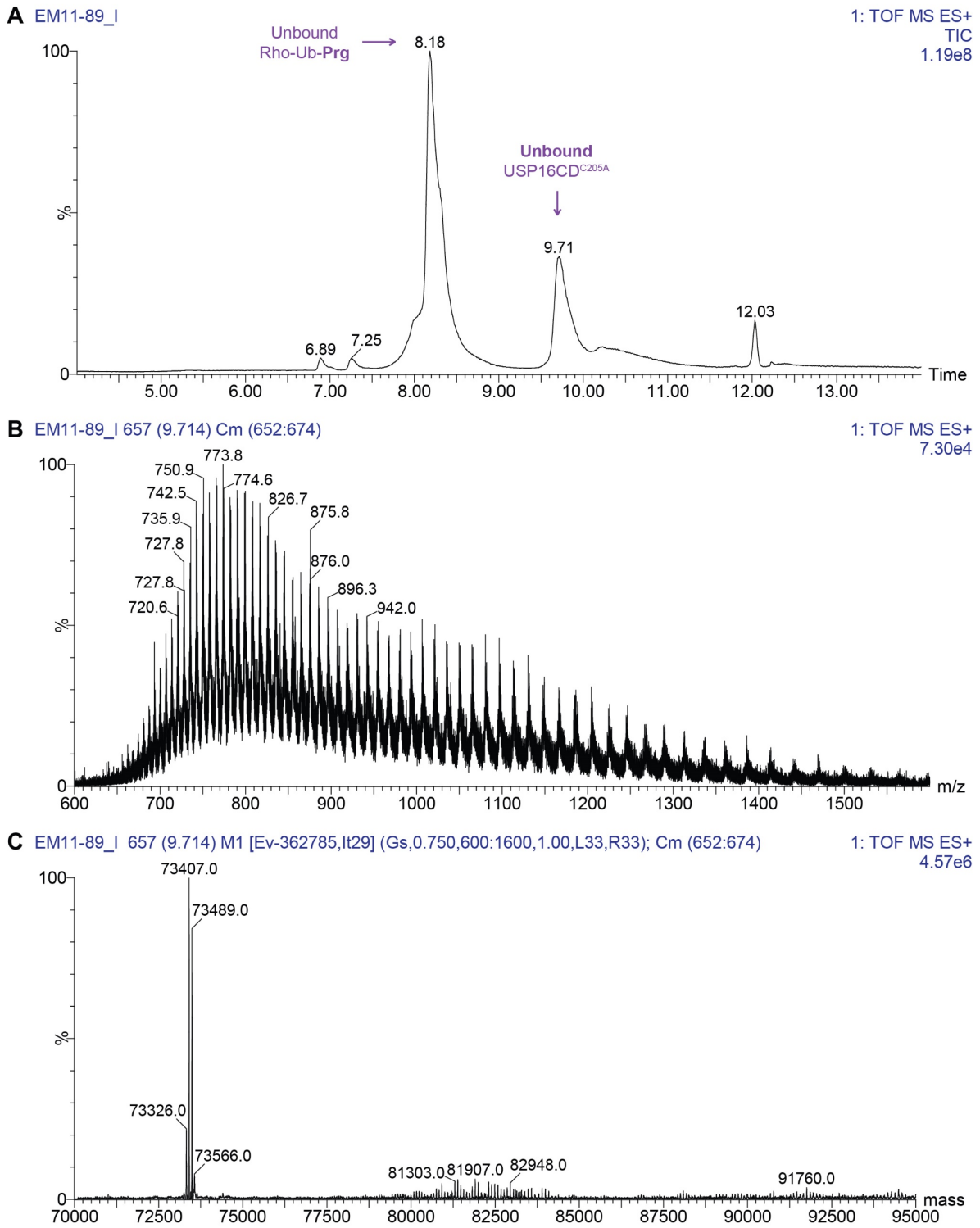


Figure S24. LC-MS data for intact **USP16CD^{C205A}** + Rho-Ub-Prg related to Figure 3C. **A**) Chromatogram. TIC (m/z = 200-2500). **B**) Spectrum of USP16(adduct). **C**) Deconvoluted mass: 73,407 + 73,489 Da (Found)/82,290 + 82,372 Da (Calc.). Covalent USP16-ABP adduct is not detected.

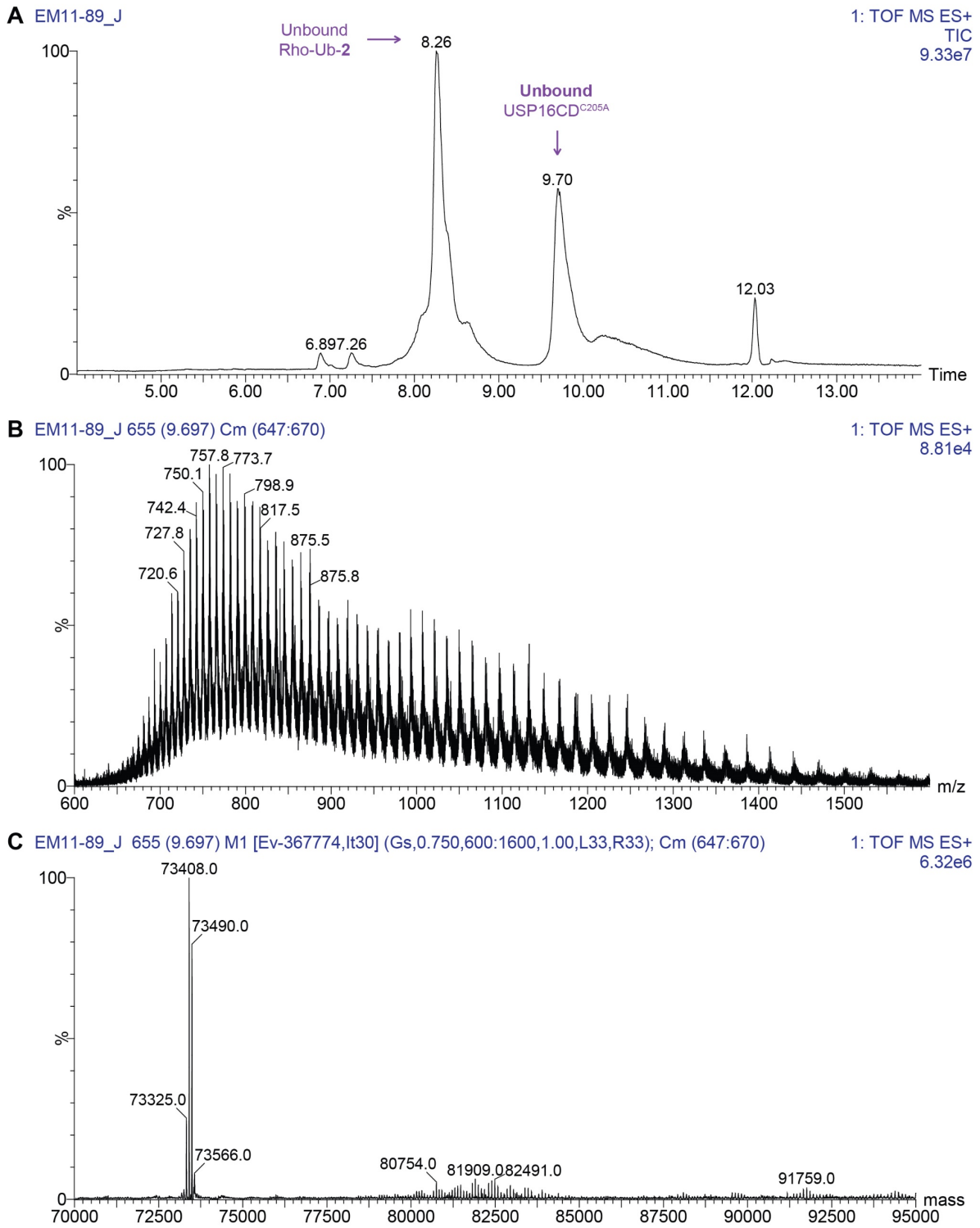


Figure S25. LC-MS data for intact **USP16CD^{C205A}** + Rho-Ub-2 related to Figure 3C. **A**) Chromatogram. TIC ($m/z = 200-2500$). **B**) Spectrum of USP16(adduct). **C**) Deconvoluted mass: 73,408 + 73,490 Da (Found)/82,304 + 82,386 Da (Calc.). Covalent USP16-ABP adduct is not detected.

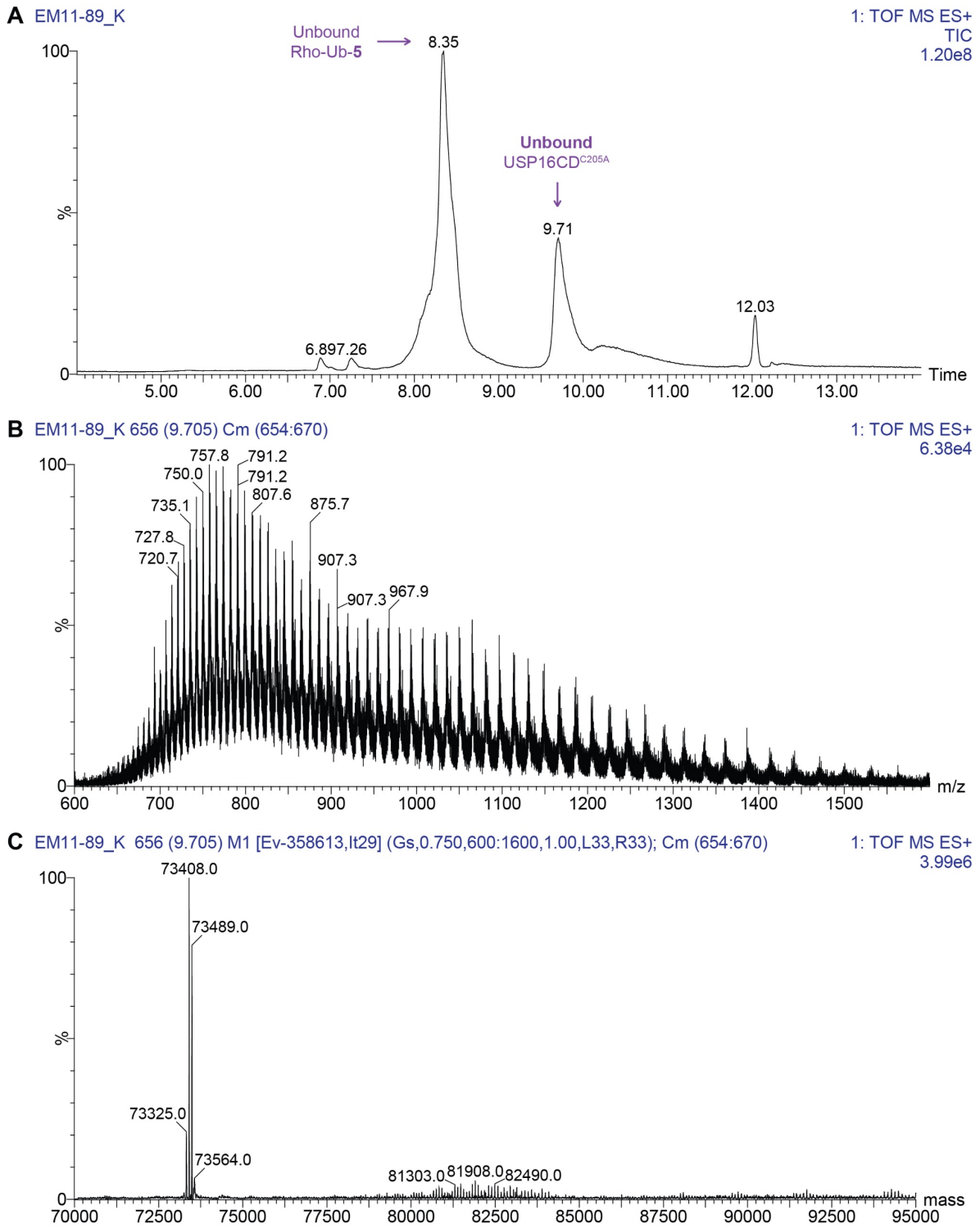


Figure S26. LC-MS data for intact **USP16CD^{C205A}** + Rho-Ub-5 related to Figure 3C. **A**) Chromatogram. TIC ($m/z = 200-2500$). **B**) Spectrum of USP16(adduct). **C**) Deconvoluted mass: 73,408 + 73,489 Da (Found)/82,318 + 82,400 Da (Calc.). Covalent USP16-ABP adduct is not detected.

Bottom-up mass spectrometric analysis of (deuterated) adducts

High-resolution mass spectrometry (HRMS) of unbound Rho-Ub-ABPs.

HRMS measurements of unbound Rho-Ub-Prg and Rho-Ub-[D₂]-Prg were performed to validate that both deuteriums are intact in Rho-Ub-[D₂]-Prg, and the mass difference is 2 Da. The values and isotope pattern for each charge state were in agreement with the calculated values (Table S4 and Figure S27).

Table S4. Calculated and detected m/z of naturally most abundant peak for each charge state.

Rho-Ub-	m/z	z					
		13	12	11	10	9	8
Prg	Calc. ^a	684.2974	741.2384	808.5319	889.2842	987.9816	1111.3534
	(Found)	(684.3000)	(741.2388)	(808.5306)	(889.2878)	(987.9859)	(1111.3591)
[D ₂]-Prg	Calc. ^b	684.4522	741.4059	808.7148	889.4855	988.2053	1111.6050
	(Found)	(684.4553)	(741.4115)	(808.7168)	(889.4891)	(988.2110)	(1111.6116)

^a Isotope model C₄₀₁H₆₄₃N₁₀₇O₁₂₀. ^b Isotope model C₄₀₁H₆₄₁D₂N₁₀₇O₁₂₀ with D = 2.0141017779.

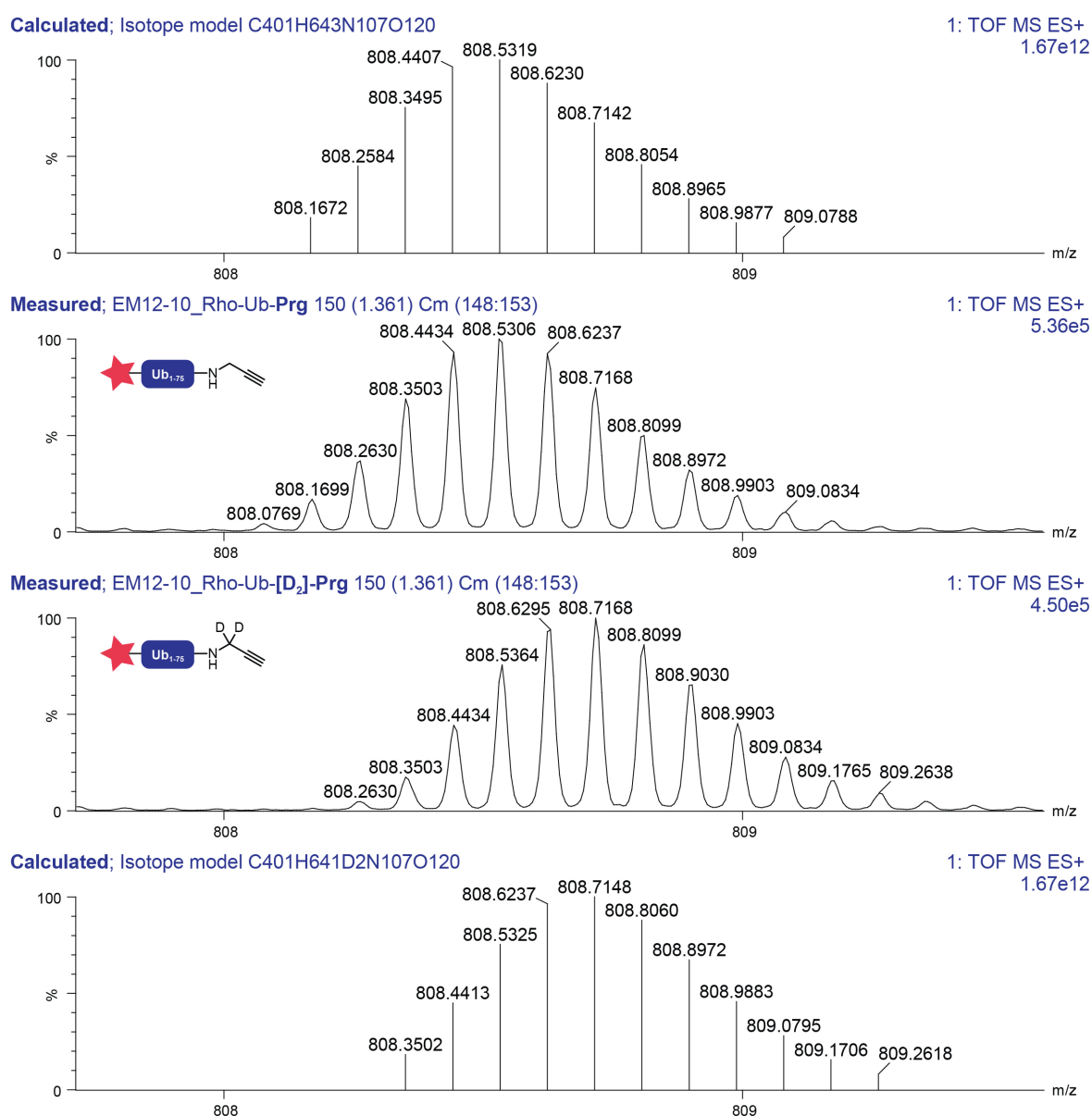


Figure S27. Measured and predicted isotope distribution of charge state z = 11 for high-resolution mass detection of Rho-Ub-Prg (C₄₀₁H₆₄₃N₁₀₇O₁₂₀) and Rho-Ub-[D₂]-Prg (C₄₀₁H₆₄₁D₂N₁₀₇O₁₂₀).

Expected peptides after alkylation and trypsin digestion (bottom-up mass spectrometric analysis)

Sequence **UCHL3^{WT}** (Uniprot; P15374) with underlined peptide containing catalytic residue (**Cys95**) after trypsin digestion;

MEGQRWLPLEANPEVTNQFLKQLGLHPNWQFVDVYGMDELLSMVPRPVCVALLLPITEKYEVFRTEEEEEKIKSQGQDVTSS
VYFMKQTISNACGTIGLIHAIANNKDKMHFESGSLTKKFLEESVMSPEERARYLENYDAIRVTHETSAHEGQTEAPSIDEKVDL
HFIALVHVDGHLIELDGRKPPFINHGETSDETLLEDAIEVCKKFMERDPDELRFNAIALSAA

Sequence **USP16CD^{WT}** (Uniprot; Q9Y5T5) with underlined peptide containing catalytic residue (**Cys205**) after trypsin digestion;

MAHHHHHHSAALEVLFGQPKGLSNLGNTCFFNAVMQNLSQTPVLRRELLKEVKMSGTIVKIEPPDLALTEPLEINLEPPGPLTLA
MSQFLNEMQETKKGVVTPKELFSQVCKKAVRFKGYQQQDSQELRLYLLDGMRAEEHQRVSKGILKAFGNSTEKLDDEELKNKVK
DYEKKKSMPFVDRIFGGELTSMIMCDQCRTVSLVHESFLDLSLPVDDQSGKKSVDKLNKKTVEDEDQDSEEEKDNDYSIKE
RSDIPSGTSKHLQKKAKKQAKKQAKNQRQQKIQGVVHLLNDICTIDHPEDSDNEAEMSLQGEVNIKSNIHSQEGVMHKEYCV
NQKDLNGQAKMIESVTDNQKSTEEVDMKNINMDNDLEVLTSPTRNNGAYLTEGSNGEVDISNGFKNLNLNAAALHPDEINI
EILNDSHTPGTKVYEVVNEDEPETAFCTLANREVFNTDECSIQHCLYQFTRNEKLRDANKLLCEVCTRRQCNGPKANIKGERKHVY
TNAKKQMLISLAPPVLTLLHLKRFQQAGFNLRKVNKHIFPEILDLPFCTLKCKNVAEENTRVLYSLYGVVEHSGTMRSGHYTAY
AKARTANSHLSNLVHLGDIPQDFEMESKGQWFHISDTHVQAVPTTKVLNSQAYLLFYERIL

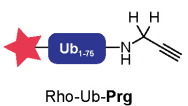
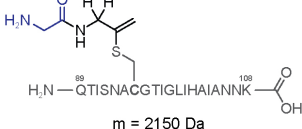
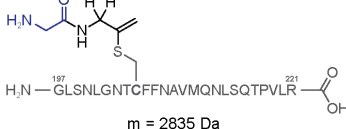
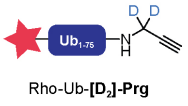
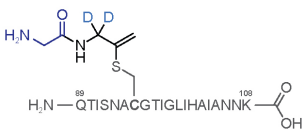
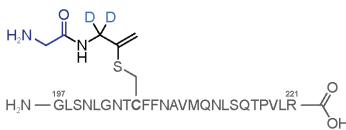
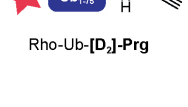
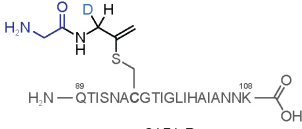
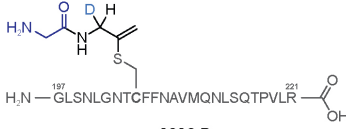
ABP	Mechanism	Adduct	UCHL3	USP16
 <p>Rho-Ub-Prg</p>	B, C, D	<i>HH-Prg</i> (+112.06366 Da)	 <p>m = 2150 Da</p>	 <p>m = 2835 Da</p>
 <p>Rho-Ub-[D₂]-Prg</p>	B, D	<i>DD-Prg</i> (+114.07622 Da)	 <p>m = 2152 Da</p>	 <p>m = 2837 Da</p>
 <p>Rho-Ub-[D₂]-Prg</p>	C	<i>DH-Prg</i> (+113.06994 Da)	 <p>m = 2151 Da</p>	 <p>m = 2836 Da</p>

Figure S28. Expected mass of peptides (no missed cleavage or oxidation) in bottom-up mass spectrometric analysis of DUB adducts with Rho-Ub-Prg and Rho-Ub-[D₂]-Prg after alkylation and trypsin digestion related to Figure 4.

Detected peptides after alkylation and trypsin digestion (bottom-up mass spectrometric analysis)

Bottom-up mass spectrometric analysis as presented in Figure 4. Detected tryptic peptides are listed in Table S5, detected fragment ions with UCHL3 can be found in Table S6. Peptides with DH-Prg (113.06994 Da) modification were not found for UCHL3/USP16 adducts with Rho-Ub-[D₂]-Prg. Full MS and MS2 spectra are provided in Figure S29 and Figure S30.

Table S5. Tryptic peptides identified with Mascot (v1.36) after alkylation and trypsin digestion of covalent adducts of Rho-Ub-ABPs with recombinant UCHL3 or USP16.*

<i>ABP adduct</i>	UCHL3 ^{WT}		USP16CD ^{WT}	
	Rho-Ub-Prg	Rho-Ub-[D ₂]-Prg	Rho-Ub-Prg	Rho-Ub-[D ₂]-Prg
<i>Peptide sequence</i>	QTISNACGTIGLIHAIANNK, C7-HH-Prg (112.06366 Da)	QTISNACGTIGLIHAIANNK, C7-DD-Prg (114.07622 Da)	GLSNLGNTCFFNAVMQNLSQTPVLR, M15-Oxidation (15.99492 Da), C9-HH-Prg (112.06366 Da)	GLSNLGNTCFFNAVMQNLSQTPVLR, M15-Oxidation (15.99492 Da), C9-DD-Prg (114.07622 Da)
<i>Charge</i>	+3	+3	+3	+3
<i>Monoisotopic m/z</i>	717.71631 Da (+0.16 mmu/+0.22 ppm)	718.38696 Da (-0.04 mmu/-0.05 ppm)	951.47675 Da (-0.84 mmu/-0.88 ppm)	952.14832 Da (-0.12 mmu/-0.12 ppm)
<i>MH⁺</i>	2151.13437 Da	2153.14634 Da	2852.41568 Da	2854.43039 Da
<i>R_T</i>	32.4201 min	32.5055 min	41.8239 min	41.9013 min
<i>Ions score</i>	88	60	62	71
<i>Percolator q-Value</i>	8.9e-4	1.4e-3	9.1e-4	9.6e-4
<i>Percolator PEP</i>	7.4e-6	2.4e-4	5.8e-5	2.1e-4
<i>Ions matched by search engine</i>	12/204	11/204	9/270	9/270
<i>Fragment match tolerance used for search</i>	20 mmu	20 mmu	20 mmu	20 mmu

* bottom-up mass spectrometric analysis related to Figure 4, Figure S28, Figure S29 and Figure S30. Peptides with DH-Prg (113.06994 Da) modification were not found for DUB adducts with Rho-Ub-[D₂]-Prg.

Table S6. Expected and detected fragment ions of UCHL3 peptide QTISNACGTIGLIHAIANNK modified with Gly-HH-Prg (m/z = 717.716³⁺) or Gly-DD-Prg (m/z = 718.387³⁺).*

b#	b-H ₂ O ⁺		b-NH ₃ ⁺		Seq.	y ⁺		y ²⁺		y#
	[H ₂]-Prg	[D ₂]-Prg	[H ₂]-Prg	[D ₂]-Prg		[H ₂]-Prg	[D ₂]-Prg	[H ₂]-Prg	[D ₂]-Prg	
1			112.03930	112.03930	Q					20
2	212.10297	212.10297	213.08698	213.08698	T	2023.07532	2025.08787	1012.04130	1013.04757	19
3	325.18703	325.18703	326.17105	326.17105	I	1922.02764	1924.04019	961.51746	962.52374	18
4	412.21906	412.21906	413.20308	413.20308	S	1808.94358	1810.95613	904.97543	905.98170	17
5	526.26199	526.26199	527.24600	527.24600	N	1721.91155	1723.92410	861.45941	862.46569	16
6	597.29910	597.29910	598.28312	598.28312	A	1607.86862	1609.88117	804.43795	805.44423	15
7	812.37195	814.38450	813.35596	815.36852	C	1536.83151	1538.84406	768.91939	769.92567	14
8	869.39341	871.40597	870.37743	972.38998	G	1321.75866	1321.75866	661.38297	661.38297	13
9	970.44109	972.45364	971.42511	973.43766	T	1264.73720	1264.73720	632.87224	632.87224	12
10	1083.55252	1085.53771	1084.50917	1086.52172	I	1163.68952	1163.68952	582.34840	582.34840	11
11	1140.54662	1142.55917	1141.53063	1143.54319	G	1050.60545	1050.60545	525.80637	525.80637	10
12	1253.63068	1255.64324	1254.61470	1256.62725	L	993.58399	993.58399	497.29563	497.29563	9
13	1366.71475	1368.72730	1367.69876	1369.71131	I	880.49993	880.49993	440.75360	440.75360	8
14	1503.77366	1505.78621	1504.75767	1506.77023	H	767.41586	767.41586	384.21157	384.21157	7
15	1574.81077	1576.82332	1575.79479	1577.80734	A	630.35695	630.35695	315.68211	315.68211	6
16	1687.89484	1689.90739	1688.87885	1690.89140	I	559.31984	559.31984	280.16356	280.16356	5
17	1758.93195	1760.94450	1759.91597	1761.92852	A	446.23577	446.23577	223.62152	223.62152	4
18	1872.97488	1874.98743	1873.95889	1875.97145	N	375.19866	375.19866	188.10297	188.10297	3
19	1987.01780	1989.03036	1988.00182	1990.01437	N	261.15573	261.15573	131.08150	131.08150	2
20					K	147.11280	147.11280	74.06004	74.06004	1

* related to bottom-up mass spectrometric analysis shown in Figure 5D. Tandem MS analysis for modified QTISNAC*GTIGLIHAIANNK peptide obtained by alkylation and trypsin digestion of covalent UCHL3 adduct with Rho-Ub-**Prg** or Rho-Ub-**[D₂]-Prg**. **Green** = detected fragment ions without modification. **Blue** = detected fragment ions with modified cysteine residue. **Bold** = fragment ion detected in both samples. Details on expected and detected peptides can be found in Figure S28, Figure S29 and Table S5.

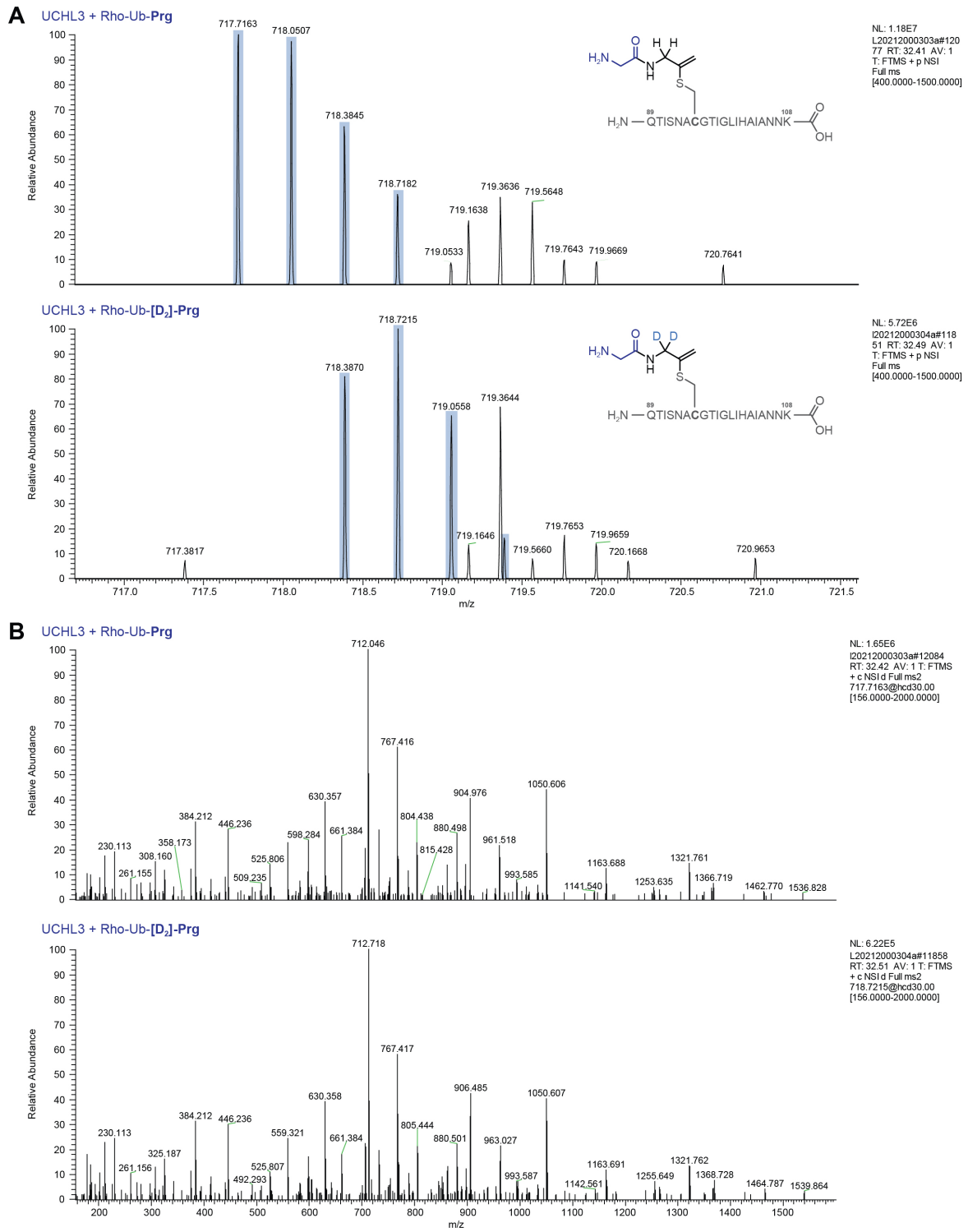


Figure S29. Bottom-up mass spectrometric analysis of UCHL3 adducts with Rho-Ub-Prg and Rho-Ub-[D₂]-Prg related to Figure 4B-D. **A**) Full MS spectrum of QTISNACGTIGLIHAIANNK peptide modified with Gly-HH-Prg (top) or Gly-DD-Prg (bottom). Relevant signals are highlighted in blue. **B**) Full MS2 spectrum of modified peptide highlighted in A. Relevant expected and detected fragment ions are listed in Table S6.

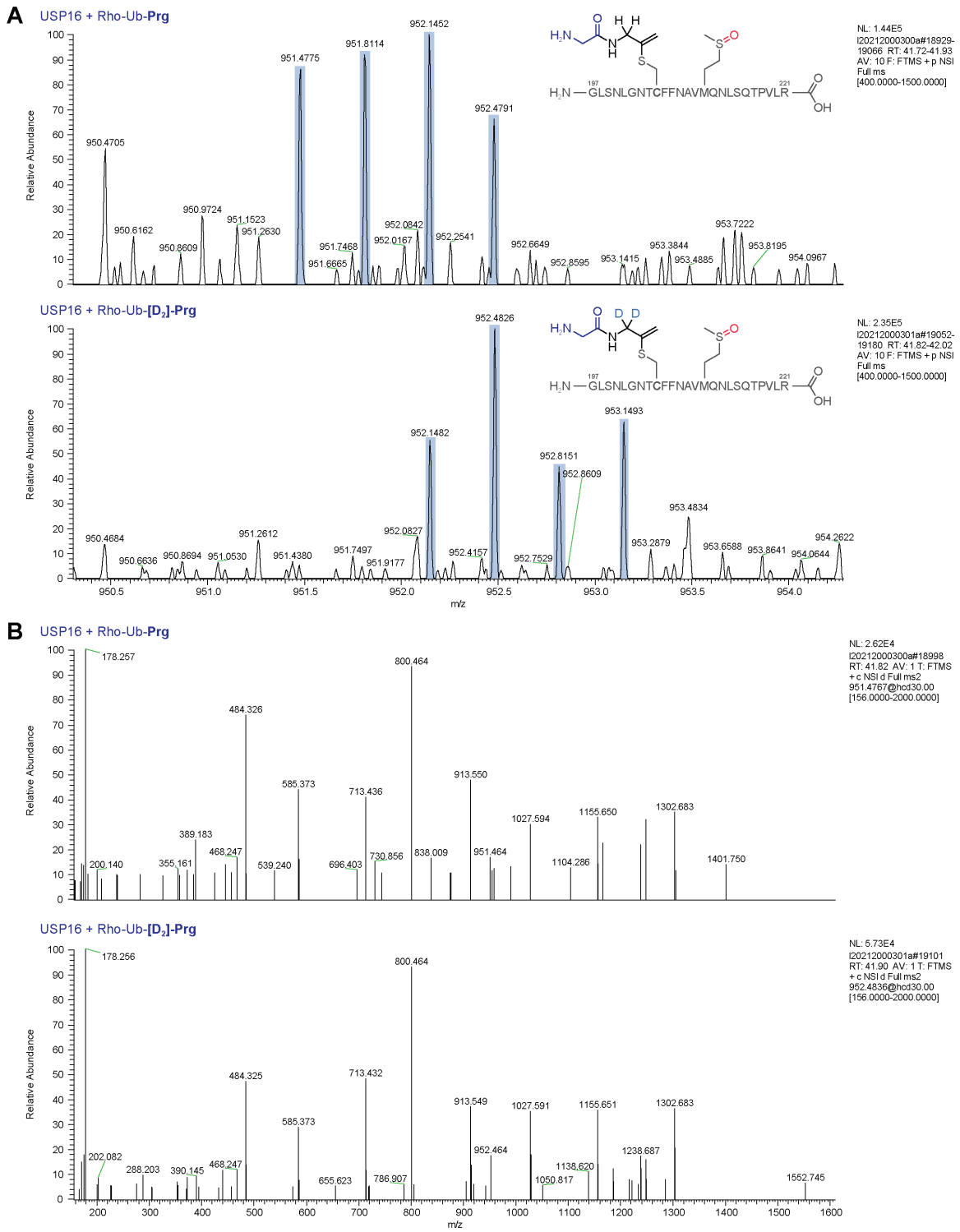


Figure S30. Bottom-up mass spectrometric analysis of USP16 adducts with Rho-Ub-Prg and Rho-Ub-[D₂]-Prg related to Figure 4B. **A**) Full MS of GLSNLGNTCCFFNAVM(ox)QNLSQTPVLR peptide modified with Gly-HH-Prg (top) or Gly-DD-Prg (bottom). Relevant signals are highlighted in blue. **B**) Full MS2 spectrum of modified peptide highlighted in A.

Thiol reactivity assay

The reaction mixture was submitted to LC-MS analysis. The mass difference of unbound ABP and GSH-adduct was clearly detected, but it was not possible to separate the unbound ABP from the GSH-adduct on the LC-MS for quantification. Instead quantification was performed based on the intensity of the naturally most abundant peak for the most common charge states ($z = 7-13$) in the ionization envelope of ubiquitin (Table S7), as is more often used for quantification in top- and middle-down mass spectrometry of ubiquitin.⁵²⁻⁵³

Adduct formation with biological thiols such as cysteine and glutathione (GSH) is an established method to assess intrinsic chemical reactivity of electrophilic warheads towards thiols.⁵⁴ In general the rate of adduct formation with GSH is much slower than adduct formation with catalytic cysteine residues; half-life for adduct formation with 5 mM GSH is in the multiple-hour range, whereas adduct formation with catalytic cysteines can be finished within minutes at the same ABP concentration (10 μ M). Most warheads used in activity-based probes and covalent inhibitors show a certain level of thiol reactivity, unactivated alkynes are unique in their ability to achieve reaction completion with targeted DUBs within minutes while not showing any detectable adduct with untargeted thiols.

Table S7. Adduct formation after incubation with 5 mM GSH for 24 hours.*

ABP	<i>t</i> (h)	Calculations		TIC ^b			
		% GSH adduct ^a	% degraded	unbound	adduct	degraded/hydrolyzed	total
Rho-Ub-Prg	0	0%	0%	10892	0	0	1.09E+04
	24		0%	10698	0	0	1.07E+04
Rho-Ub-2	0	0%	0%	8796	0	0	8.80E+03
	24		0%	8009	0	0	8.01E+03
Rho-Ub-3	0	0%	60%	2857	0	4214	7.07E+03
	24		65%	1740	0	3162	4.90E+03
Rho-Ub-4	0	0%	0%	11060	0	0	1.11E+04
	24		0%	9627	0	0	9.63E+03
Rho-Ub-7	0	0%	0%	11534	0	0	1.15E+04
	24		0%	7602	0	0	7.60E+03
Rho-Ub-5	0	0%	0%	11433	0	0	1.14E+04
	24		0%	10768	0	0	1.08E+04
Rho-Ub-8	0	0%	0%	13157	0	0	1.32E+04
	24		0%	11345	0	0	1.13E+04
Rho-Ub-9	0	0%	0%	14167	0	0	1.42E+04
	24		0%	11973	0	0	1.20E+04
Rho-Ub-10	0	0%	0%	14255	0	0	1.43E+04
	24		0%	13938	0	0	1.39E+04
Rho-Ub-Prp	0	0%	0%	15452	0	0	1.55E+04
	24		0%	13570	0	0	1.36E+04
Rho-Ub-18	0	70%	0%	2280	0	0	2.28E+03
	24		0%	547	1305	0	1.85E+03
Rho-Ub-VME	0	80%	0%	12675	0	0	1.27E+04
	24		0%	2737	11041	0	1.38E+04

* related to Figure S4C. ^a GSH adduct detected after incubation of 10 μ M Rho-Ub-ABP with 5 mM GSH in PBS pH7.4 for 24 hrs. Equation; % GSH adduct = 100%*(TIC adduct)/(total TIC). ^b Sum of naturally most abundant peak for charge states $z = 7-13$. m/z values used for quantification are reported in Table S8.

Table S8. m/z values of each charge state used for quantification of unbound ABP and GSH adduct.*

ABP	State ^a	M (Da)	m/z ^b						
			z = 13	z = 12	z = 11	z = 10	z = 9	z = 8	z = 7
Rho-Ub-Prg	A	8883	684.2	741.2	808.5	889.2	987.9	1111.3	1270.0
	B	9190	707.9	766.8	836.5	920.0	1022.1	1149.8	1313.9
	C	8901	685.7	742.8	810.2	891.1	990.0	1113.6	1272.6
Rho-Ub-2	A	8897	685.4	742.3	809.7	890.6	989.4	1113.0	1271.9
	B	9204	709.0	768.0	837.7	921.4	1023.7	1151.5	1315.9
	C	8915	686.8	743.9	811.5	892.5	991.6	1115.4	1274.6
Rho-Ub-3	A	8959	690.1	747.5	815.4	896.8	996.3	1120.9	1280.7
	B	9266	713.8	773.2	843.4	927.6	1030.6	1159.3	1324.7
	C	8977	691.5	749.0	817.0	898.7	998.4	1123.1	1283.3
Rho-Ub-4	A	8897	685.3	742.4	809.7	890.6	989.5	1113.0	1271.9
	B	9204	709.0	768.0	837.7	921.4	1023.7	1151.5	1315.9
	C	8915	686.8	743.9	811.5	892.5	991.6	1115.4	1274.6
Rho-Ub-7	A	8959	690.1	747.5	815.3	896.8	996.4	1120.8	1280.7
	B	9266	713.8	773.2	843.4	927.6	1030.6	1159.3	1324.7
	C	8977	691.5	749.1	817.1	898.7	998.4	1123.1	1283.4
Rho-Ub-5	A	8912	686.4	743.5	811.0	892.0	991.0	1114.9	1273.9
	B	9219	710.2	769.3	839.1	922.9	1025.3	1153.4	1318.0
	C	8930	687.9	745.2	812.8	894.0	993.2	1117.3	1276.7
Rho-Ub-8	A	8951	689.4	746.8	814.6	896.0	995.5	1119.7	1279.7
	B	9258	713.2	772.5	842.6	926.8	1029.7	1158.3	1323.6
	C	8969	690.9	748.4	816.4	897.9	997.6	1122.1	1282.3
Rho-Ub-9	A	8897	685.3	742.3	809.6	890.5	989.5	1113.1	1271.9
	B	9204	709.0	768.0	837.7	921.4	1023.7	1151.5	1315.9
	C	8915	686.8	743.9	811.5	892.5	991.6	1115.4	1274.6
Rho-Ub-10	A	8897	685.3	742.3	809.7	890.5	989.4	1113.0	1271.9
	B	9204	709.0	768.0	837.7	921.4	1023.7	1151.5	1315.9
	C	8915	686.8	743.9	811.5	892.5	991.6	1115.4	1274.6
Rho-Ub-Prp	A	8887	684.5	741.4	808.8	889.6	988.3	1111.8	1270.4
	B	9194	708.2	767.2	836.8	920.4	1022.6	1150.3	1314.4
	C	8905	686.0	743.1	810.5	891.5	990.4	1114.1	1273.1
Rho-Ub-18	A	8951	689.5	746.9	814.6	896.0	995.5	1119.8	1279.7
	B	9258	713.1	772.5	842.5	926.8	1029.5	1158.2	1323.4
	C	8969	690.9	748.4	816.4	897.9	997.6	1122.1	1282.3
Rho-Ub-VME	A	8943	688.8	746.2	813.9	895.2	994.5	1118.7	1278.5
	B	9250	712.5	771.8	841.8	926.0	1028.7	1157.2	1322.4
	C	8961	690.3	747.8	815.6	897.1	996.7	1121.1	1281.1

* related to Figure S4C and Table S7. Detection of Rho-Ub-ABP and derivatives by LC-MS in ES+ mode; m/z = (M+zH⁺)/z. ^a A = unreacted/unmodified ABP. B = ABP-GSH adduct (+302). C = hydrolyzed (+18) or otherwise degraded ABP. ^b Values in *italics* are expected/calculated values, not detected.

Materials and Methods; ABP Synthesis

General. Solvents and reagents for (peptide) synthesis were purchased from various suppliers (listed in Table S9) and are used as received. Linear solid phase synthesis of Ub was performed according to established method reported by our group.¹ Data processing of LC-MS analysis was performed using Waters MassLynx Mass Spectrometry Software V4.2. Deconvoluted mass was obtained from the electrospray ionization mass spectrum envelope (average isotopes) with the MaxEnt1 function. The calculated mass of Ub (derivatives) is obtained with ChemDraw Professional 16.0.1.4 (PerkinElmer Informatics, Inc.) by calculating the molecular weight of the complete structure.

General method; Trial Cleavage and LC-MS analysis of reaction progress

A small sample is incubated with Trial Cleavage Mix (92.5:2.5:2.5:2.5 TFA/water/*i*Pr₃SiH/DODt) for 30 minutes at 38 °C under gentle agitation. Resin-bound samples are then transferred to a filter tip and filtered prior to continuation. The reaction mixture or filtrate is treated with cold 1:1 Et₂O/pentane (v/v) to precipitate the product, centrifuged and the soluble material is removed by suction. The precipitate is washed twice with cold Et₂O, and remaining Et₂O is removed by submitting to a gentle air flow. The solid material is dissolved in DMSO, and reaction progress is analyzed by LC-MS. LC-MS analysis of crude reaction mixtures and purification fractions was performed on a Waters Alliance 2795 Separation Module system equipped with Waters 2996 Photodiode Array Detector (λ = 190-750 nm), Waters Xbridge C18 column (130 Å, 3.5 μ m, 2.1 x 30 mm) and LCT Premier Orthogonal Acceleration Time of Flight Mass Spectrometer (*m/z* = 300-2000). Samples were run with a 3 minute gradient (run time 6 min) using two mobile phases; 1% MeCN + 0.1% FA in water and 1% water + 0.1% FA in MeCN (flow rate = 0.8 mL/min).

Time (min)	1% water + 0.1% FA in MeCN (%)	1% MeCN + 0.1% FA in water (%)
0:00	5.0	95.0
0.20	5.0	95.0
3:20	95.0	5.0
4.20	95.0	5.0
4.40	5.0	95.0
6.20	5.0	95.0

General method; LC-MS analysis of purified ABPs

Stock solutions of pure ABP (500 μ M in DMSO) were diluted 100-fold in 0.1% FA in water, and 10 μ L was injected for LC-MS analysis. LC-MS analysis of pure ABPs was performed on a Waters ACQUITY UPLC H-class System equipped with Waters ACQUITY Quaternary Solvent Manager (QSM), Waters ACQUITY UPLC Photodiode Array (PDA) e λ Detector (λ = 210-800 nm), Waters ACQUITY UPLC Protein BEH C4 Column (300 Å, 1.7 μ m, 2.1 x 50 mm) and LCT Premier Orthogonal Acceleration Time of Flight Mass Spectrometer (*m/z* = 100-1600) in ES+ mode. Samples were run with a 7 minute gradient (run time 10 min) using three mobile phases detailed below (flow rate = 0.5 mL/min).

Time (min)	Water (%)	MeCN (%)	2.5% FA in water/MeCN (%)
0:00	94.0	2.0	4.0
0.50	94.0	2.0	4.0
7.50	0.0	96.0	4.0
8.00	0.0	96.0	4.0
8.10	94.0	2.0	4.0
10.00	94.0	2.0	4.0

Table S9. Building blocks, reagents and solvents for ABP synthesis.*

Compound	Abbreviation	CAS#	Source or reference
Building blocks			
Fmoc Gly TentaGel® R Trt resin	Gly-Trt	-	Rapp Polymere GmbH, #RA1213
3',6'-bis((<i>tert</i> -butoxycarbonyl)amino)-3-oxo-3 <i>H</i> -spiro[isobenzofuran-1,9'-xanthene]-5-carboxylic acid	(Boc) ₂ Rho-OH 11	-	In-house synthesis ⁵⁵
Propargylamine	Prg	2450-71-7	SigmaAldrich, #P50900
1-Amino-2-butyne hydrochloride	2	50329-23-2	In-house synthesis ⁵⁶
3-Phenylprop-2-yn-1-amine hydrochloride	3	30011-36-0	Enamine, #EN300-26681
1-Methyl-prop-2-ynylamine hydrochloride	4	30389-17-4	Chem-Impex, #18527
1-Phenylprop-2-yn-1-amine hydrochloride	7	157022-35-0	Enamine, #EN300-190354
2-Methyl-3-butyn-2-amine	5	2978-58-7	SigmaAldrich, #687189
1-Ethynylcyclohexylamine	8	30389-18-5	SigmaAldrich, #177024
1-Amino-3-butyne	9	14044-63-4	SigmaAldrich, #715190
<i>N</i> -Methylpropargylamine	10	35161-71-8	SigmaAldrich, #150223
Propylamine	Prp	107-10-8	Fluka Analytical, #82100
Prop-2-yn-1,1- <i>d</i> ₂ -1-amine hydrochloride	[D₂]-Prg	-	In-house synthesis, <i>this work</i>
4,4,4-Trifluorobut-2-yn-1-amine hydrochloride	18	-	In-house synthesis, <i>this work</i>
Methyl (<i>E</i>)-4-aminobut-2-enoate hydrochloride	VME	141973-57-1	In-house synthesis ⁵⁷
Reagents			
(Benzotriazol-1-yloxy)tripyrrolidino-phosphonium hexafluorophosphate)	PyBOP	128625-52-5	SigmaAldrich, #851009
<i>N,N</i> -Diisopropylethylamine	DIPEA	7087-68-5	Biosolve, #041533
1,1,1,3,3,3-hexafluoroisopropylalcohol	HFIP	920-66-1	Chem-Impex, #00080
Piperidine	-	110-89-4	Biosolve, #16183301
Triisopropylsilane	<i>i</i> Pr ₃ SiH	6485-79-6	SigmaAldrich, #233781
2,2'-(Ethylenedioxy)diethanethiol	DODt	14970-87-7	SigmaAldrich, #465178
Phenol	PhOH	108-95-2	SigmaAldrich, #328111
Trifluoroacetic acid	TFA	76-05-1	Biosolve, #20233320
Formic acid	FA	64-18-6	SigmaAldrich, #33015
Solvents			
<i>N</i> -Methyl-pyrrolidone	NMP	872-50-4	Biosolve, #13563202
1,2-Dichloroethane	DCE	107-06-2	Acros Organics, #406820025
Diethyl ether	Et ₂ O	60-29-7	Biosolve, #5280501
<i>n</i> -Pentane	Pentane	109-66-0	Biosolve, #16050502
Dimethyl sulfoxide	DMSO	67-68-5	Biosolve, #4470501
Dichloromethane	DCM	75-09-2	Biosolve, #13790502
<i>N,N</i> -Dimethylformamide	DMF	68-12-2	Biosolve, #4190501
Acetonitrile	MeCN	75-05-8	Biosolve, #012013

* Peptide building blocks are listed in Table S10 (SI-53).

Step I. SPPS

Ubiquitin Δ G on trityl-resin was prepared by linear solid phase peptide synthesis on a Syro II Automated Peptide Synthesizer (MultiSynTech GmbH, Germany) as described previously.¹ Briefly, Glycine-loaded trityl resin (Rapp Polymere, Germany, #RA1213) was incubated twice for 25 minutes with Fmoc-protected amino acids (4 eq.), DIPEA (8 eq.) and PyBOP (4 eq.) in NMP, followed by Fmoc removal by incubating three times for 2 minutes with 20% piperidine/NMP (v/v). This procedure was repeated for each amino acid coupling cycle, with a total of 68 cycles. Details on acid-labile side chain protecting groups (PG) and coupling of Fmoc-protected (di)peptide building blocks are provided in Table S10 (SI-53).

Step II. Rhodamine coupling

Rhodamine coupling to the N-terminus was performed as described previously.⁵⁵ Briefly, (Boc)₂Rho-OH **11** (4 eq.), PyBOP (4 eq.) and DIPEA (8 eq.) were dissolved in NMP, and the preactivated mixture was added to NH₂-Ub₁₋₇₅(PG)-resin (1 eq.), and incubated overnight. The resin was washed with NMP and DCM, after which trial cleavage was performed to evaluate reaction progress. The resin-bound material was either resubmitted to reach reaction completion or used in the next step.

Step III. Cleavage from resin

Resin cleavage was performed as described previously.¹ Briefly, (Boc)₂Rho-Ub₁₋₇₅(PG)-resin was washed with DCM to remove all NMP, and then twice incubated for 30 minutes at room temperature with 20% HFIP/DCM (v/v). The combined filtrate was collected, and the solvent was removed by rotary evaporation. Residual HFIP was removed by co-evaporation 2-3 times with DCE (to prevent formation of HFIP ester in next steps) and dried to use in the next step.

Step IV. Amine coupling

Amine coupling was performed as described previously.¹ Briefly, (Boc)₂Rho-Ub₁₋₇₅(PG)-OH was dissolved in DCM or DMF, and incubated overnight with amine (4 eq.), DIPEA (8 eq.) and PyBOP (4 eq.). DCM was removed by rotary evaporation or N₂ (g) shower. DMF was removed by dilution of the reaction mixture in MeCN/water (1:1) and subsequently lyophilized. Trial cleavage was performed to evaluate reaction progress by LC-MS. The residue was either resubmitted to coupling conditions until reaction completion was reached or submitted to global deprotection conditions.

Step V. Global deprotection

Global deprotection was performed as described previously.⁵ Briefly, (Boc)₂Rho-Ub₁₋₇₅(PG)-warhead was incubated for 2.5-3 hours with freshly prepared Cleavemix (90:5:2.5:2.5 TFA/water/*i*Pr₃SiH/PhOH) under gentle agitation at room temperature to remove protecting groups from all amino acid sidechains. Then cold 3:1 Et₂O/pentane (v/v) was added to precipitate the product. The reaction mixture was spun down in the centrifuge (2000 rpm, 5 minutes, 4 °C), supernatant was removed, and the pellet was washed twice with cold Et₂O. The remaining solvent was removed by a N₂ shower. The solid crude material was dissolved in DMSO and carefully diluted 10-fold in (warm) water (containing 0.05% TFA if required), filtered and submitted to preparative RP-HPLC purification. LC-MS analysis of purified ABPs was conducted according to General Method described above.

RP-HPLC purification

Method A. RP-HPLC purifications (max. 0.5 mL/run) were performed on a Waters AutoPurification HPLC/MS System equipped with a 2767 Sample Manager, 2545 Binary Gradient Module, two 515 HPLC pumps, SFO Fluid Organizer, 2998 Photodiode Array Detector (λ = 210-650 nm), 3100 Mass Detector (m/z = 100-1500), and a Waters Xbridge BEH C18 OBD Prep. Column (130 Å, 5 μ m, 19 x 150 mm). Column was pre-equilibrated depending on the gradient (prerun time 8 min), and samples (0.45 mL/run) were run with a 15 minute gradient detailed below (run time 21 min) using water and MeCN as mobile phases (flow rate = 30 mL/min), with additional at column dilution (ACD) of 1.5% TFA in MeCN (flow rate = 1 mL/min). Fraction collection was triggered by mass detection; after column

separation, 0.02% of the sample was diverted and sent to the mass detector. Fractions containing the correct mass were collected, pooled and lyophilized to obtain product as a pink powder.

Time (min)	A1		A2	
	Water (%)	MeCN (%)	Water (%)	MeCN (%)
0:00	90.0	10.0	82.0	18.0
2.50	90.0	10.0	82.0	18.0
17.50	60.0	40.0	52.0	48.0
19.50	5.0	95.0	5.0	95.0
20.90	5.0	95.0	5.0	95.0
21.00	95.0	5.0	95.0	5.0

Method B. RP-HPLC purifications (max. 5 mL/run) were performed on a Shimadzu LC-20AT HPLC system equipped with a SPD-20A UV/Vis detector, RF-20A Fluorescence Detector ($\lambda_{\text{ex}} = 507 \text{ nm}$, $\lambda_{\text{em}} = 529 \text{ nm}$), FRC-10A fraction collector and a Waters XBridge BEH C18 Prep. Column (130 Å, 5 μm , 10 x 150 mm). Samples were run with a 15 minute gradient detailed below (run time 22.1 min) using 0.05% TFA in water (v/v) and 0.05% TFA in MeCN (v/v) as mobile phases (flow rate = 6.5 mL/min). Sample collection was triggered by UV/Vis intensity. Pure fractions (checked by LC-MS) were pooled and lyophilized to obtain products as a pink powder.

Time (min)	0.05% TFA in water (%)	0.05% TFA in MeCN (%)
1.00	95.0	5.0
2.00	90.0	10.0
17.00	30.0	70.0
17.10	5.0	95.0
19.00	5.0	95.0
19.10	95.0	5.0
22.00	95.0	5.0
22.10	95.0	5.0

Method C. RP-HPLC purifications (max. 20 mL/run) were performed on a Waters HPLC equipped with a Waters 2489 UV/Vis detector, Waters fraction collector III and a Waters XBridge BEH C18 OBD Prep. Column (130 Å, 5 μm , 30 x 150 mm). Samples were run with a 13 minute gradient detailed below (run time 25 min) using water, MeCN and 1% TFA in water (v/v) as mobile phases (flow rate = 37.5 mL/min). Fraction collection was triggered by UV intensity ($\lambda = 210 \text{ nm}$). Pure fractions (checked by LC-MS) were pooled and lyophilized to obtain products as a pink powder.

Time (min)	Water (%)	MeCN (%)	1% TFA in water (%)
0:00	90.0	5.0	5.0
5.00	90.0	5.0	5.0
7.00	75.0	20.0	5.0
18.00	50.0	45.0	5.0
18.50	0.0	95.0	5.0
21.50	0.0	95.0	5.0
21.60	90.0	5.0	5.0
25.00	90.0	5.0	5.0

Supporting Data; ABP Synthesis

Step I. Solid Phase Peptide Synthesis (SPPS)

NH₂-Ub₁₋₇₅(PG)-resin was synthesized on trityl resin preloaded with Glycine, building the peptide chains from C-terminus to N-terminus according to traditional SPPS procedure by coupling amino acids with Fmoc-protected N-terminus. Coupling sequence has previously been optimized for incorporation of Fmoc-protected dipeptides.¹ Amino acids have acid-labile protection groups on reactive side chains to prevent cross-reactivity and truncations (Table S10), which are all removed in the final global deprotection step. Met1 (methionine) was replaced by its close isostere Nle (norleucine) to prevent oxidation, which typically does not affect recognition by DUBs but can reduce cleavage efficiency of linear diUb chains.⁵⁸⁻⁵⁹

Sequence Ub₁₋₇₅^{Met1Nle}

(Nle)QIFVKTLTG KTITLEVEPS DTIENVKAKI QDKEGIPPDQ QRLIFAGKQL EDGRTLSDYN IQKESTLHLV LRLRG

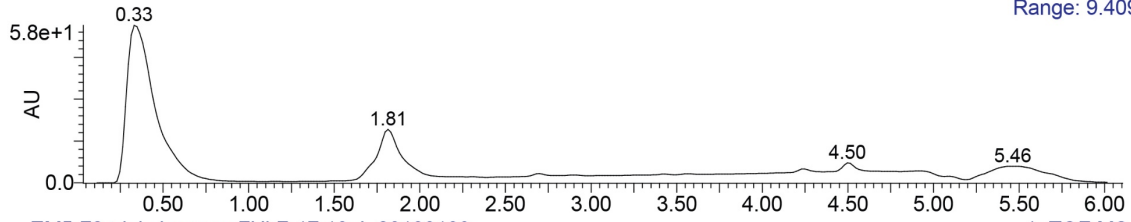
Table S10. Fmoc-protected L-Amino acids and dipeptides.

AA	Reagent	CAS#	Cat# *	Coupled in cycle #
R	Fmoc-Arg(Pbf)-OH	154445-77-9	852067	1, 3, 18, 29
L	Fmoc-Leu-OH	35661-60-0	852011	2, 4, 6, 8, 22, 28, 56
V	Fmoc-Val-OH	68858-20-8	852021	5, 45, 54, 64
H	Fmoc-His(Trt)-OH	109425-51-6	852032	7
ST	Fmoc-Ser(tBu)-Thr($\Psi^{\text{Me,Me}}$ pro)-OH	-	852192	9
E	Fmoc-Glu(OtBu)-OH	71989-18-9	852009	10, 21, 37, 47, 53, 55
K	Fmoc-Lys(Boc)-OH	71989-26-9	852012	11, 24, 38, 42, 44, 59, 63
Q	Fmoc-Gln(Trt)-OH	132327-80-1	852045	12, 23, 30, 31, 40, 67
I	Fmoc-Ile-OH	71989-23-6	852010	13, 27, 35, 41, 48, 66
N	Fmoc-Asn(Trt)-OH	132388-59-1	852044	14, 46
Y	Fmoc-Tyr(tBu)-OH	71989-38-3	852020	15
D	Fmoc-Asp(OtBu)-OH	71989-14-5	852005	16, 32, 39, 50
LS	Fmoc-Leu-Ser($\Psi^{\text{Me,Me}}$ pro)-OH	339531-50-9	852179	17
T	Fmoc-Thr(tBu)-OH	71989-35-0	852000	19, 49, 58, 62
DG	Fmoc-Asp(OtBu)-(Dmb)Gly-OH	900152-72-9	852115	20
AG	Fmoc-Ala-(Dmb)Gly-OH	-	852108	25
F	Fmoc-Phe-OH	35661-40-6	852016	26, 65
P	Fmoc-Pro-OH	71989-31-6	852017	33, 34, 52
G	Fmoc-Gly-OH	29022-11-5	852001	36, 60
A	Fmoc-Ala-OH	35661-39-3	852003	43
S	Fmoc-Ser(tBu)-OH	71989-33-8	852019	51
IT	Fmoc-Ile-Thr($\Psi^{\text{Me,Me}}$ pro)-OH	957780-52-8	852193	57
LT	Fmoc-Leu-Thr($\Psi^{\text{Me,Me}}$ pro)-OH	955048-89-2	852184	61
Nle	Fmoc-Nle-OH	77284-32-3	852014	68

* Brand: Novabiochem. Supplier: Merck.

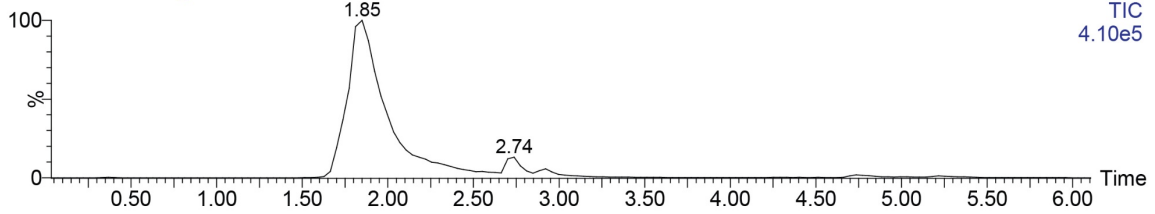
A EM5-72 trial cleavage 7Ub7-17 10uL 20180109

3: Diode Array
Range: 9.409e+1



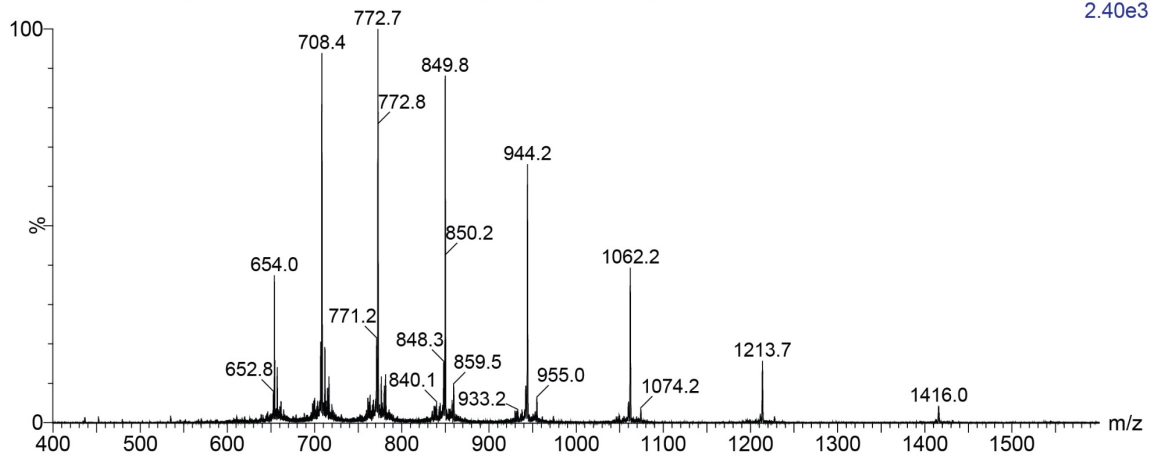
EM5-72 trial cleavage 7Ub7-17 10uL 20180109

1: TOF MS ES+
TIC
4.10e5



B EM5-72 trial cleavage 7Ub7-17 10uL 20180109 50 (1.849) Cm (49:52)

1: TOF MS ES+
2.40e3



C EM5-72 trial cleavage 7Ub7-17 10uL 20180109 50 (1.849) M1 [Ev0,It19] (Gs,0.750,400:1600,1.00,L33,R33); Cm (49:52)

9.69e4

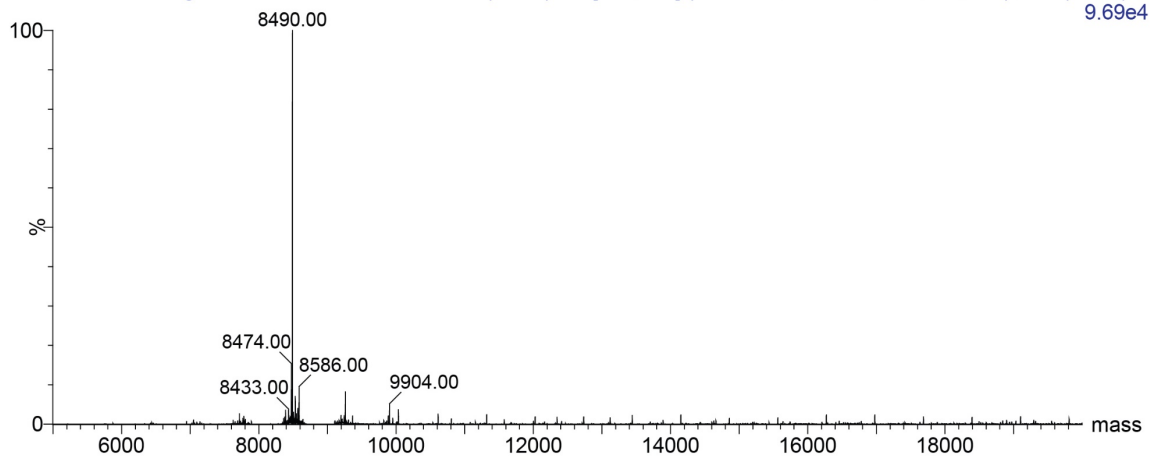


Figure S31. Analytical data for crude NH₂-Ub₁₋₇₅-OH related to Figure 1 and Figure S1B. **A**) Chromatogram. Top; UV chromatogram ($\lambda = 190\text{-}600\text{ nm}$). Bottom; TIC ($m/z = 300\text{-}2000$). **B**) Spectrum of main peak. **C**) Deconvoluted mass: 8490 Da (Found)/8489.78 Da (Calc.).

Step II + III. Rhodamine coupling + resin cleavage

N,N'-Boc₂-5-carboxy-Rhodamine or (Boc)₂Rho-OH **11** was synthesized according to published procedure.⁵⁵ Treatment with HFIP in DCM cleaves bond between Glycine and Trityl resin, while protecting groups on the amino acid side chains remain intact. Global deprotection and cleavage from resin was performed by trial cleavage on a small sample to enable analysis of reaction progress, since resin and protecting groups are not compatible with LC-MS analysis.

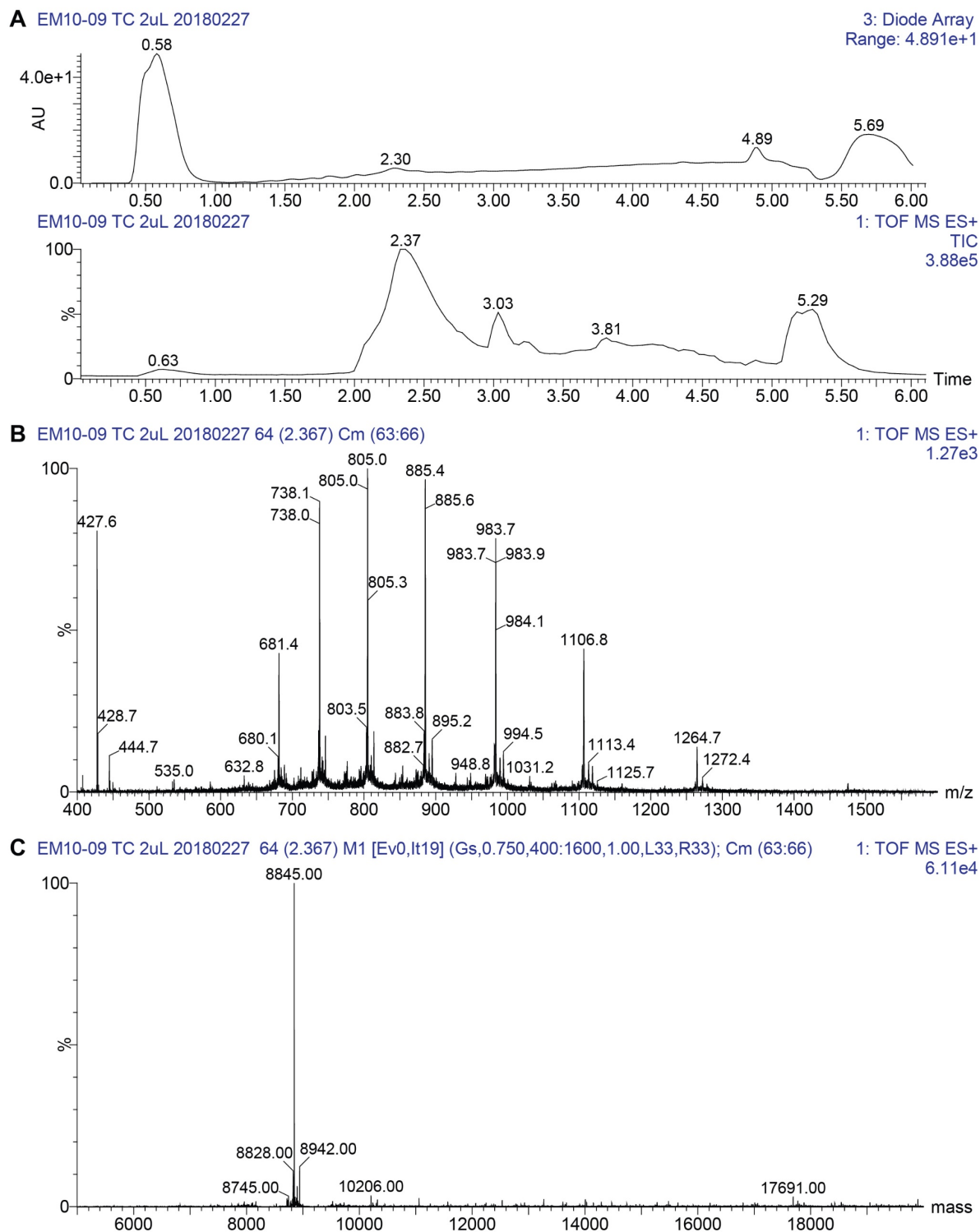


Figure S32. Analytical data for crude Rho-Ub₁₋₇₅-OH related to Figure 1 and Figure S1B. **A**) Chromatogram. Top; UV chromatogram ($\lambda = 190-600$ nm). Bottom; TIC ($m/z = 300-2000$). **B**) Spectrum of main peak. **C**) Deconvoluted mass: 8845 Da (Found)/8846.12 Da (Calc.).

Step IV + V. Warhead coupling, global deprotection and purification

Amines were obtained from commercial sources or by chemical synthesis (Table S9). Chemical synthesis of amines **[D₂]-Prg** and **18** is discussed from SI-70 onward. Amide couplings were performed with DMF or DCM as the solvent. RP-HPLC purification method is determined by the synthesis scale. Rho-Ub-ABPs were obtained as solid pink powder. Rho-Ub-**3** is prone to hydrolysis or possibly (acid-catalyzed) hydration resulting in hydrolyzed Rho-Ub-**3b** (M+18) and could thus only be obtained as a mixture.

Synthesis details

Rho-Ub ₁₋₇₅ - Prg	(Boc) ₂ Rho-Ub ₁₋₇₅ (PG)-OH (10 μmol) was incubated with propargylamine in DCM, and purified by RP-HPLC method C to yield Rho-Ub ₁₋₇₅ - Prg . LC-MS R _t = 3.42 min, M = 8883 Da (Calc. 8883.18 Da).
Rho-Ub ₁₋₇₅ - 2	(Boc) ₂ Rho-Ub ₁₋₇₅ (PG)-OH (2 μmol) was incubated with 1-amino-2-butyne hydrochloride in DCM, and purified by RP-HPLC method B to yield Rho-Ub ₁₋₇₅ - 2 . LC-MS R _t = 3.46 min, M = 8897 Da (Calc. 8897.21 Da).
Rho-Ub ₁₋₇₅ - 3	(Boc) ₂ Rho-Ub ₁₋₇₅ (PG)-OH (2 μmol) was incubated with 3-phenylprop-2-yn-1-amine hydrochloride in DCM, and purified by RP-HPLC method B to yield a 7:10 mixture of Rho-Ub ₁₋₇₅ - 3 and hydrolyzed Rho-Ub ₁₋₇₅ - 3b . LC-MS R _t = 3.51 min, M = 8959 + 8977 Da (Calc. 8959.28 Da).
Rho-Ub ₁₋₇₅ - 4	(Boc) ₂ Rho-Ub ₁₋₇₅ (PG)-OH (2 μmol) was incubated with 1-methyl-prop-2-ynylamine hydrochloride in DMF, and purified by RP-HPLC method A2 to yield Rho-Ub ₁₋₇₅ - 4 . LC-MS R _t = 3.44 min, M = 8897 Da (Calc. 8897.21 Da).
Rho-Ub ₁₋₇₅ - 7	(Boc) ₂ Rho-Ub ₁₋₇₅ (PG)-OH (2 μmol) was incubated with 1-phenylprop-2-yn-1-amine hydrochloride in DMF, and purified by RP-HPLC method A2 to yield Rho-Ub ₁₋₇₅ - 7 . LC-MS R _t = 3.49 min, M = 8959 Da (Calc. 8959.28 Da).
Rho-Ub ₁₋₇₅ - 5	(Boc) ₂ Rho-Ub ₁₋₇₅ (PG)-OH (10 μmol) was incubated with 2-methyl-3-butyne-2-amine in DCM, and purified by RP-HPLC method C to yield Rho-Ub ₁₋₇₅ - 5 . LC-MS R _t = 3.44 min, M = 8912 Da (Calc. 8911.24 Da).
Rho-Ub ₁₋₇₅ - 8	(Boc) ₂ Rho-Ub ₁₋₇₅ (PG)-OH (2 μmol) was incubated with 1-ethynylcyclohexylamine in DMF, and purified by RP-HPLC method A2 to yield Rho-Ub ₁₋₇₅ - 8 . LC-MS R _t = 3.49 min, M = 8951 Da (Calc. 8951.30 Da).
Rho-Ub ₁₋₇₅ - 9	(Boc) ₂ Rho-Ub ₁₋₇₅ (PG)-OH (2 μmol) was incubated with 1-amino-3-butyne in DMF, and purified by RP-HPLC method A1 to yield Rho-Ub ₁₋₇₅ - 9 . LC-MS R _t = 3.42 min, M = 8897 Da (Calc. 8897.21 Da).
Rho-Ub ₁₋₇₅ - 10	(Boc) ₂ Rho-Ub ₁₋₇₅ (PG)-OH (2 μmol) was incubated with <i>N</i> -Methylpropargylamine in DMF, and purified by RP-HPLC method A2 to yield Rho-Ub ₁₋₇₅ - 10 . LC-MS R _t = 3.44 min, M = 8897 Da (Calc. 8897.21 Da).
Rho-Ub ₁₋₇₅ - Prp	(Boc) ₂ Rho-Ub ₁₋₇₅ (PG)-OH (2 μmol) was incubated with propylamine in DMF, and purified by RP-HPLC method A1 to yield Rho-Ub ₁₋₇₅ - Prp . LC-MS R _t = 3.44 min, M = 8887 Da (Calc. 8887.22 Da).
Rho-Ub ₁₋₇₅ - [D₂]-Prg	(Boc) ₂ Rho-Ub ₁₋₇₅ (PG)-OH (2 μmol) was incubated with prop-2-yn-1,1- <i>d</i> ₂ -1-amine hydrochloride in DCM, and purified by RP-HPLC method B to yield Rho-Ub ₁₋₇₅ - [D₂]-Prg . LC-MS R _t = 3.39 min, M = 8885 Da (Calc. 8885.20 Da).
Rho-Ub ₁₋₇₅ - 18	(Boc) ₂ Rho-Ub ₁₋₇₅ (PG)-OH (2 μmol) was incubated with 4,4,4-trifluorobut-2-yn-1-amine hydrochloride in DCM, and purified by RP-HPLC method B to yield Rho-Ub ₁₋₇₅ - 18 . LC-MS R _t = 3.46 min, M = 8951 Da (Calc. 8951.18 Da).
Rho-Ub ₁₋₇₅ - VME	(Boc) ₂ Rho-Ub ₁₋₇₅ (PG)-OH (4 μmol) was incubated with methyl (<i>E</i>)-4-aminobut-2-enoate hydrochloride in DCM, and purified by RP-HPLC method C to yield Rho-Ub ₁₋₇₅ - VME . LC-MS R _t = 3.40 min, M = 8942 Da (Calc. 8943.24 Da).

LC-MS spectra of Rho-Ub-ABPs

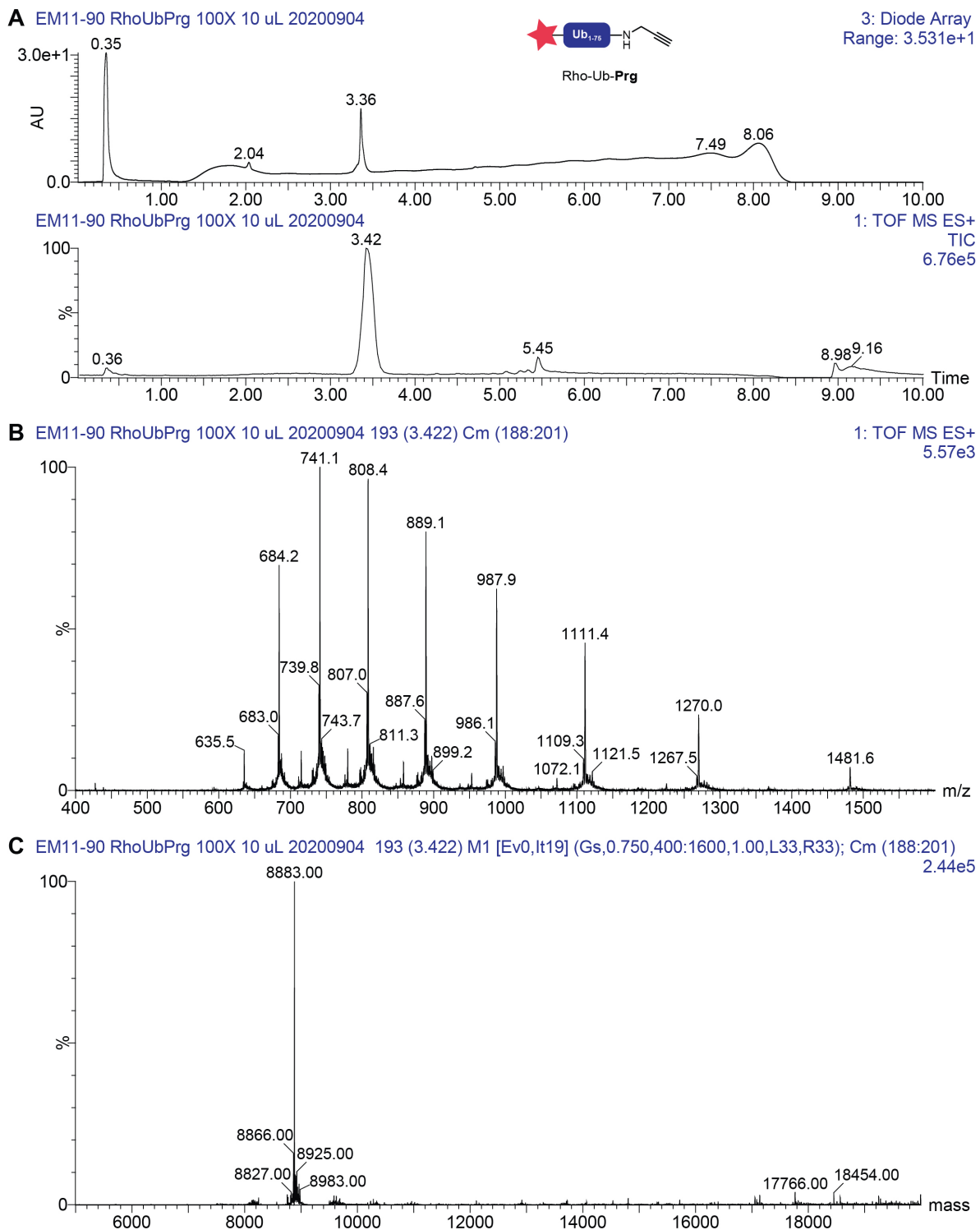
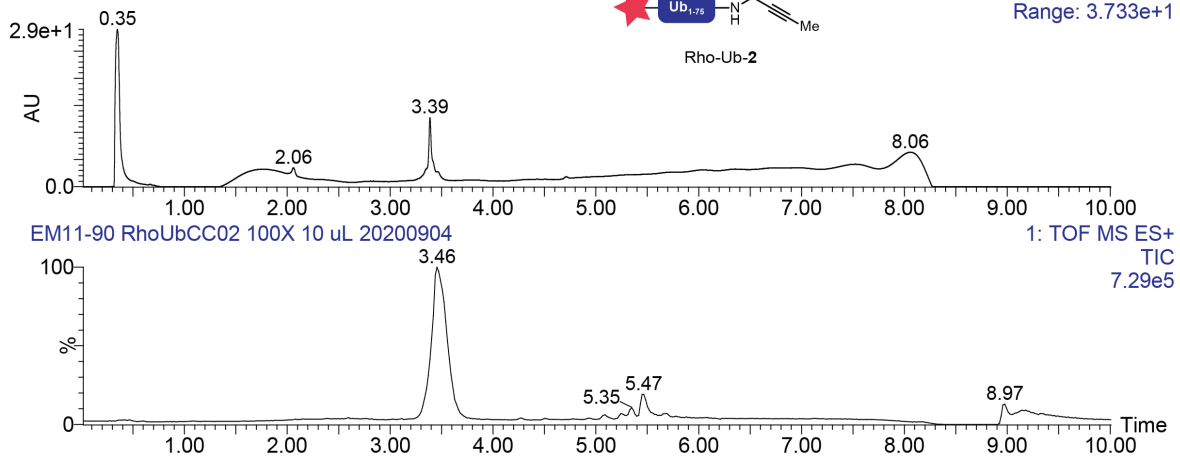
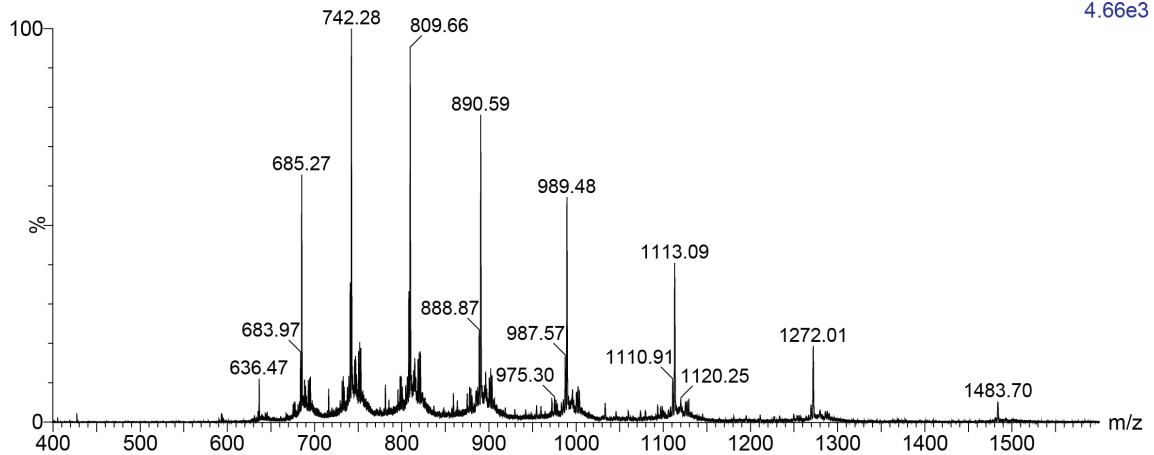


Figure S33. Analytical LC-MS data for Rho-Ub₁₋₇₅-Prg. **A**) Chromatogram. Top; UV chromatogram ($\lambda = 210\text{-}800$ nm). Bottom; TIC ($m/z = 100\text{-}1600$). **B**) Spectrum of main peak. **C**) Deconvoluted mass: 8883 Da (Found)/8883.18 Da (Calc.).

A EM11-90 RhoUbCC02 100X 10 uL 20200904



B EM11-90 RhoUbCC02 100X 10 uL 20200905 195 (3.455) Cm (190:203)



C EM11-90 RhoUbCC02 100X 10 uL 20200905 195 (3.455) M1 [Ev0,It19] (Gs,0.750,400:1600,1.00,L33,R33); Cm (190:203)
2.19e5

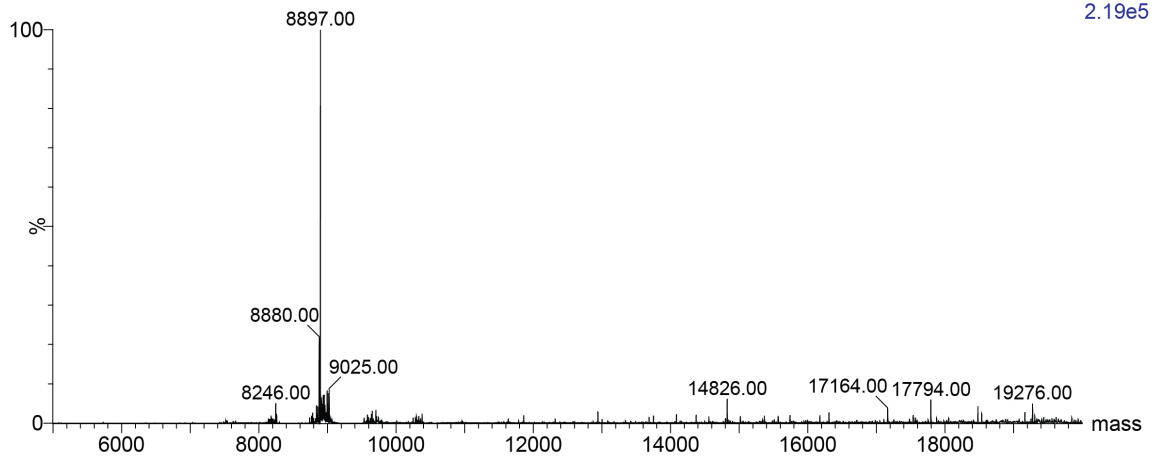
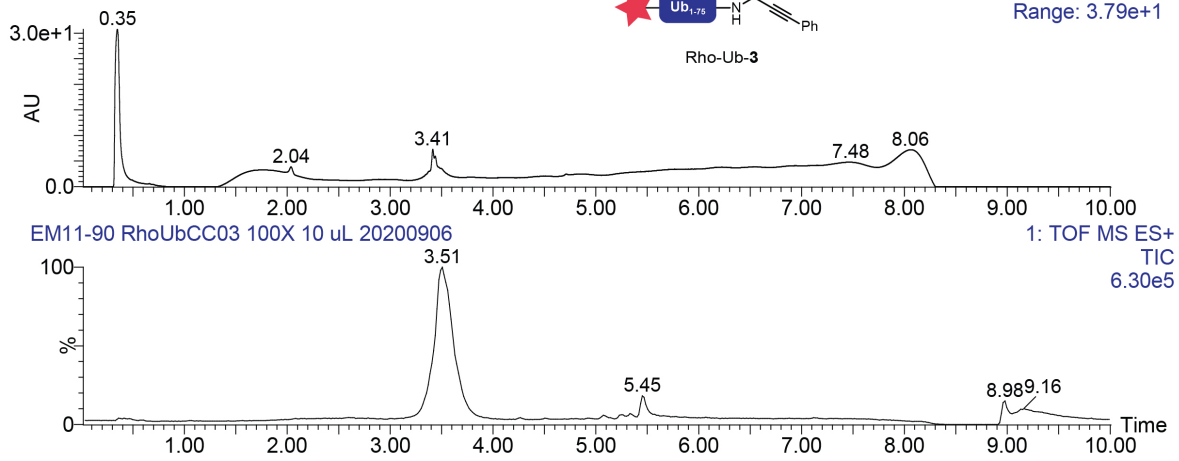
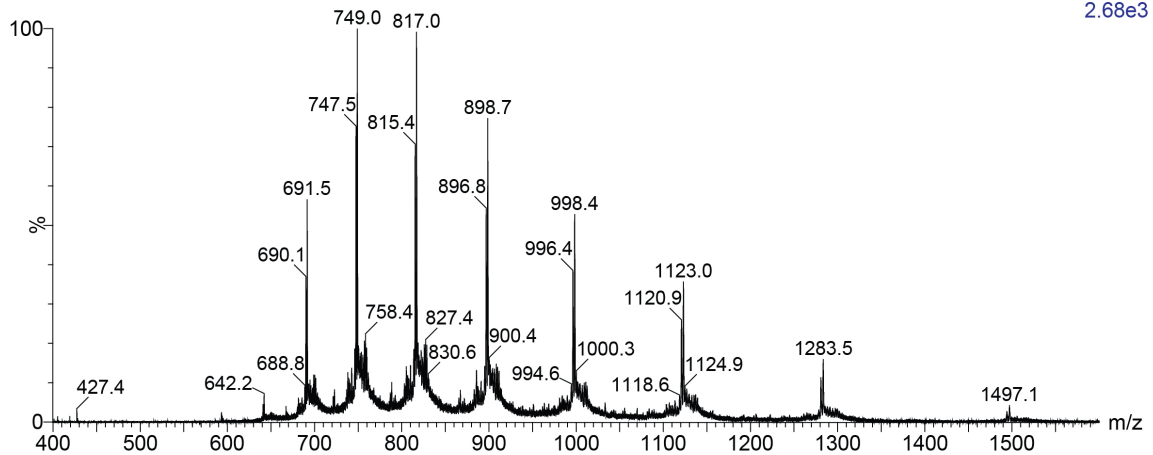


Figure S34. Analytical LC-MS data for Rho-Ub₁₋₇₅-2. **A**) Chromatogram. Top; UV chromatogram ($\lambda = 210-800$ nm). Bottom; TIC ($m/z = 100-1600$). **B**) Spectrum of main peak. **C**) Deconvoluted mass: 8897 Da (Found)/8897.21 Da (Calc.).

A EM11-90 RhoUbCC03 100X 10 uL 20200906



B EM11-90 RhoUbCC03 100X 10 uL 20200906 198 (3.507) Cm (193:204)



C EM11-90 RhoUbCC03 100X 10 uL 20200906 198 (3.507) M1 [Ev0,It19] (Gs,0.750,400:1600,1.00,L33,R33); Cm (193:204)
1.01e5

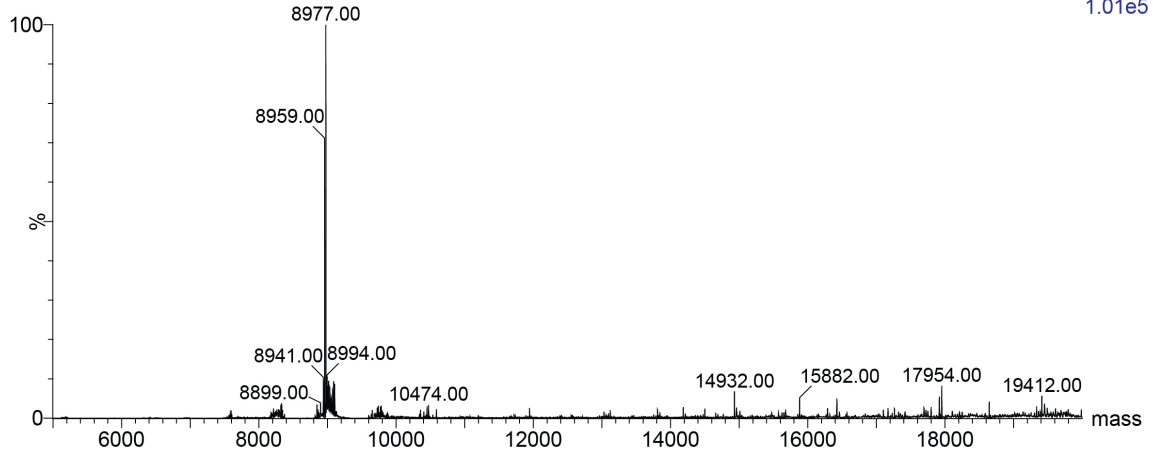
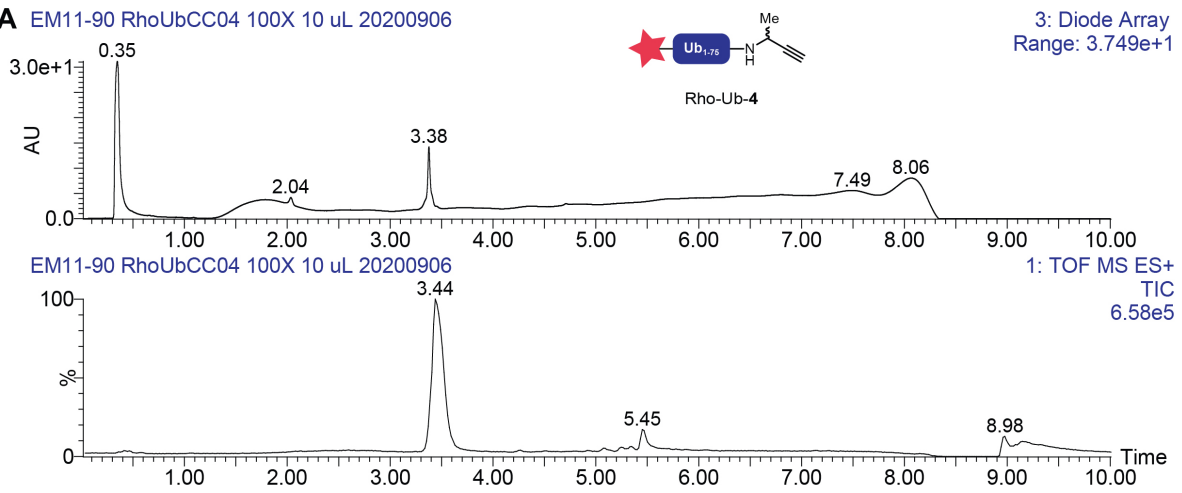
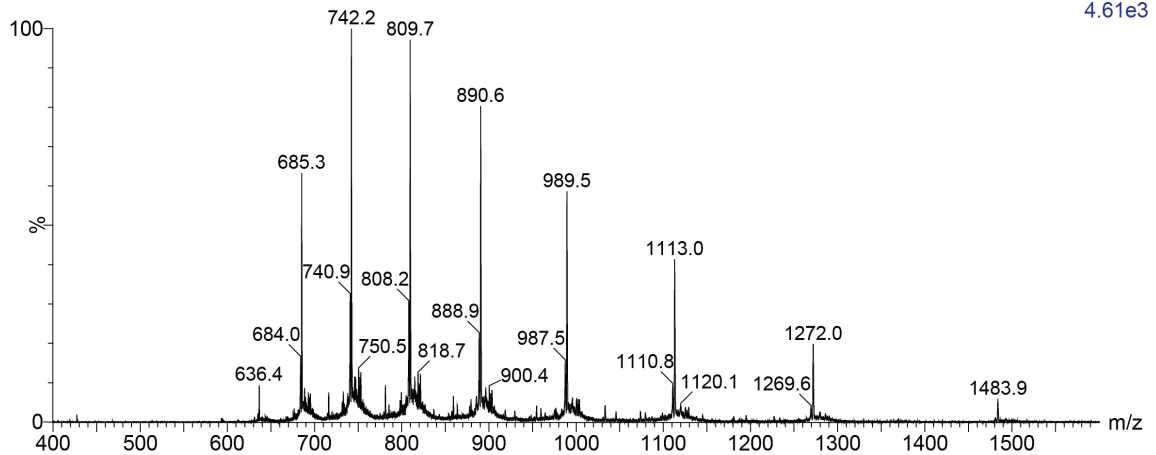


Figure S35. Analytical LC-MS data for Rho-Ub₁₋₇₅-**3**. **A**) Chromatogram. Top; UV chromatogram ($\lambda = 210\text{-}800$ nm). Bottom; TIC ($m/z = 100\text{-}1600$). **B**) Spectrum of main peak. **C**) Deconvoluted mass: 8959 + 8977 Da (Found) /8959.28 Da (Calc.). 7:10 mixture of desired Rho-Ub₁₋₇₅-**3** and hydrolysis product (M+18).

A EM11-90 RhoUbCC04 100X 10 uL 20200906



B EM11-90 RhoUbCC04 100X 10 uL 20200906 194 (3.439) Cm (190:201)



C EM11-90 RhoUbCC04 100X 10 uL 20200906 194 (3.439) M1 [Ev0,It19] (Gs,0.750,400:1600,1.00,L33,R33); Cm (190:201)
2.17e5

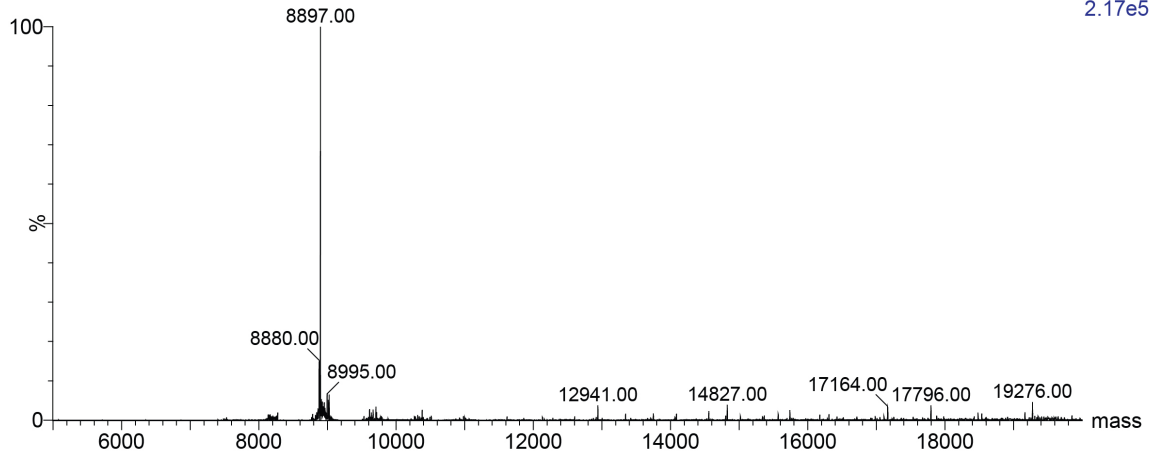
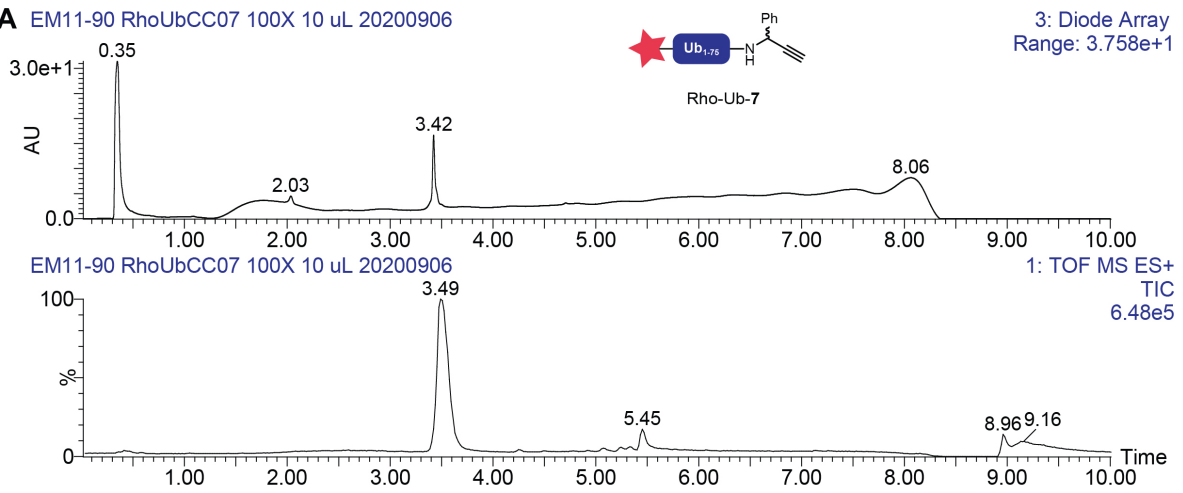
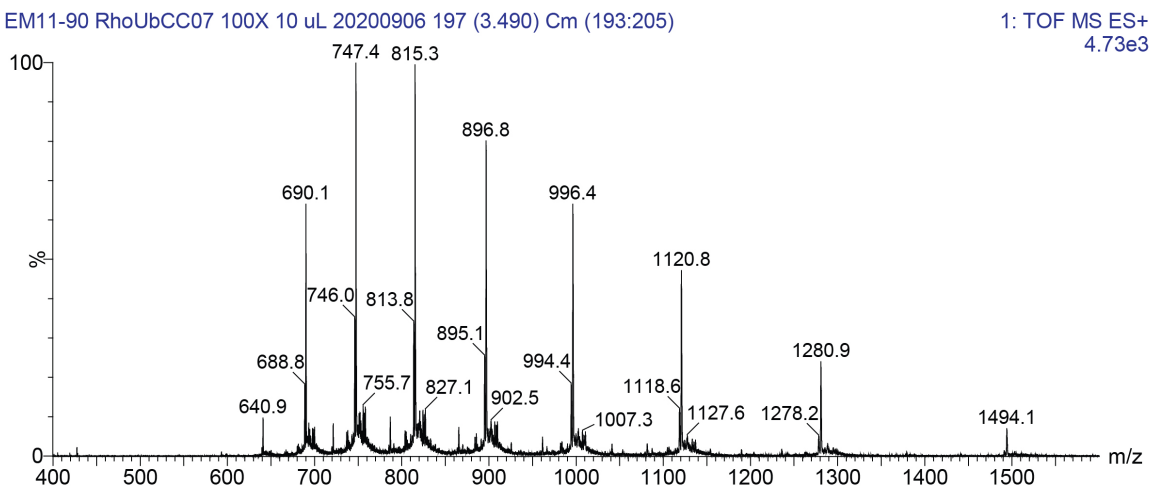


Figure S36. Analytical LC-MS data for Rho-Ub₁₋₇₅-4. **A**) Chromatogram. Top; UV chromatogram ($\lambda = 210-800$ nm). Bottom; TIC ($m/z = 100-1600$). **B**) Spectrum of main peak. **C**) Deconvoluted mass: 8897 Da (Found)/8897.21 Da (Calc.).

A EM11-90 RhoUbCC07 100X 10 uL 20200906



B EM11-90 RhoUbCC07 100X 10 uL 20200906 197 (3.490) Cm (193:205)



C EM11-90 RhoUbCC07 100X 10 uL 20200906 197 (3.490) M1 [Ev0,It19] (Gs,0.750,400:1600,1.00,L33,R33); Cm (193:205)
2.26e5

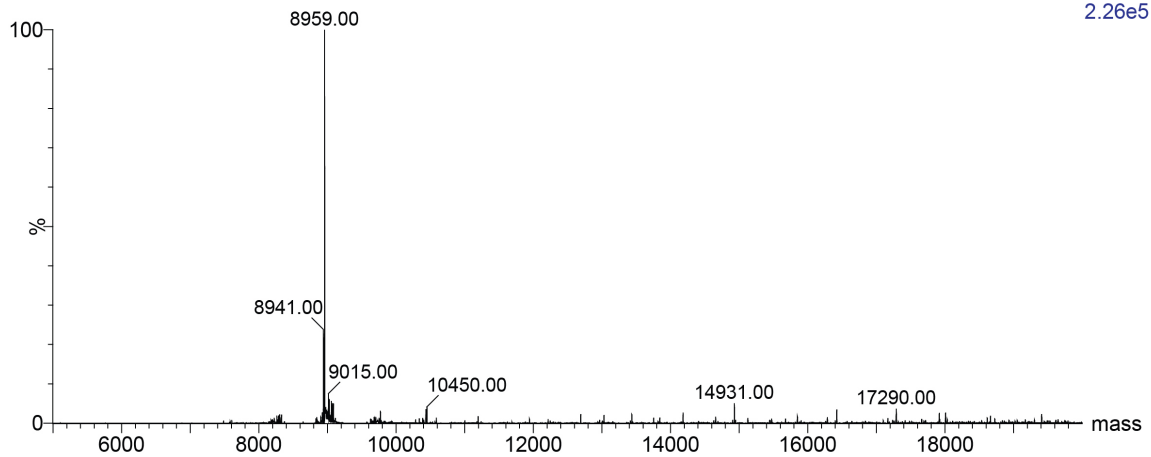
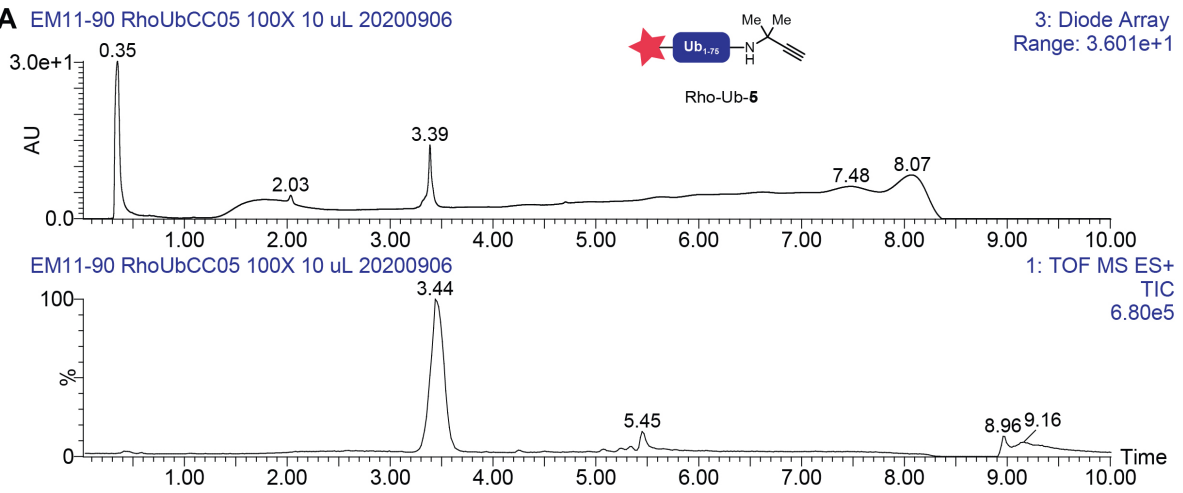
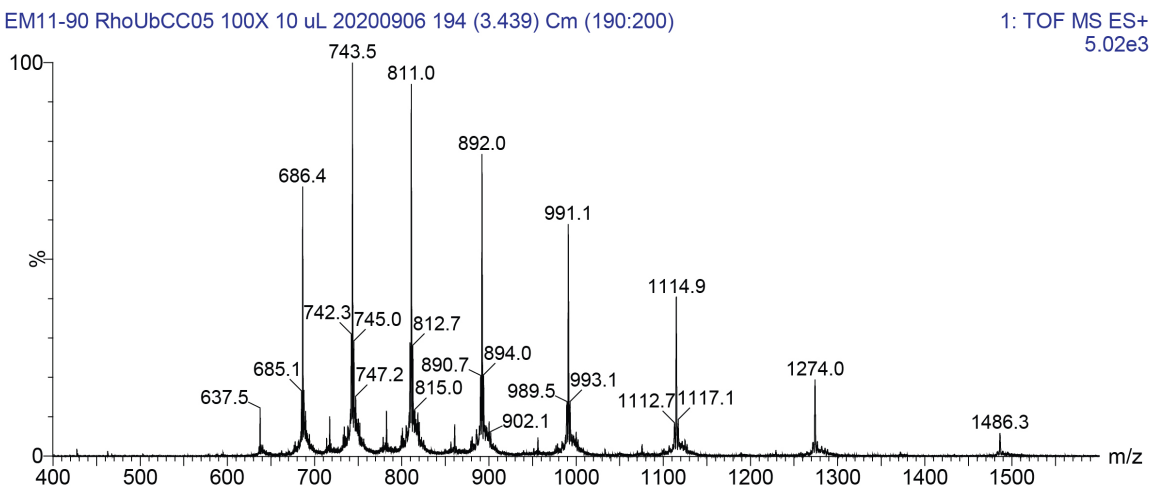


Figure S37. Analytical LC-MS data for Rho-Ub₁₋₇₅-7. **A**) Chromatogram. Top; UV chromatogram ($\lambda = 210$ -800 nm). Bottom; TIC (m/z = 100-1600). **B**) Spectrum of main peak. **C**) Deconvoluted mass: 8959 Da (Found)/8959.28 Da (Calc.).

A EM11-90 RhoUbCC05 100X 10 uL 20200906



B EM11-90 RhoUbCC05 100X 10 uL 20200906 194 (3.439) Cm (190:200)



C EM11-90 RhoUbCC05 100X 10 uL 20200906 194 (3.439) M1 [Ev0,It19] (Gs,0.750,400:1600,1.00,L33,R33); Cm (190:200)

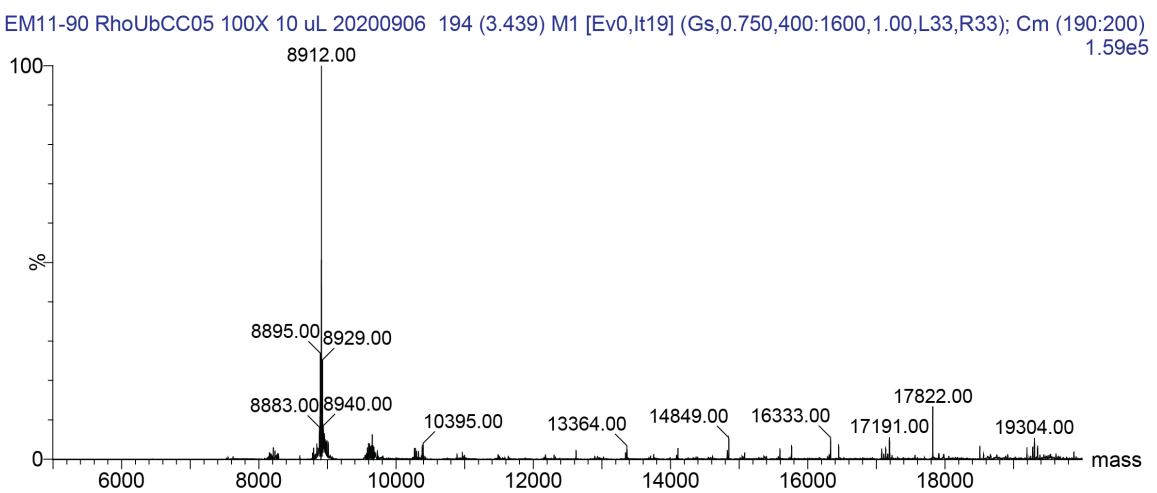
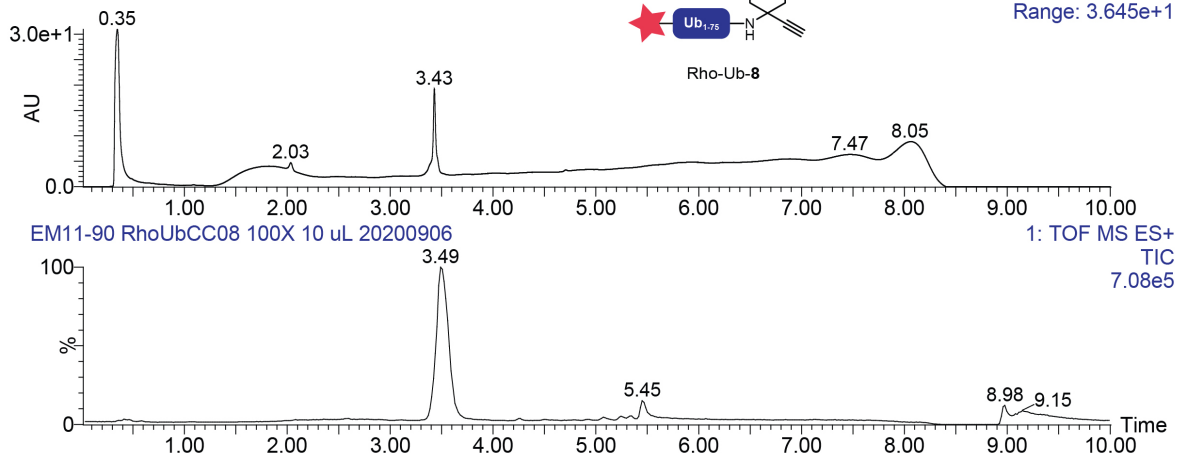
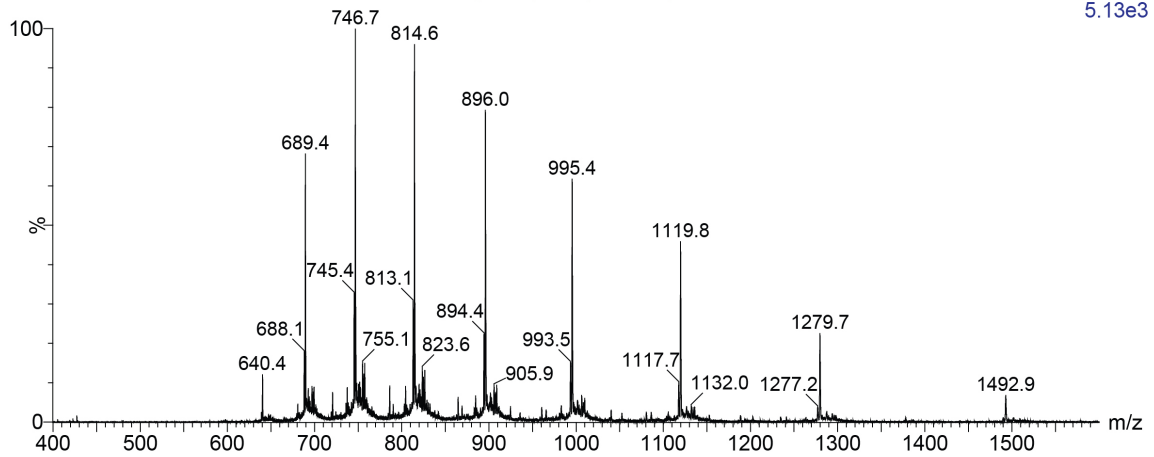


Figure S38. Analytical LC-MS data for Rho-Ub₁₋₇₅-5. **A**) Chromatogram. Top; UV chromatogram ($\lambda = 210-800$ nm). Bottom; TIC ($m/z = 100-1600$). **B**) Spectrum of main peak. **C**) Deconvoluted mass: 8912 Da (Found)/8911.24 Da (Calc.).

A EM11-90 RhoUbCC08 100X 10 uL 20200906



B EM11-90 RhoUbCC08 100X 10 uL 20200906 197 (3.490) Cm (194:203)



C EM11-90 RhoUbCC08 100X 10 uL 20200906 197 (3.490) M1 [Ev0,It19] (Gs,0.750,400:1600,1.00,L33,R33); Cm (194:203)
2.26e5

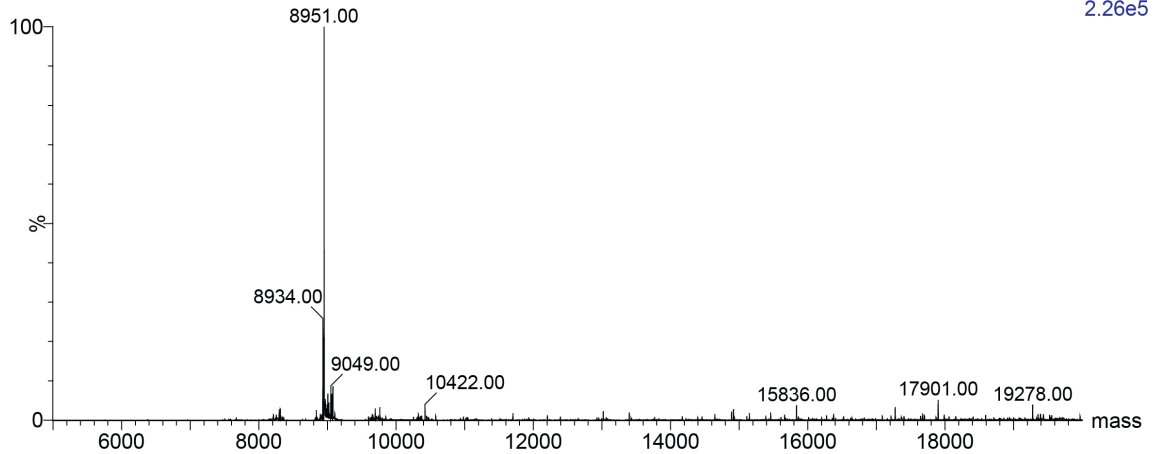
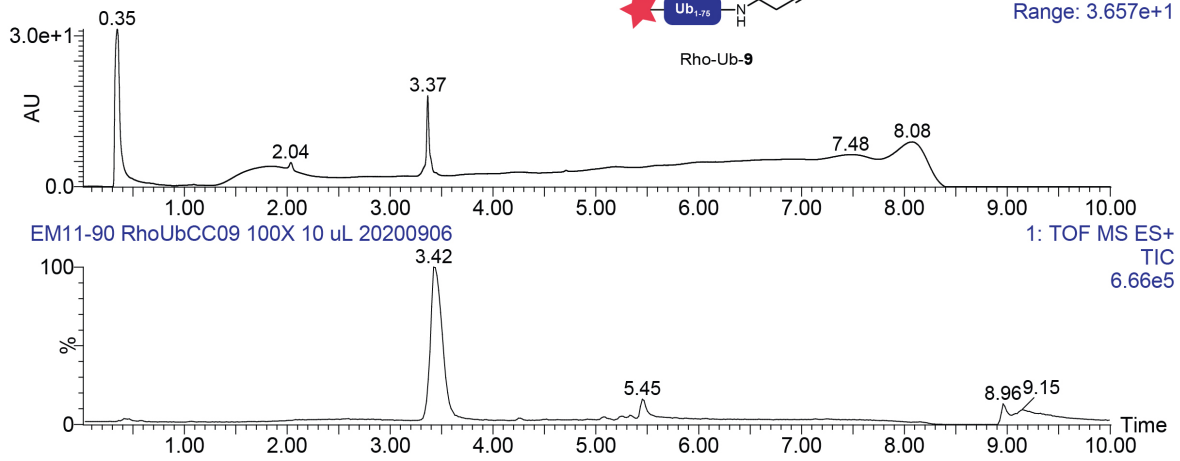
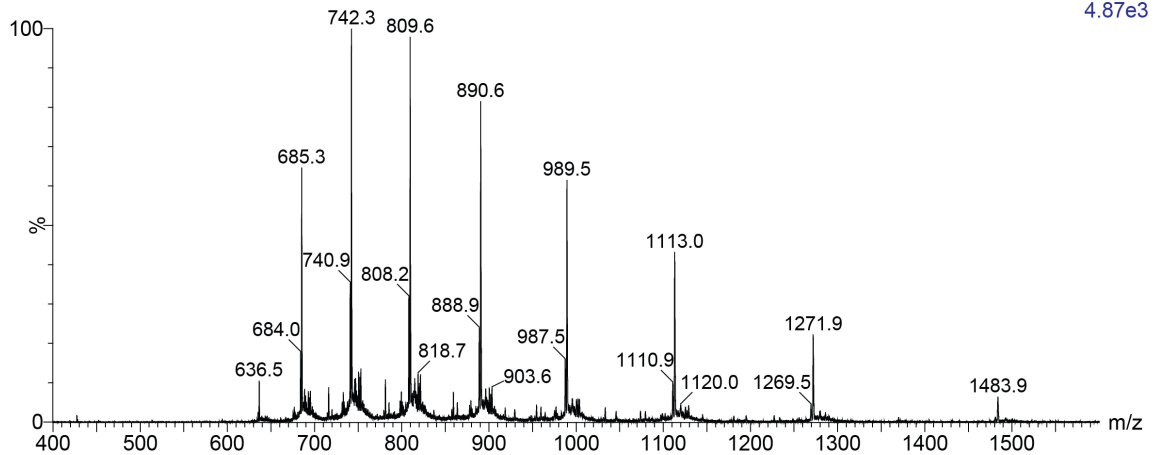


Figure S39. Analytical LC-MS data for Rho-Ub₁₋₇₅-8. **A**) Chromatogram. Top; UV chromatogram ($\lambda = 210-800$ nm). Bottom; TIC ($m/z = 100-1600$). **B**) Spectrum of main peak. **C**) Deconvoluted mass: 8951 Da (Found)/8951.30 Da (Calc.).

A EM11-90 RhoUbCC09 100X 10 uL 20200906



B EM11-90 RhoUbCC09 100X 10 uL 20200906 193 (3.422) Cm (190:200)



C EM11-90 RhoUbCC09 100X 10 uL 20200906 193 (3.422) M1 [Ev0,It19] (Gs,0.750,400:1600,1.00,L33,R33); Cm (190:200)
2.35e5

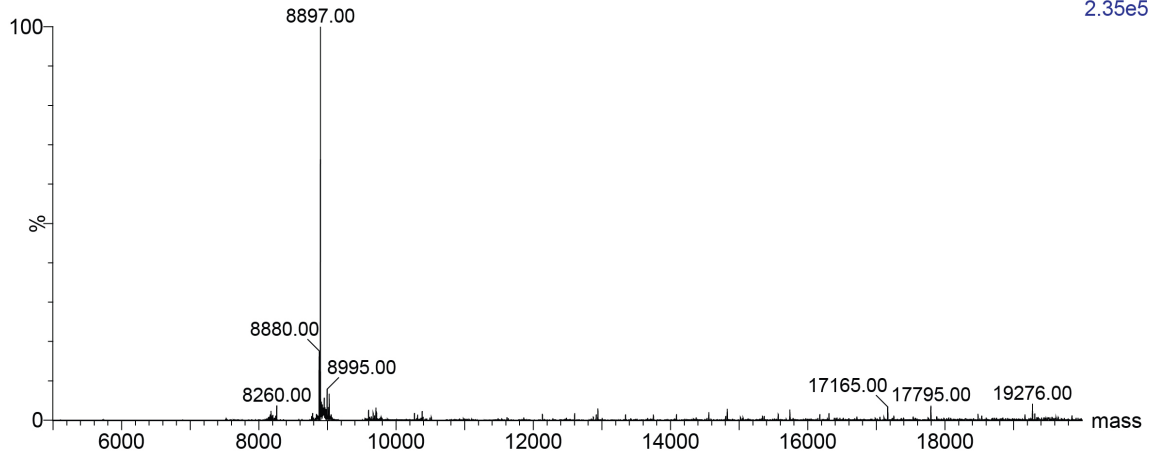
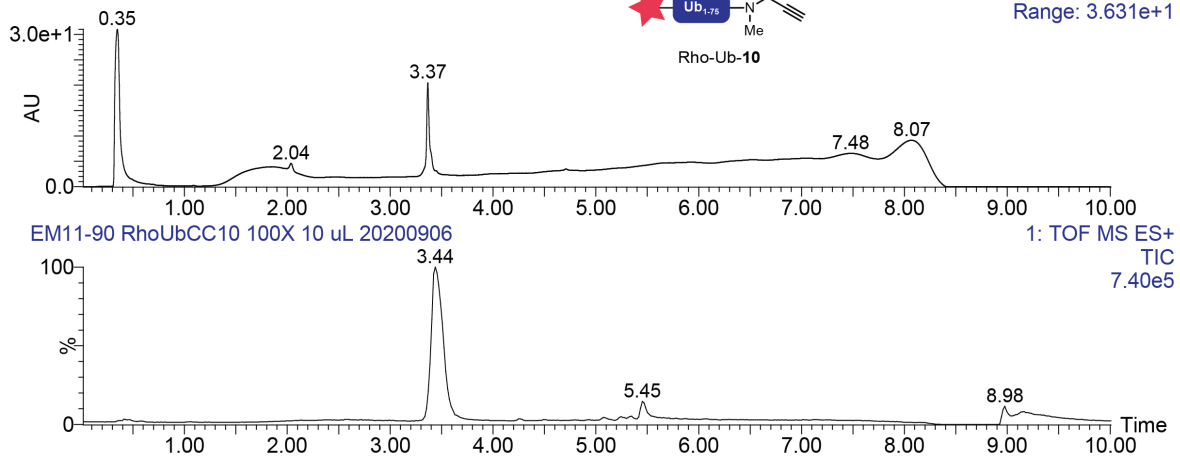
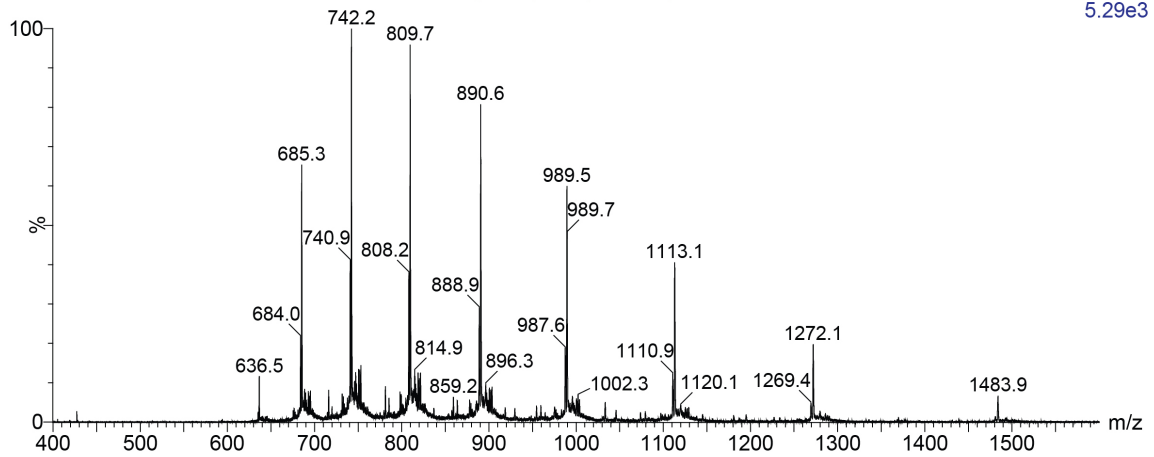


Figure S40. Analytical LC-MS data for Rho-Ub₁₋₇₅-9. **A**) Chromatogram. Top; UV chromatogram ($\lambda = 210-800$ nm). Bottom; TIC ($m/z = 100-1600$). **B**) Spectrum of main peak. **C**) Deconvoluted mass: 8897 Da (Found)/8897.21 Da (Calc.).

A EM11-90 RhoUbCC10 100X 10 uL 20200906



B EM11-90 RhoUbCC10 100X 10 uL 20200906 194 (3.439) Cm (190:202)



C EM11-90 RhoUbCC10 100X 10 uL 20200906 194 (3.439) M1 [Ev0,It19] (Gs,0.750,400:1600,1.00,L33,R33); Cm (190:202)
2.38e5

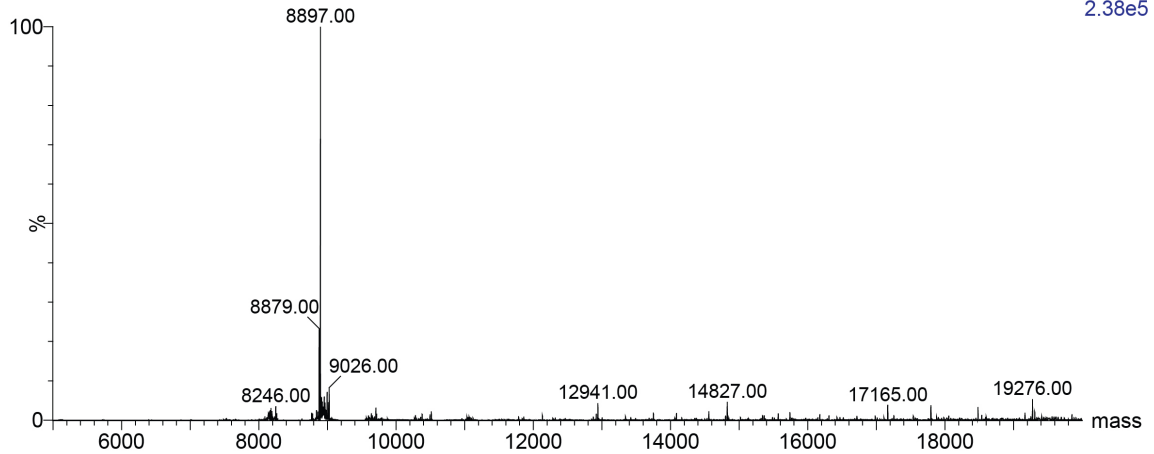
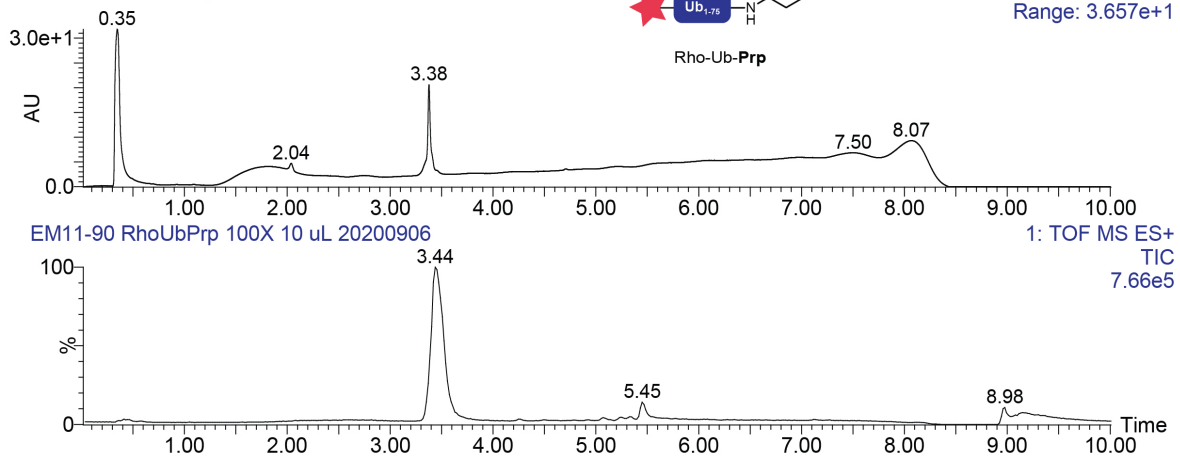
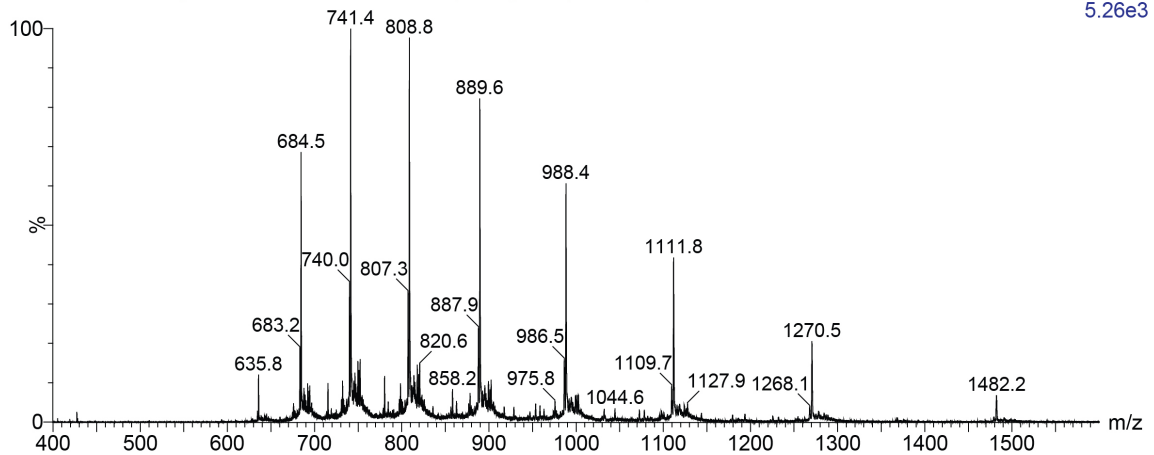


Figure S41. Analytical LC-MS data for Rho-Ub₁₋₇₅-**10**. **A**) Chromatogram. Top; UV chromatogram ($\lambda = 210\text{-}800$ nm). Bottom; TIC ($m/z = 100\text{-}1600$). **B**) Spectrum of main peak. **C**) Deconvoluted mass: 8897 Da (Found)/8897.21 Da (Calc.).

A EM11-90 RhoUbPrp 100X 10 uL 20200906



B EM11-90 RhoUbPrp 100X 10 uL 20200906 194 (3.438) Cm (190:203)



C EM11-90 RhoUbPrp 100X 10 uL 20200906 194 (3.438) M1 [Ev0,It19] (Gs,0.750,400:1600,1.00,L33,R33); Cm (190:203)

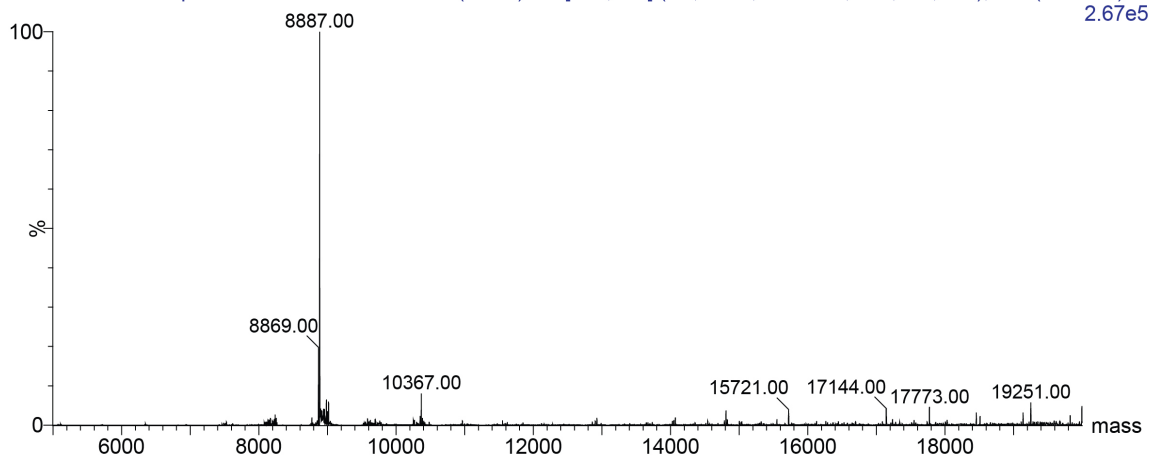
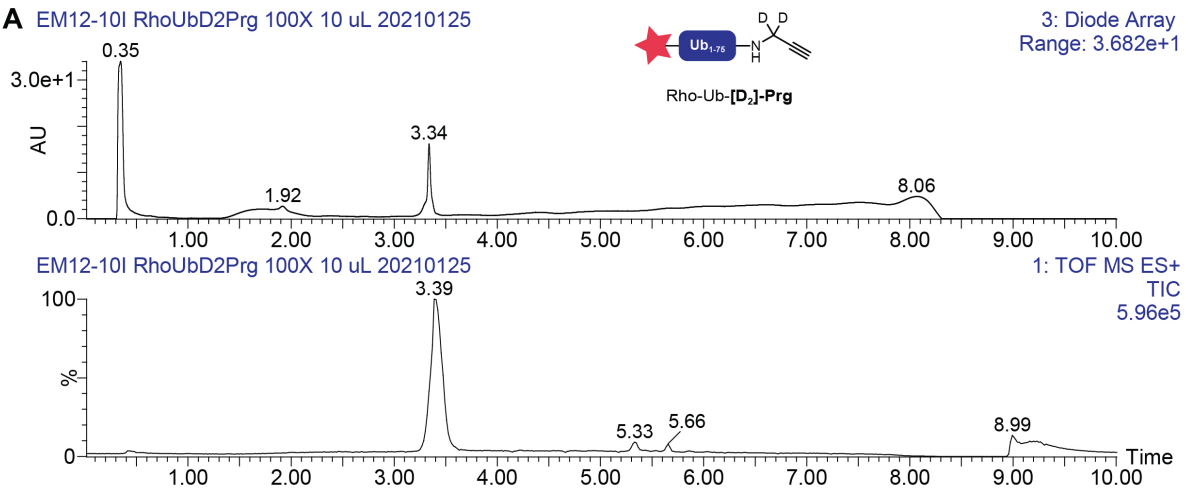
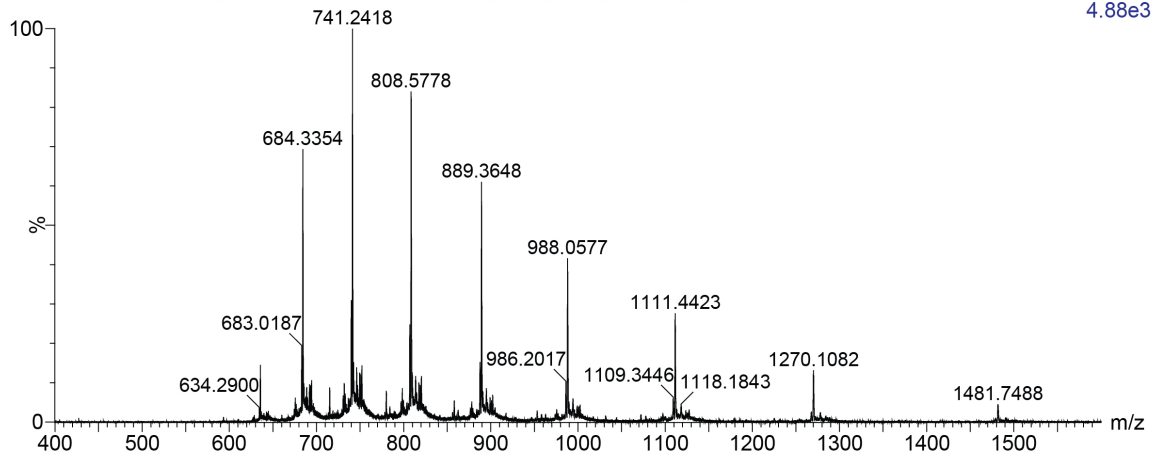


Figure S42. Analytical LC-MS data for Rho-Ub₁₋₇₅-Prp. **A**) Chromatogram. Top; UV chromatogram ($\lambda = 210\text{-}800$ nm). Bottom; TIC ($m/z = 100\text{-}1600$). **B**) Spectrum of main peak. **C**) Deconvoluted mass: 8887 Da (Found)/8887.22 Da (Calc.).

A EM12-10I RhoUbD2Prg 100X 10 uL 20210125



B EM12-10I RhoUbD2Prg 100X 10 uL 20210125 191 (3.388) Cm (186:201)



C EM12-10I RhoUbD2Prg 100X 10 uL 20210125 191 (3.388) M1 [Ev-148573,lt40] (Gs,0.750,600:1600,1.00,L33,R33)

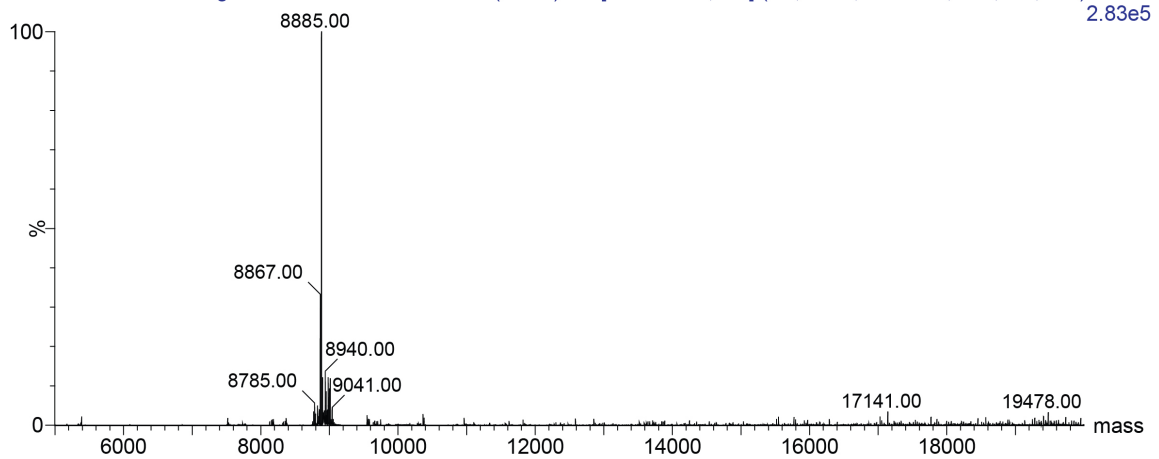
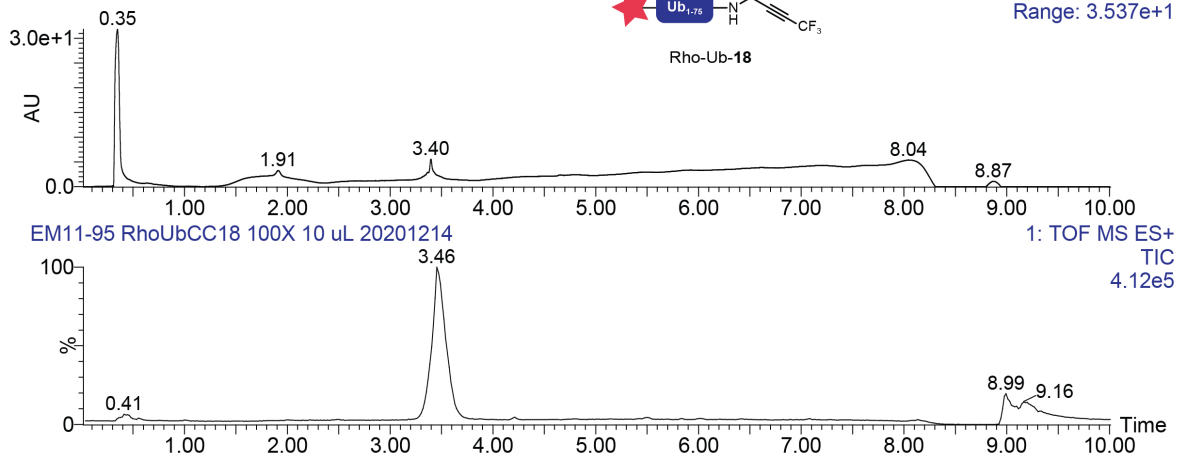
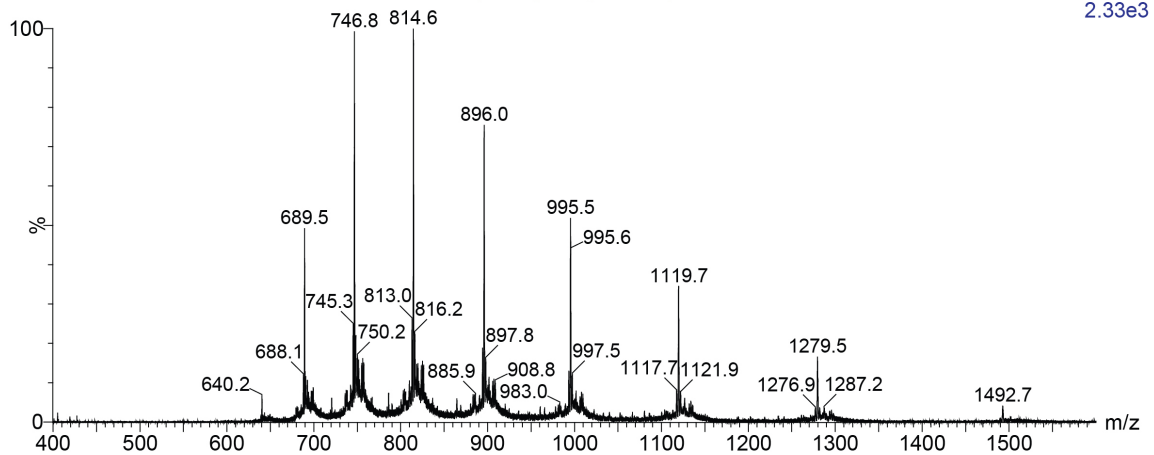


Figure S43. Analytical LC-MS data for Rho-Ub₁₋₇₅-[D₂]-Prg. **A**) Chromatogram. Top; UV chromatogram ($\lambda = 210-800$ nm). Bottom; TIC ($m/z = 100-1600$). **B**) Spectrum of main peak. **C**) Deconvoluted mass: 8885 Da (Found) /8885.20 Da (Calc.).

A EM11-95 RhoUbCC18 100X 10 uL 20201214



B EM11-95 RhoUbCC18 100X 10 uL 20201214 195 (3.456) Cm (192:202)



C EM11-95 RhoUbCC18 100X 10 uL 195 (3.456) M1 [Ev-166270,t43] (Gs,0.750,400:1600,1.00,L33,R33); Cm (192:202)

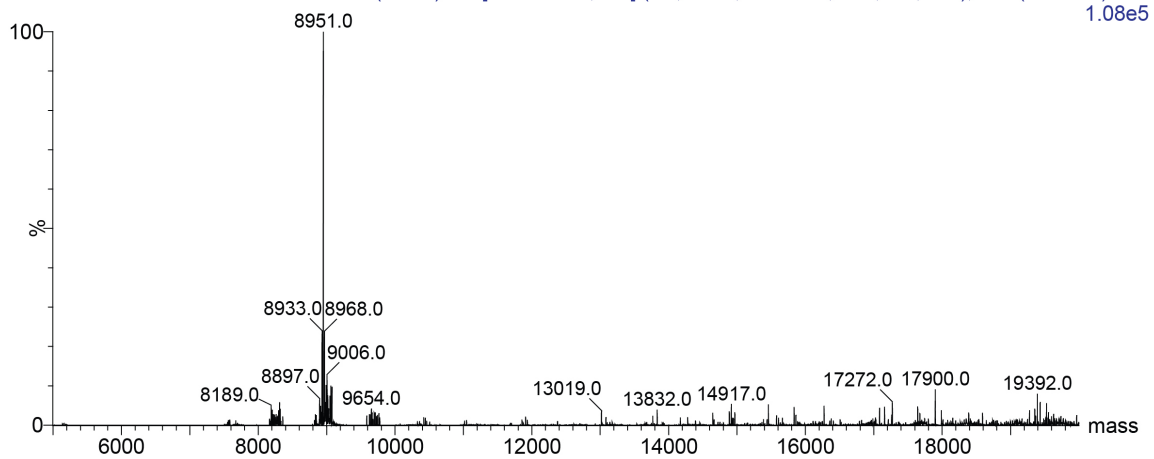
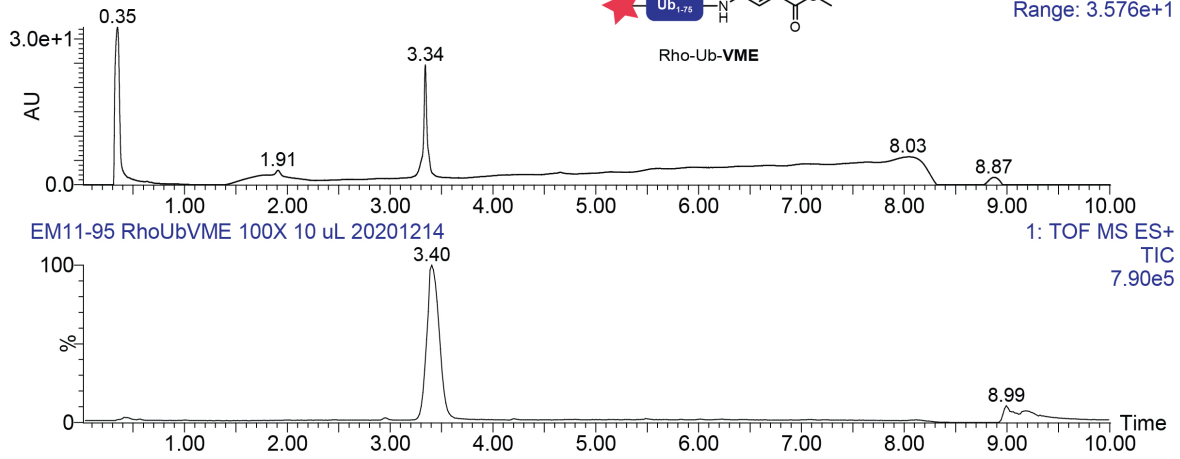
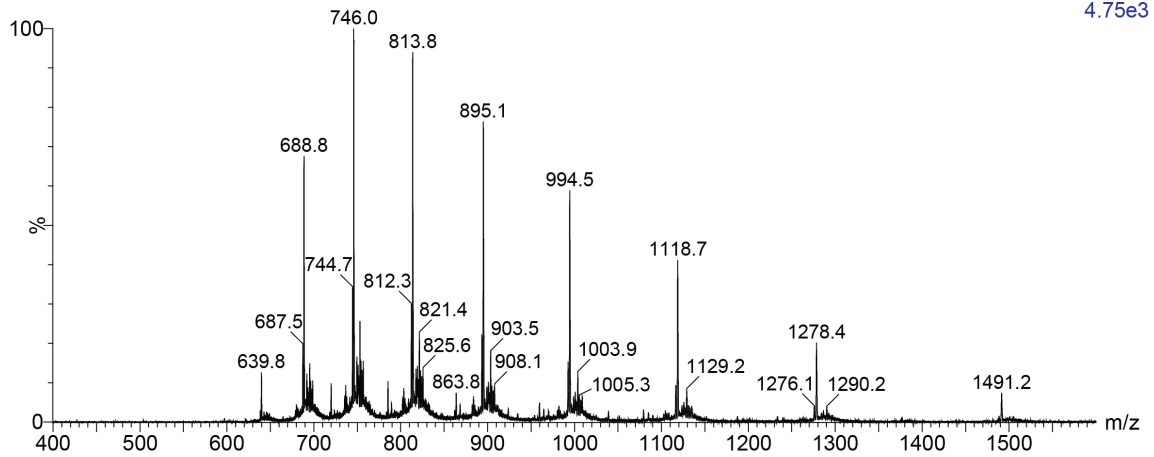


Figure S44. Analytical LC-MS data for Rho-Ub₁₋₇₅-**18**. **A**) Chromatogram. Top; UV chromatogram ($\lambda = 210\text{-}800$ nm). Bottom; TIC ($m/z = 100\text{-}1600$). **B**) Spectrum of main peak. **C**) Deconvoluted mass: 8951 Da (Found)/8951.18 Da (Calc.).

A EM11-95 RhoUbVME 100X 10 uL 20201214



B EM11-95 RhoUbVME 100X 10 uL 20201214 192 (3.405) Cm (189:197)



C EM11-95 RhoUbVME 100X 10 uL 192 (3.405) M1 [Ev-189837,lt47] (Gs,0.750,400:1600,1.00,L33,R33); Cm (189:197)

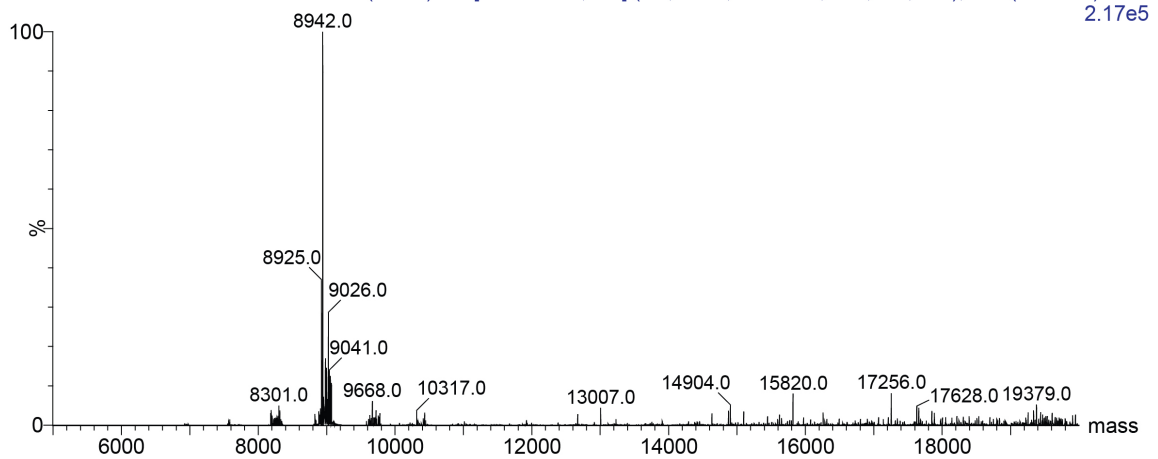


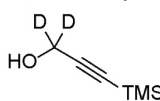
Figure S45. Analytical LC-MS data for Rho-Ub₁₋₇₅-VME. **A**) Chromatogram. Top; UV chromatogram ($\lambda = 210\text{-}800$ nm). Bottom; TIC ($m/z = 100\text{-}1600$). **B**) Spectrum of main peak. **C**) Deconvoluted mass: 8942 Da (Found)/8943.24 Da (Calc.).

Materials and Methods; Chemical Synthesis

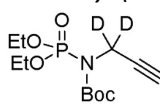
General. All commercially available reagents and solvents were used as purchased. Reported yields are not optimized. Nuclear magnetic resonance (NMR) spectra were recorded on a Bruker Avance 300 (300 MHz for ^1H , 75.00 MHz for ^{13}C) using the residual solvent as internal standard (^1H : 7.26 ppm for CDCl_3 , 2.50 ppm for $\text{DMSO}-d_6$ and 3.31 ppm for MeOD. ^{13}C : 77.16 ppm for CDCl_3 , 39.52 ppm for $\text{DMSO}-d_6$ and 49.00 ppm for MeOD). Chemical shifts (δ) are given in ppm and coupling constants (J) are quoted in hertz (Hz). Resonances are described as s (singlet), d (doublet), t (triplet), q (quartet), p (quintet), b (broad) and m (multiplet) or combinations thereof. The quaternary CD_2 carbon in ^{13}C NMR of deuterated compounds is detected/reported as quintet (p) due to J_{CD} -coupling with ^2D ($n = 2$, splitting pattern $2n+1$). Carbons in vicinity of trifluoromethyl group in ^{13}C NMR are detected/reported as quartet due to J_{CF} -coupling with ^{19}F ($n = 3$, splitting pattern $n+1$, up to $^4J_{\text{CF}}$). Thin Layer Chromatography (TLC) was performed using TLC plates from Merck (SiO_2 , Kieselgel 60 F254 neutral, on aluminum with fluorescence indicator) and compounds were visualized by KMnO_4 or ninhydrin staining. Flash Column Chromatography (FCC) purifications were performed using Grace Davisil Silica Gel (particle size 40–63 μm , pore diameter 60 \AA) and the indicated eluent.

Synthesis of amine [**D**]**-Prg**

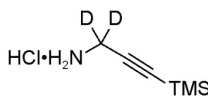
3-(trimethylsilyl)prop-2-yn-1,1- d_2 -1-ol **12**.

 A 1 M solution of lithium aluminum deuteride in diethyl ether (2.2 mL, 2.2 mmol) was cooled to $-78\text{ }^\circ\text{C}$ and diluted with anhydrous diethyl ether (8 mL). After stirring for 1 hour, a solution of ethyl 3-(trimethylsilyl)propiolate (1.0 gr, 5.87 mmol) in anhydrous diethyl ether (2 mL) was added in portions over 1 hour. The mixture was allowed to stir at room temperature for 18 hrs after which the reaction was quenched by addition of 1N aqueous HCl solution (10 mL) and the layers were separated. The aqueous layer was extracted with diethyl ether and the combined organic layers were dried over Na_2SO_4 , filtered and carefully concentrated on a rotary evaporator (850 mbar, $42\text{ }^\circ\text{C}$) to avoid loss of the product. Intermediate **12** was obtained as a pale yellow oil (832 mg, quant.) with some remnant diethyl ether, and used crude in the next step. Spectral data was in agreement with structure and reported data.⁶⁰ TLC $R_f = 0.67$ (1:1 EtOAc/heptane). ^1H NMR (300 MHz, CDCl_3) δ 0.17 (s, 9H). ^{13}C NMR (75 MHz, CDCl_3) δ 104.00, 90.79, 51.26 (p, $J = 22.6$ Hz), -0.07 .

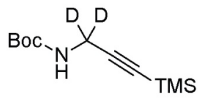
tert-butyl (diethoxyphosphoryl)(3-(trimethylsilyl)prop-2-yn-1-yl-1,1- d_2)carbamate **13**.

 Adjustment of reported procedure for conversion of alcohols into amines under Mitsunobu conditions.⁸ Crude deuterated 3-(trimethylsilyl)propargyl alcohol **12** (5.87 mmol), triphenylphosphine (1.77 gr, 6.74 mmol) and diethyl N-(tert-butoxycarbonyl)phosphoramidate (1.49 gr, 5.87 mmol, 1 eq.) were dissolved in anhydrous THF (30 mL). The reaction mixture was flushed with argon and subsequently cooled to $0\text{ }^\circ\text{C}$. Diisopropyl azodicarboxylate (1.33 mL, 6.74 mmol) was added dropwise to the reaction over 10 minutes. Cooling was removed and the reaction mixture was stirred at room temperature for 18 hrs. The solvent was removed *in vacuo* and the crude reaction mixture containing intermediate **13** was directly submitted to the next step.

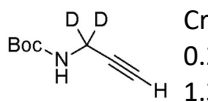
3-(trimethylsilyl)prop-2-yn-1,1-d₂-1-amine hydrochloride **14**.

 Adjustment of reported procedure.² Crude *tert*-butyl (diethoxyphosphoryl)(3-(trimethylsilyl)prop-2-yn-1-yl-1,1-d₂)carbamate **13** was dissolved in anhydrous toluene (40 mL) in a two-neck flask equipped with an inlet for gaseous hydrogen chloride and an outlet toward a strong alkaline solution to neutralize the acidic gas. Hydrogen chloride (g) was generated continuously (*in situ*) by slow dropwise addition of hydrogen chloride (37% aq.) onto powdered calcium chloride in a separate sealed flask, and bubbled through the reaction mixture for 2 hours. Then the reaction mixture was sealed and left to stir overnight. The reaction mixture was filtered, the residue was triturated with diethyl ether (3x) and dried *in vacuo* to give product. Additional product was obtained by removal of solvent from the filtrate *in vacuo*, followed by trituration with diethyl ether and toluene. Intermediate **14** was obtained as a white solid (426 mg, 2.57 mmol, 44% over 3 steps). TLC R_f = 0.21 (5% MeOH/DCM). ¹H NMR (300 MHz, DMSO-*d*₆) δ 8.45 (s, 3H), 0.17 (s, 9H). ¹³C NMR (75 MHz, DMSO-*d*₆) δ 99.00, 91.24, 28.53 (p, *J* = 22.3 Hz), -0.35.

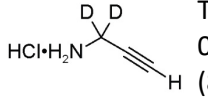
tert-butyl (3-(trimethylsilyl)prop-2-yn-1-yl-1,1-d₂)carbamate **15**.

 To 3-(trimethylsilyl)prop-2-yn-1,1-d₂-1-amine hydrochloride **14** (42.9 mg, 0.26 mmol) were added DCM (0.8 mL) and triethylamine (72 μL, 0.52 mmol, 2 eq.). The suspension was stirred at room temperature for 10 minutes prior to addition of *tert*-butyl dicarbonate (56.5 mg, 0.26 mmol, 1 eq.), and additional triethylamine (72 μL, 0.52 mmol, 2 eq.) in DCM (2 mL). The clear solution was stirred for 60 min (until full conversion of the starting material was detected by TLC) and concentrated by rotary evaporation to give a white solid. The material was treated with ethyl acetate, water and 1N aq. KHSO₄. The organic layer was extracted with saturated aq. NaHCO₃ solution, dried over Na₂SO₄, filtered and concentrated to give a colorless oil (63.4 mg) containing a 2:1 mixture of intermediate **15** with unreacted Boc anhydride. The material was used in the next step without further purification. TLC R_f = 0.87 (5% MeOH/DCM), R_f = 0.72 (1:1 EtOAc/heptane). ¹H NMR (300 MHz, CDCl₃) δ 4.64 (s, 1H), 1.45 (s, 9H), 0.15 (s, 9H).

tert-butyl (prop-2-yn-1-yl-1,1-d₂)carbamate **16**.

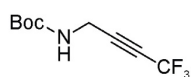
 Crude *tert*-butyl (3-(trimethylsilyl)prop-2-yn-1-yl-1,1-d₂)carbamate **15** (63.4 mg, max. 0.26 mmol) was dissolved in methanol (3 mL), to which potassium carbonate (184 mg, 1.33 mmol, 5 eq.) was added. The suspension was stirred at room temperature for 30 min, when full conversion was detected by TLC analysis. The reaction mixture was diluted with ethyl acetate and water and layers were separated. The organic layer was extracted with water and brine, dried over Na₂SO₄, filtered and carefully concentrated *in vacuo* to give intermediate **16** as a colorless oil (26.4 mg, 0.17 mmol, 65% over 2 steps). Note; Exposure of intermediate **16** to high vacuum for a few minutes can result in significant loss of material. TLC R_f = 0.74 (5% MeOH/DCM), R_f = 0.64 (1:1 EtOAc/heptane). ¹H NMR (300 MHz, CDCl₃) δ 4.73 (s, 1H), 2.20 (s, 1H), 1.44 (s, 9H).

prop-2-yn-1,1-d₂-1-amine hydrochloride [**D**₂]-Prg.

 To a mixture of 3-(trimethylsilyl)prop-2-yn-1,1-d₂-1-amine hydrochloride **14** (20 mg, 0.12 mmol), di-*tert*-butyl dicarbonate (29 mg, 0.13 mmol) and potassium carbonate (83 mg, 0.60 mmol) were added methanol (0.5 mL) and water (0.5 mL). The reaction mixture was stirred at room temperature for 18 hrs, and volatiles (methanol) were removed by rotary evaporation upon reaction completion (as detected by TLC, analytical details for deuterated Boc-propargylamine **16** described above). The reaction mixture was resuspended in ethyl acetate and extracted with water. The organic layer was dried over Na₂SO₄, filtered and carefully concentrated by rotary evaporation. Crude Boc-protected propargylamine **16** was dissolved in methanol (1.5 mL) to which was added 4N hydrogen chloride in dioxane (1 mL, 4 mmol), and the reaction mixture was left to stir 18 hrs. Then the solvent was removed *in vacuo*, and the precipitate was triturated with diethyl ether to obtain hydrochloride salt of deuterated propargylamine [**D**₂]-Prg as a white solid (10 mg, 0.064 mmol, 53%). TLC R_f = 0.02 (5% MeOH/DCM). ¹H NMR (300 MHz, DMSO-*d*₆) δ 8.37 (s, 3H), 3.58 (s, 1H). ¹³C NMR (75 MHz, DMSO-*d*₆) δ 77.84, 76.88, 27.67 (p, *J* = 22.4 Hz).

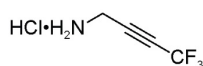
Synthesis of amine **18**

tert-butyl (4,4,4-trifluorobut-2-yn-1-yl)carbamate **17**.



Adjustment of reported procedure for copper(I)-catalyzed trifluoromethylation of terminal alkynes.⁶ A flask was charged with copper(I) iodide (1.43 gr, 7.5 mmol), potassium carbonate (2.07 gr, 15 mmol), tetramethylethylenediamine (1.12 mL, 7.5 mmol) in DMF (23 mL). The dark blue reaction mixture was stirred vigorously under an atmosphere of air at room temperature for 15 min. trimethyl(trifluoromethyl)silane (1.5 mL, 10 mmol) was added and the resulting dark green reaction mixture was stirred for 5 min under air atmosphere prior to cooling to 0 °C. A solution of *N*-*tert*-butoxycarbonyl-1-amino-3-propyne (776 mg, 5 mmol) and trimethyl(trifluoromethyl)silane (1.5 mL, 10 mmol) in DMF (23 mL), already cooled to 0 °C, was added dropwise in 10 min. The reaction mixture was stirred at 0 °C for 30 min under air atmosphere after which the cooling was removed and the dark blue reaction mixture was left to stir at room temperature for 18 hrs. The dark green solution was diluted with water and extracted with diethyl ether (2x). The combined organic layers were extracted with water (2x) and brine, dried over MgSO₄ and filtered. The solution was diluted with DCM and transferred to a pad of Hyflo which was washed with diethyl ether. The mixture was concentrated to give a crude 2:1 mixture of desired product **17** and undesired dimer **19**, which could be separated by FCC (1:4 EtOAc/heptane) to give intermediate **17** as a yellow oil (260.3 mg, 1.2 mmol, 23%). TLC R_f = 0.76 (1:1 EtOAc/heptane). ¹H NMR (300 MHz, CDCl₃) δ 4.80 (s, 1H), 4.06 (s, 2H), 1.46 (s, 9H). ¹³C NMR (75 MHz, CDCl₃) δ 155.12, 113.99 (q, *J* = 257.4 Hz), 84.28 (q, *J* = 6.3 Hz), 80.94, 70.39 (q, *J* = 52.6 Hz), 30.06, 28.40.

4,4,4-trifluorobut-2-yn-1-amine hydrochloride **18**.



To *tert*-butyl (4,4,4-trifluorobut-2-yn-1-yl)carbamate **17** (120 mg, 0.54 mmol) was added 4N HCl in dioxane (2 mL, 8 mmol) and the reaction mixture was stirred for 90 min at room temperature. After 5 minutes a precipitate started to form. Volatiles were removed by rotary evaporation and the material was triturated with diethyl ether to give amine **18** as a white solid (78.1 mg, 0.49 mmol, 91%). TLC R_f = 0.00 (1:1 EtOAc/heptane). ¹H NMR (300 MHz, DMSO-*d*₆) δ = 8.85 (s, 3H), 4.05 (q, *J* = 3.4 Hz, 2H). ¹³C NMR (75 MHz, DMSO-*d*₆) δ = 113.42 (q, *J* = 256.6 Hz), 84.18 (q, *J* = 7.3 Hz), 70.86 (q, *J* = 52.3 Hz), 27.73. Note; product decomposition was observed within a few hours at high concentration in DMSO-*d*₆, therefore NMR measurements of the electrophilic hydrochloride salt was conducted in deuterated methanol. ¹H NMR (300 MHz, MeOD) δ 4.08 (q, *J* = 3.2 Hz, 2H). ¹³C NMR (75 MHz, MeOD) δ 115.05 (q, *J* = 257.1 Hz), 81.91 (q, *J* = 6.3 Hz), 73.77 (q, *J* = 53.5 Hz), 29.36.

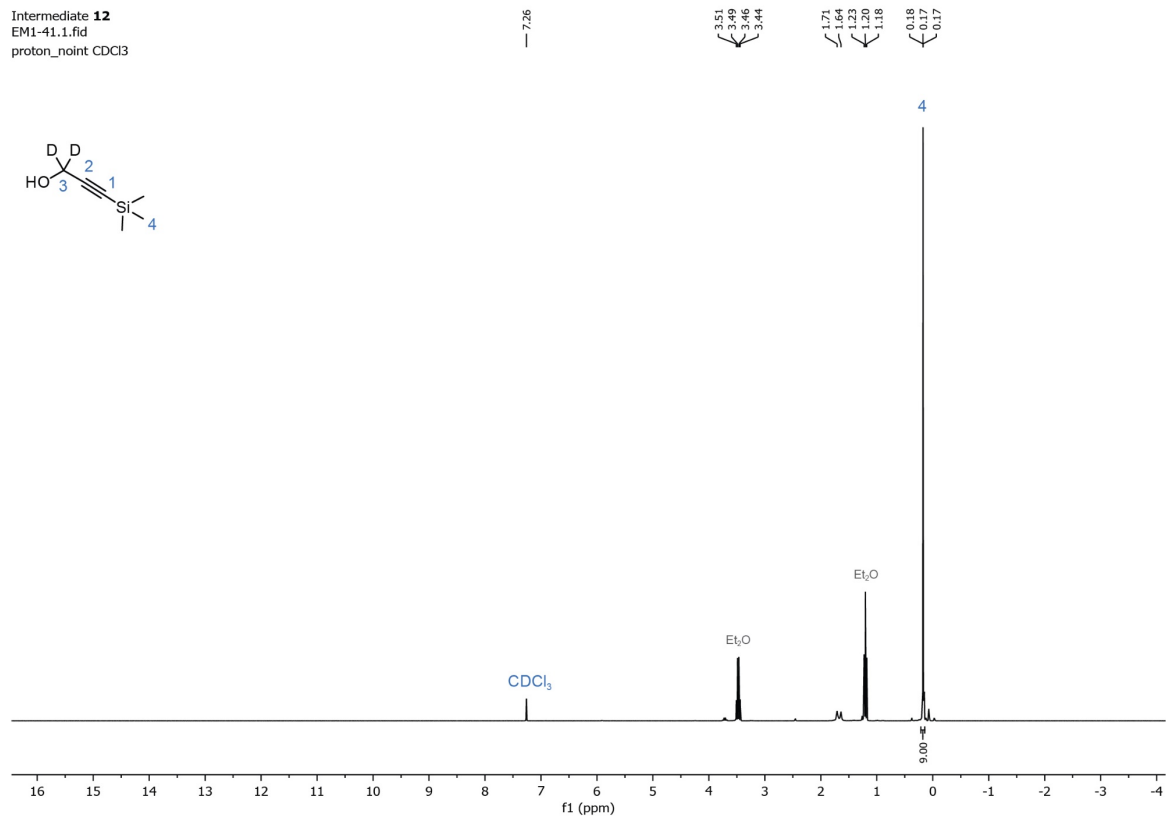
di-*tert*-butyl hexa-2,4-diyne-1,6-diyl dicarbamate **19**.



Dimer **19** is formed as undesired Glaser-Hay product in the copper(I)-catalyzed synthesis of trifluoromethylated alkyne **17** in presence of TMEDA. Dimer **19** was isolated as a colorless oil after separation by FCC (1:4 EtOAc/heptane). TLC R_f = 0.62 (1:1 EtOAc/heptane). ¹H NMR (300 MHz, CDCl₃) δ 4.69 (s, 2H), 3.99 (d, *J* = 5.4 Hz, 4H), 1.44 (s, 18H). ¹³C NMR (75 MHz, CDCl₃) δ 155.22, 80.44, 74.90, 67.47, 31.16, 28.46.

NMR Spectra

Intermediate **12**
EM1-41.1.fid
proton_noint CDCl₃



Intermediate **12**
EM1-41.3.fid
13C-CPD_noint CDCl₃

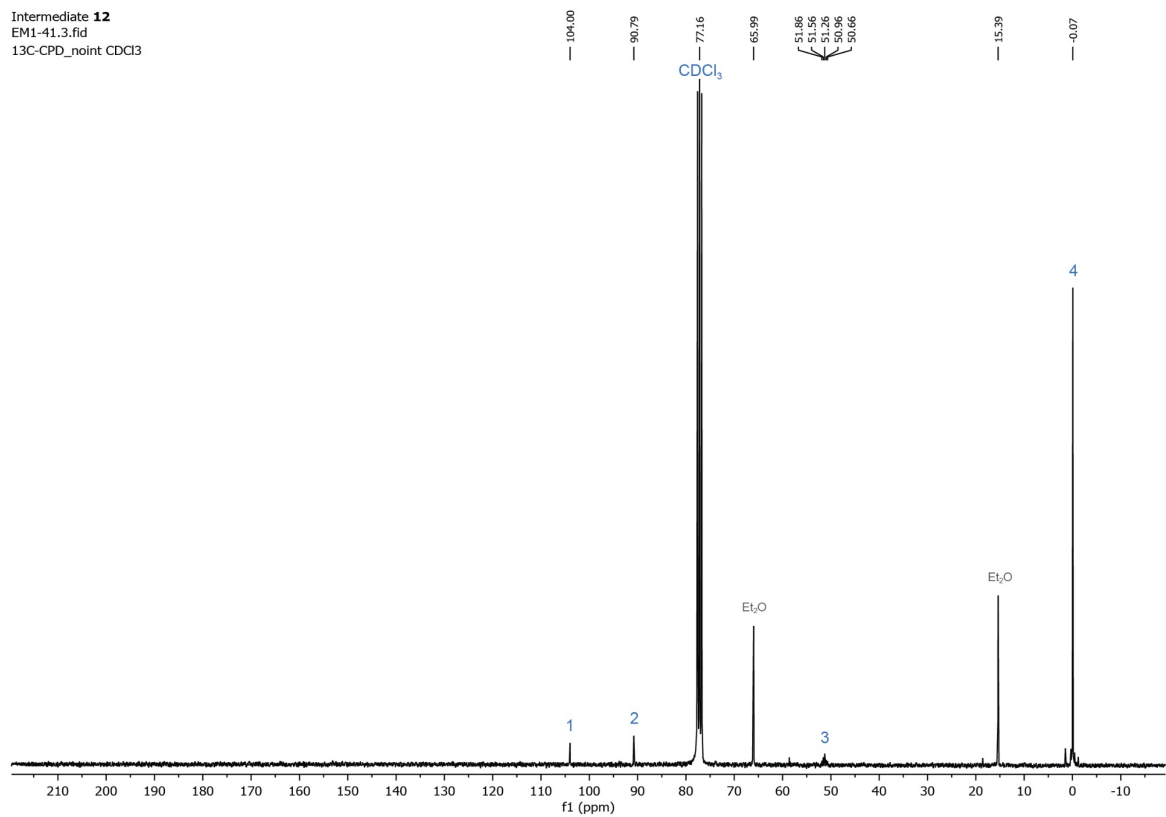
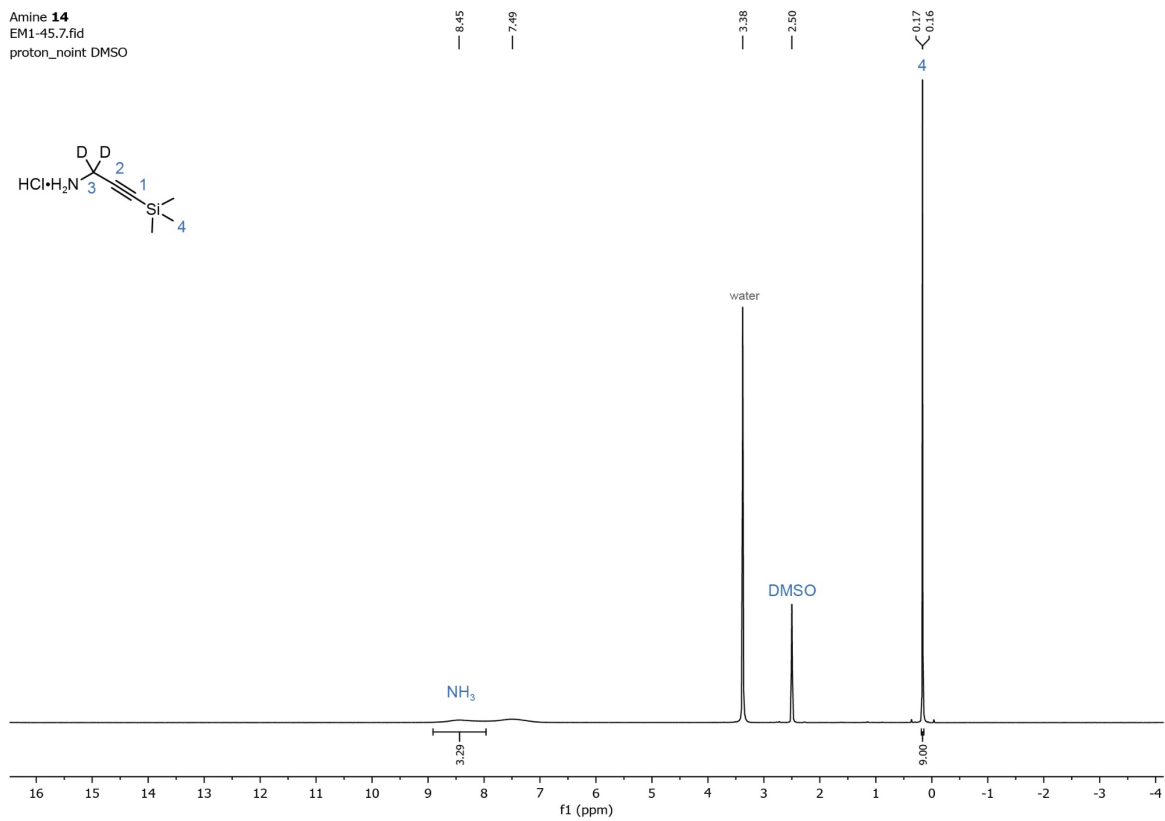


Figure S46. ¹H NMR + ¹³C NMR spectra of crude **12**.

Amine **14**
EM1-45.7.fid
proton_noint DMSO



Amine **14**
EM1-45.8.fid
13C-CPD DMSO

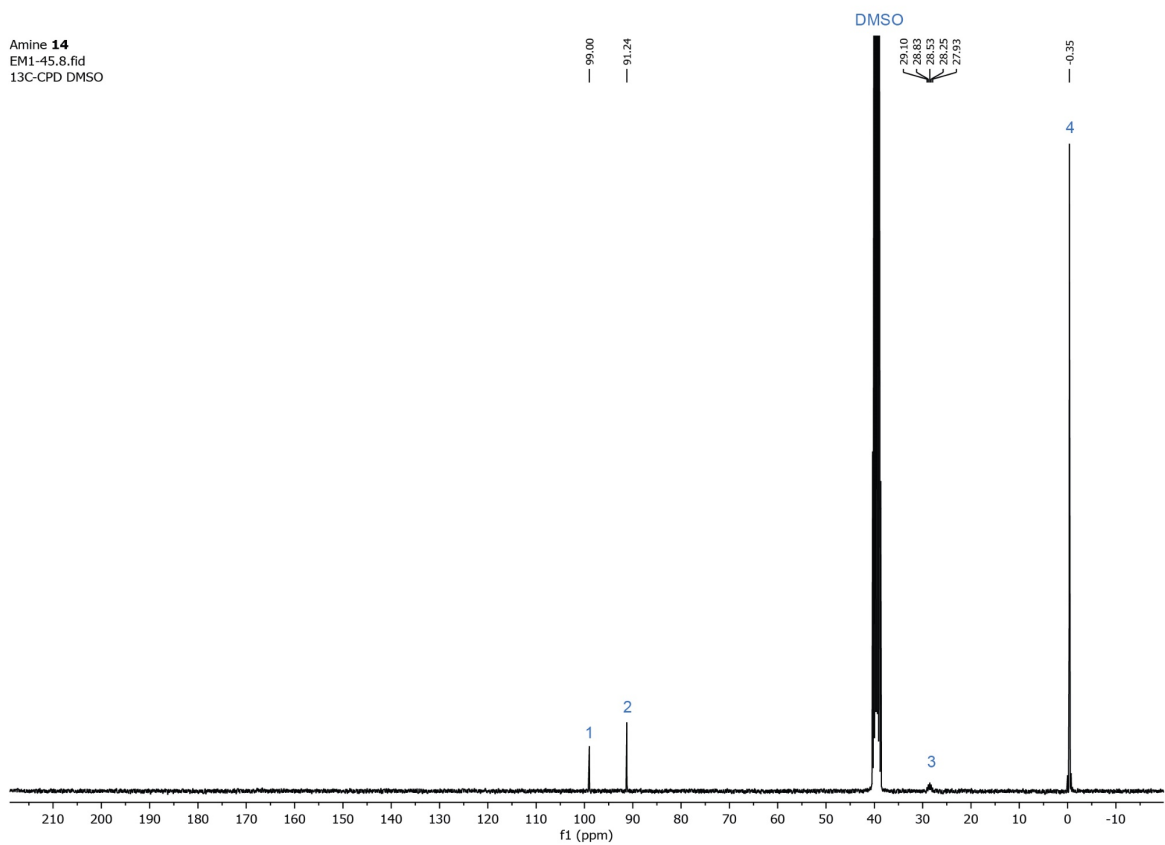


Figure S47. ¹H NMR + ¹³C NMR spectra of **14**.

Intermediate **15**
EM12-02.5.fid
proton_noint CDCl₃

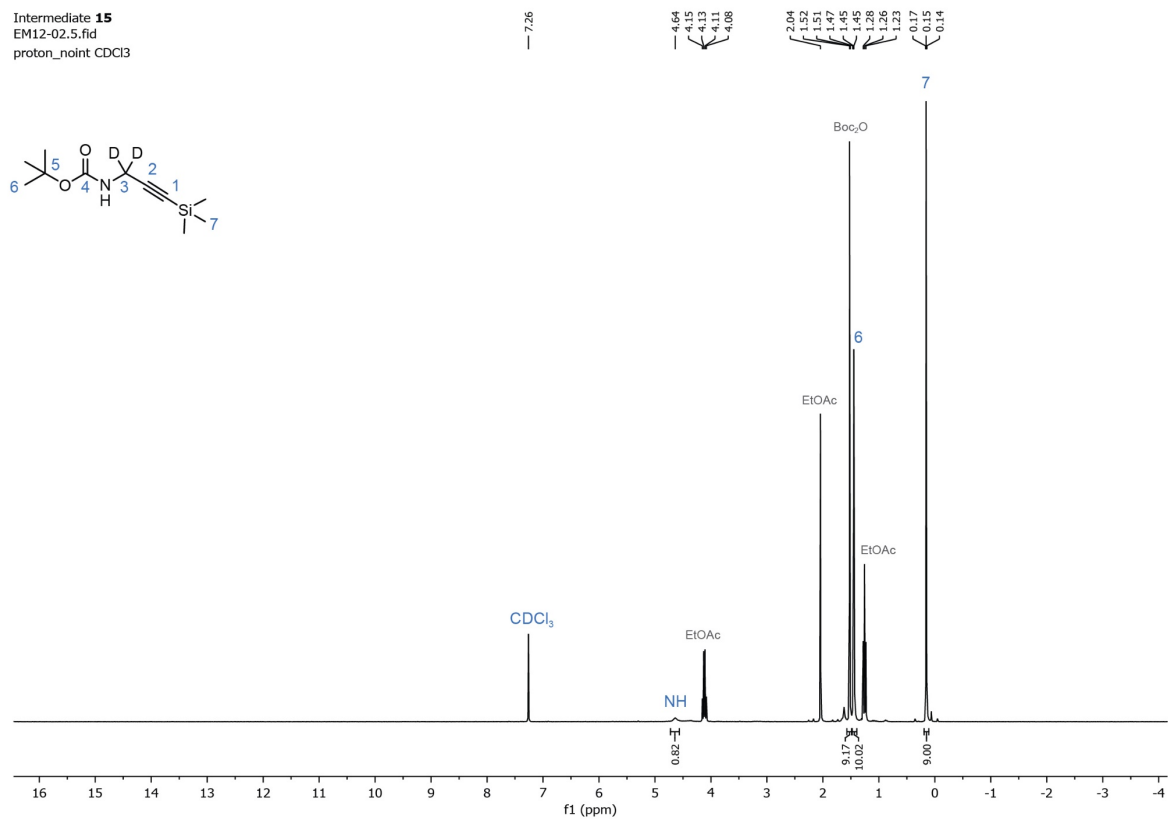


Figure S48. ¹H NMR spectrum of crude **15**.

Intermediate **16**
EM12-03.1.fid
proton_noint CDCl₃

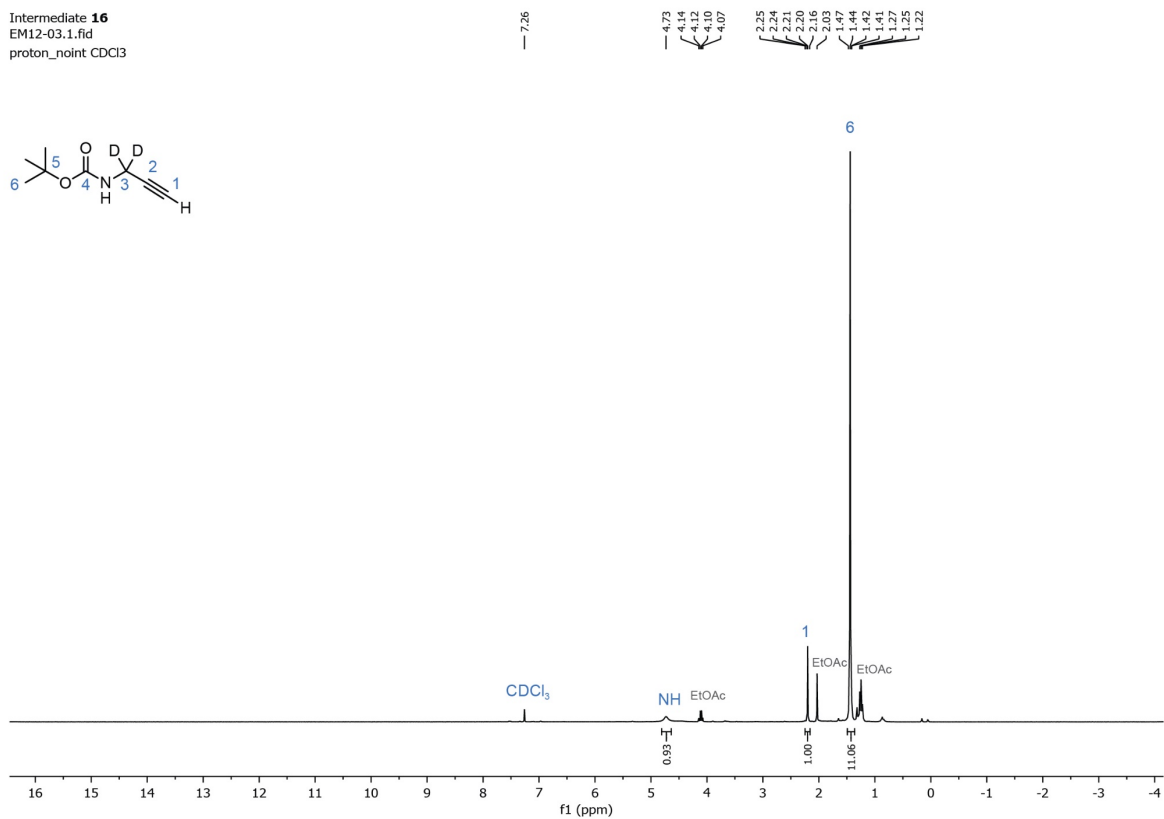
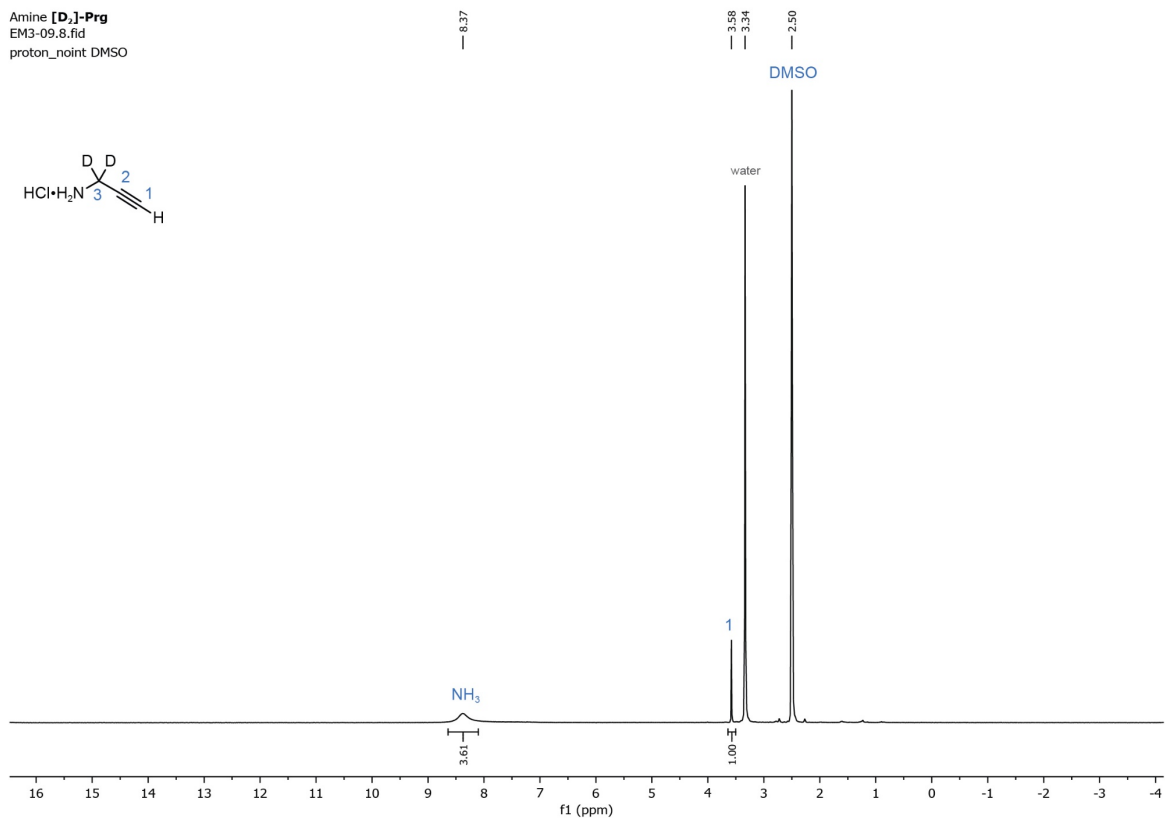


Figure S49. ¹H NMR spectrum of crude **16**.

Amine [D₂]-Prg
EM3-09.8.fid
proton_noint DMSO



Amine [D₂]-Prg
EM12-05.3.fid
13C-CPD_noint DMSO

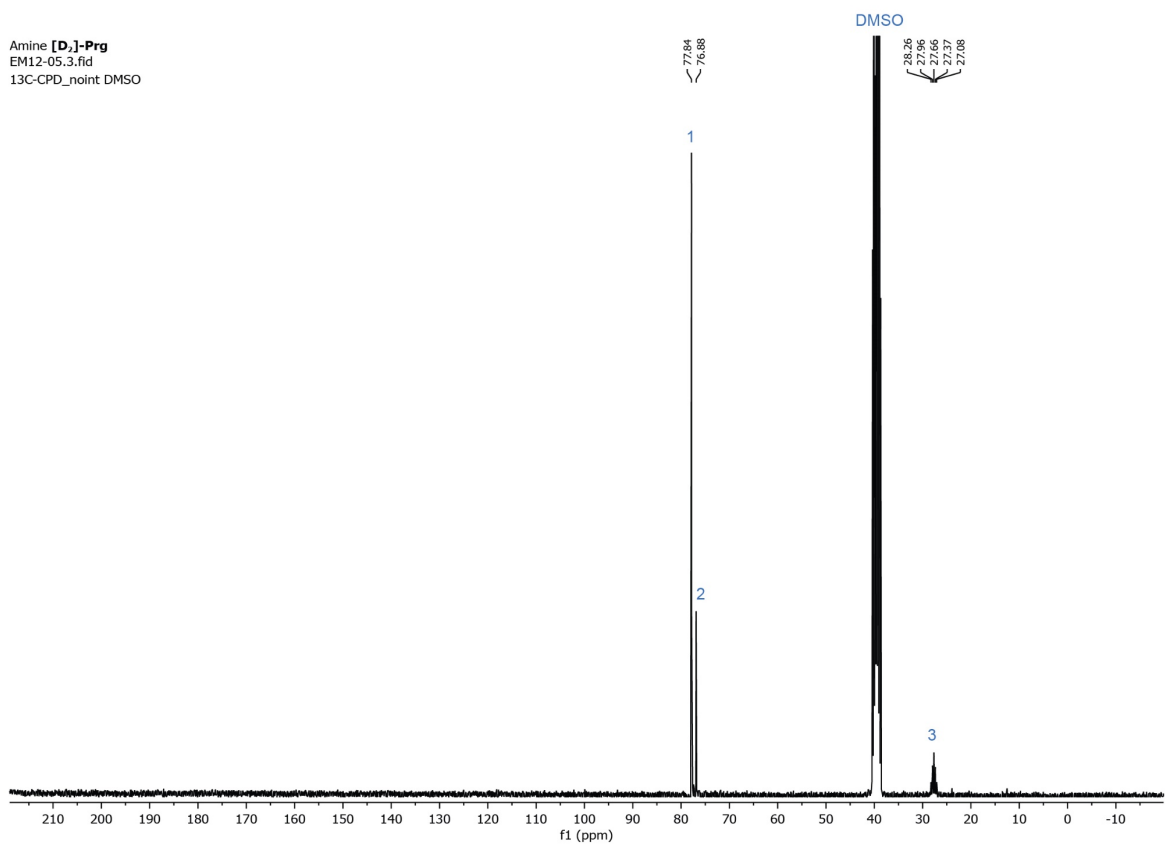
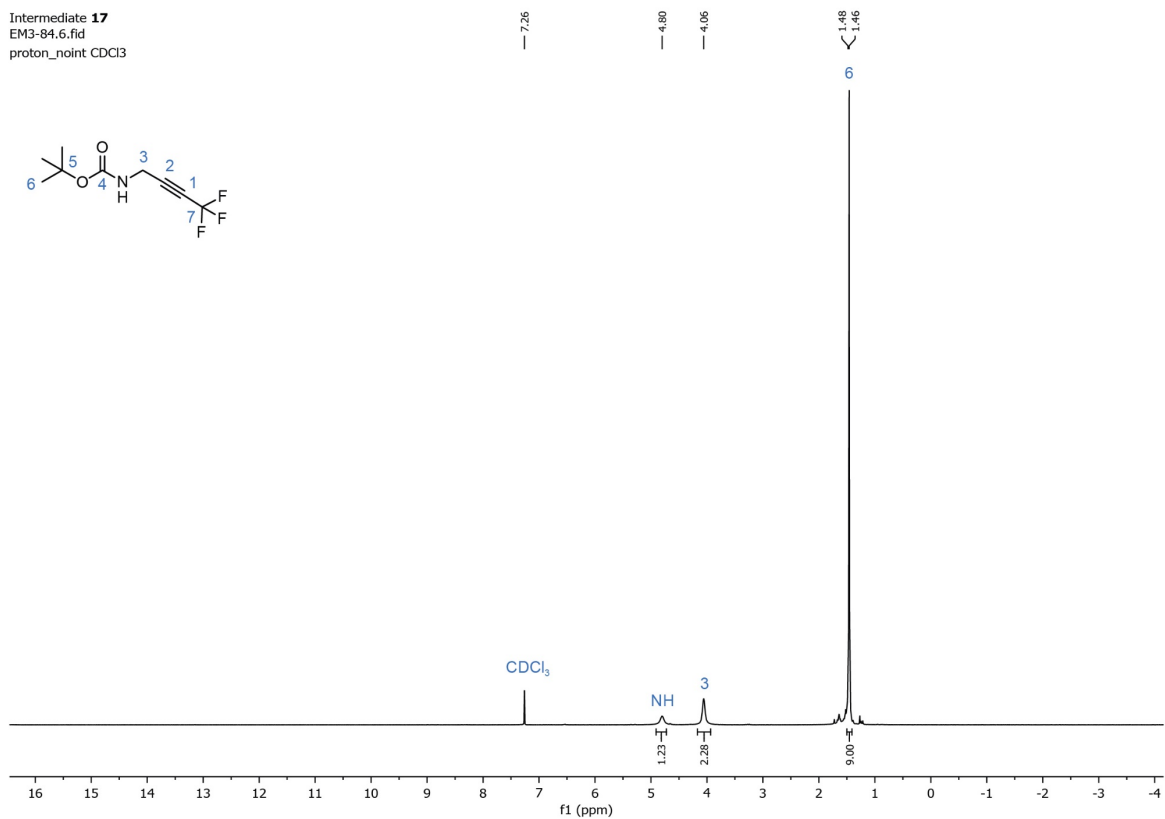


Figure S50. ¹H NMR + ¹³C NMR spectra of [D₂]-Prg.

Intermediate **17**
EM3-84.6.fid
proton_noint CDCl₃



Intermediate **17**
EM3-84.7.fid
13C-CPD_noint CDCl₃

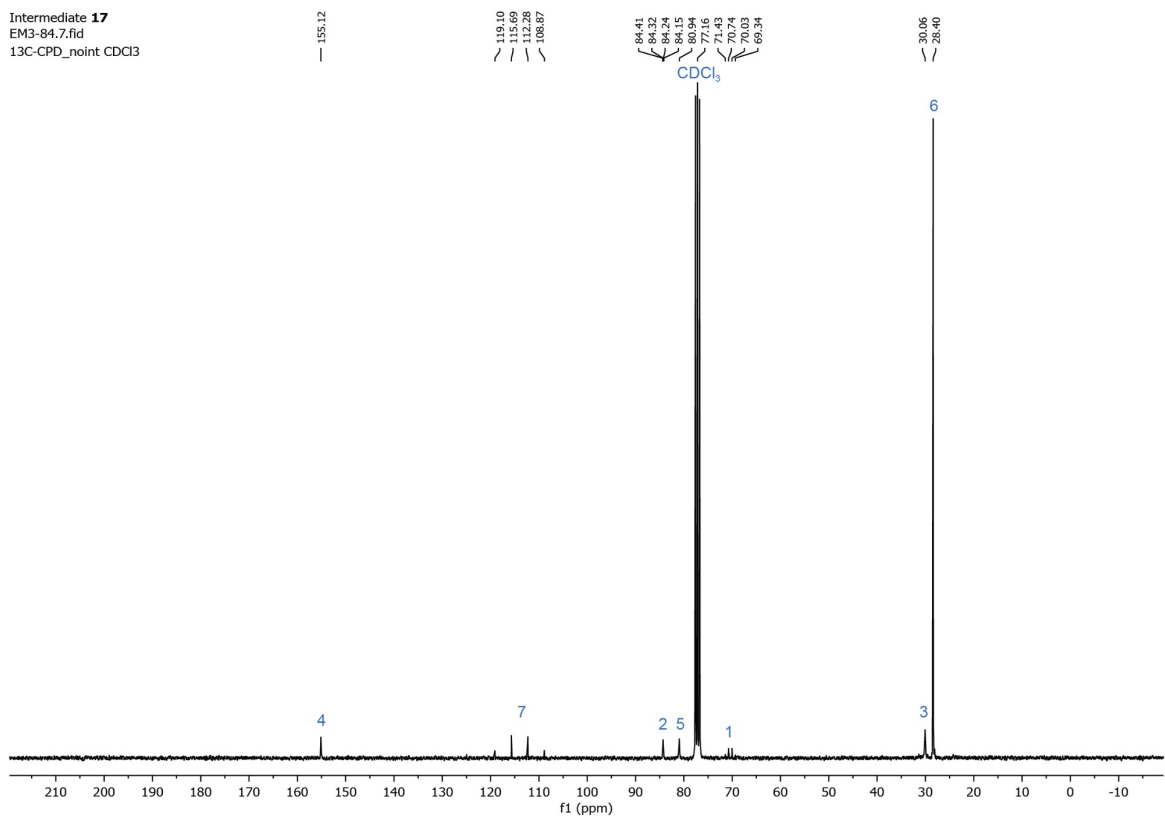
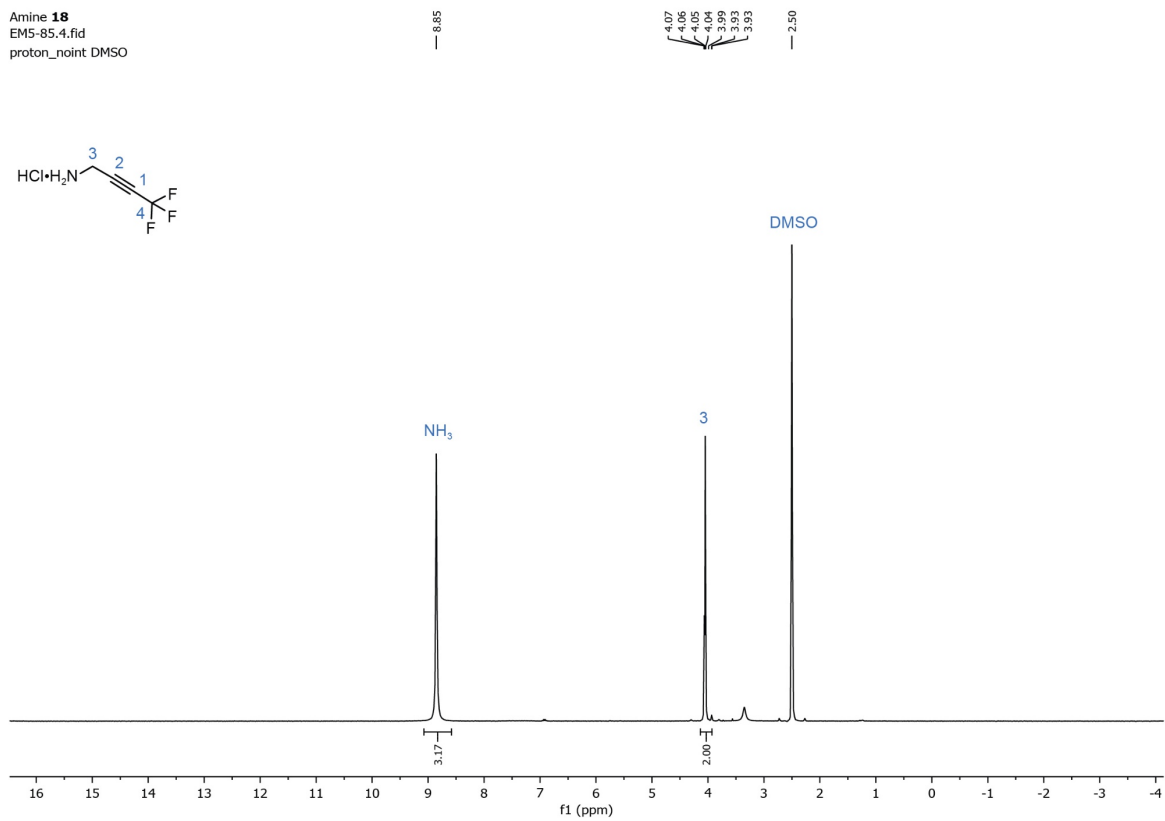


Figure S51. ¹H NMR + ¹³C NMR spectra of **17**.

Amine **18**
EMS-85.4.fid
proton_noint DMSO



Amine **18**
EMS-85.5.fid
13C-CPD DMSO

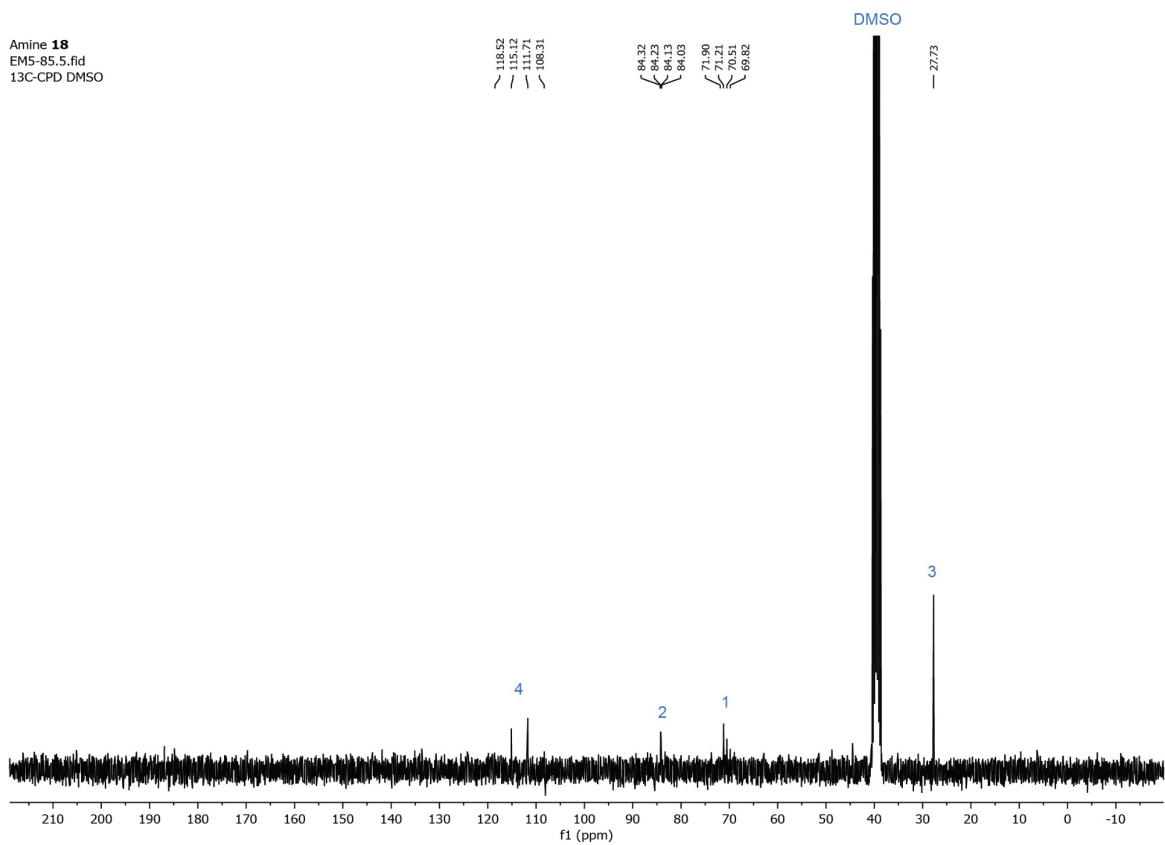
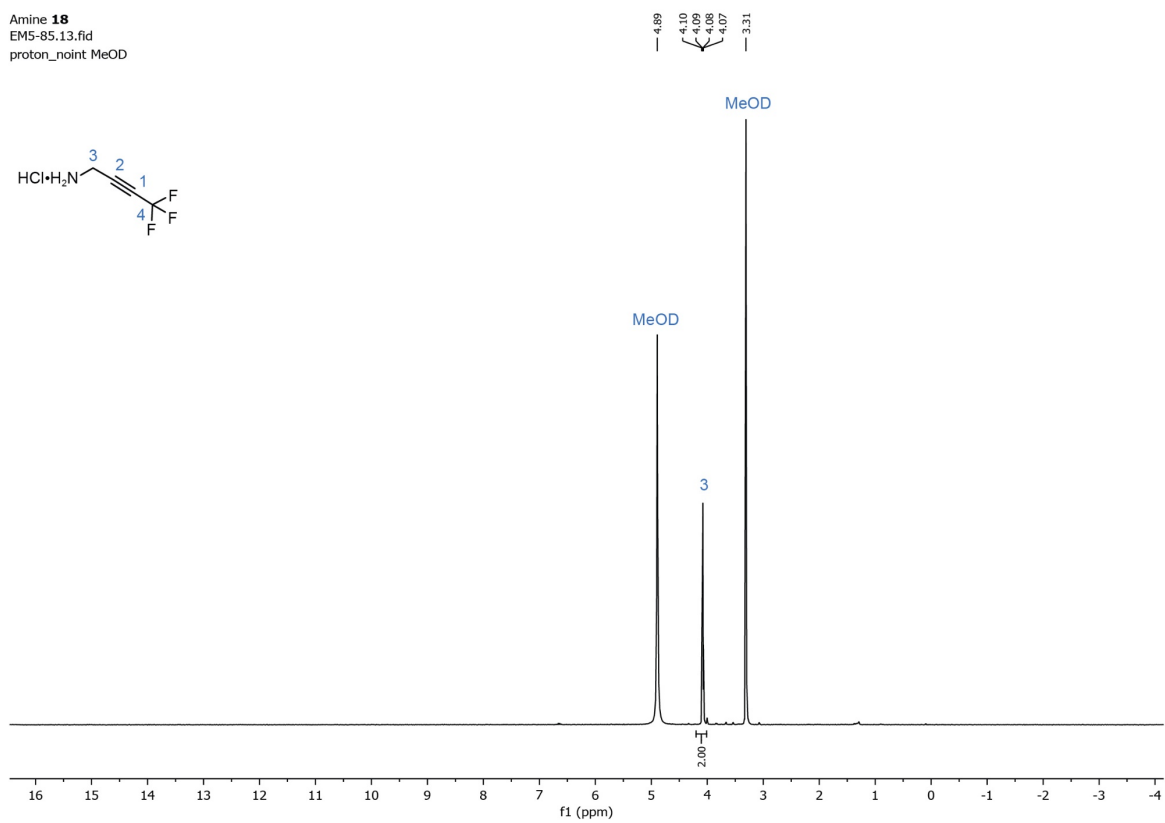


Figure S52. ¹H NMR + ¹³C NMR spectra of **18** in DMSO-d₆.

Amine **18**
EM5-85.13.fid
proton_noint MeOD



Amine **18**
EM5-85.12.fid
13C-CPD_noint MeOD

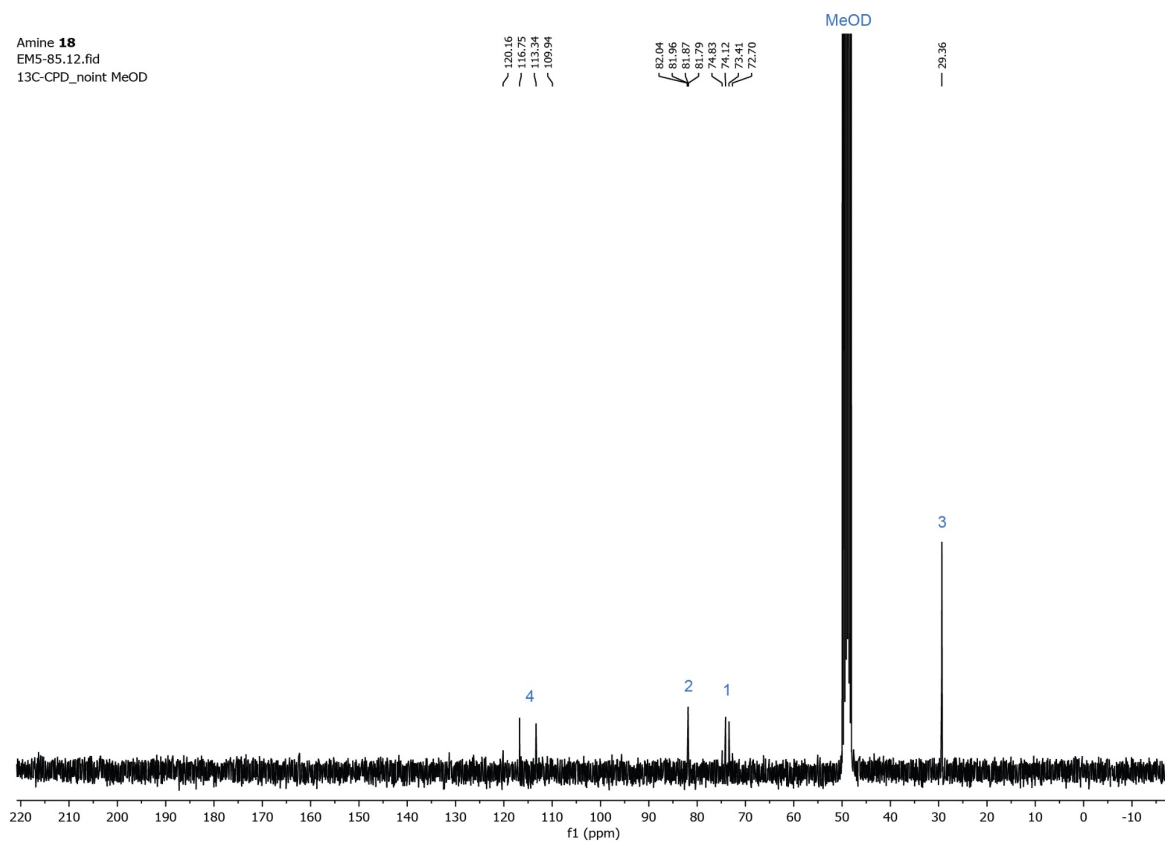
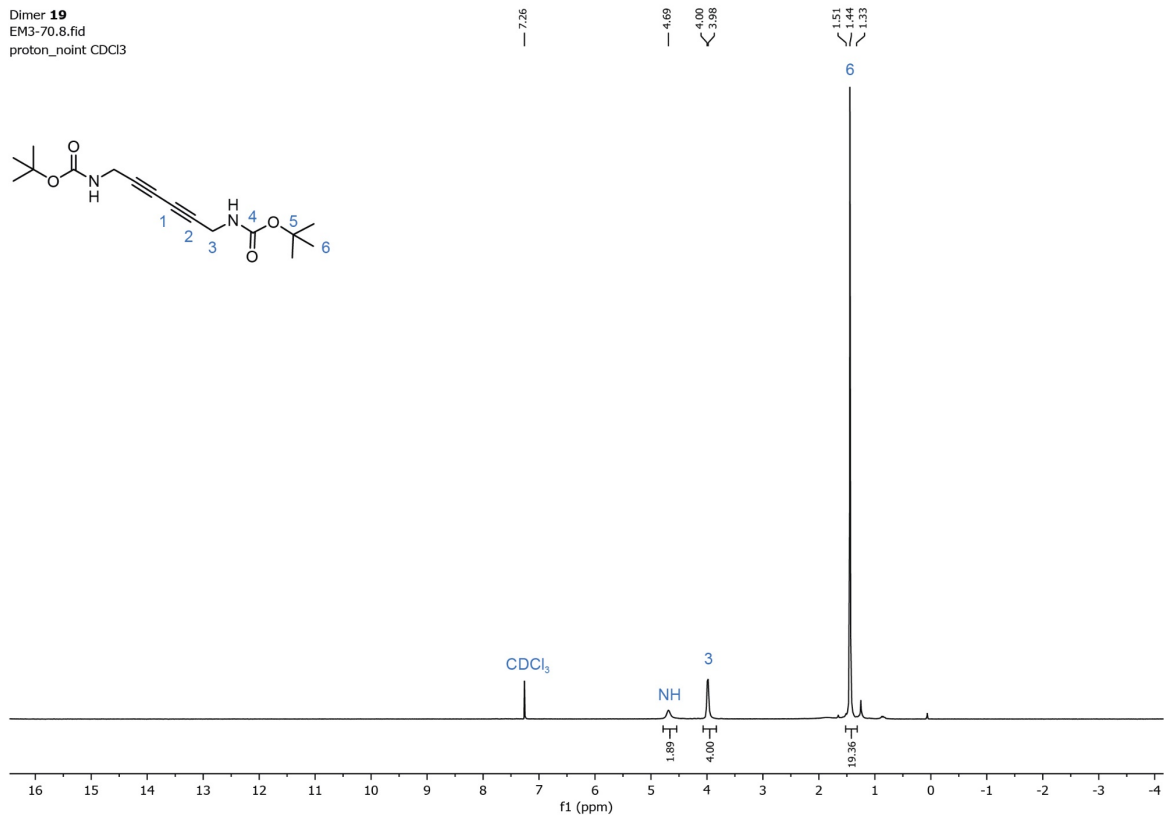


Figure S53. ^1H NMR + ^{13}C NMR spectra of **18** in MeOD.

Dimer **19**
EM3-70.8.fid
proton_noint CDCl₃



Dimer **19**
EM3-70.9.fid
13C-CPD_noint CDCl₃

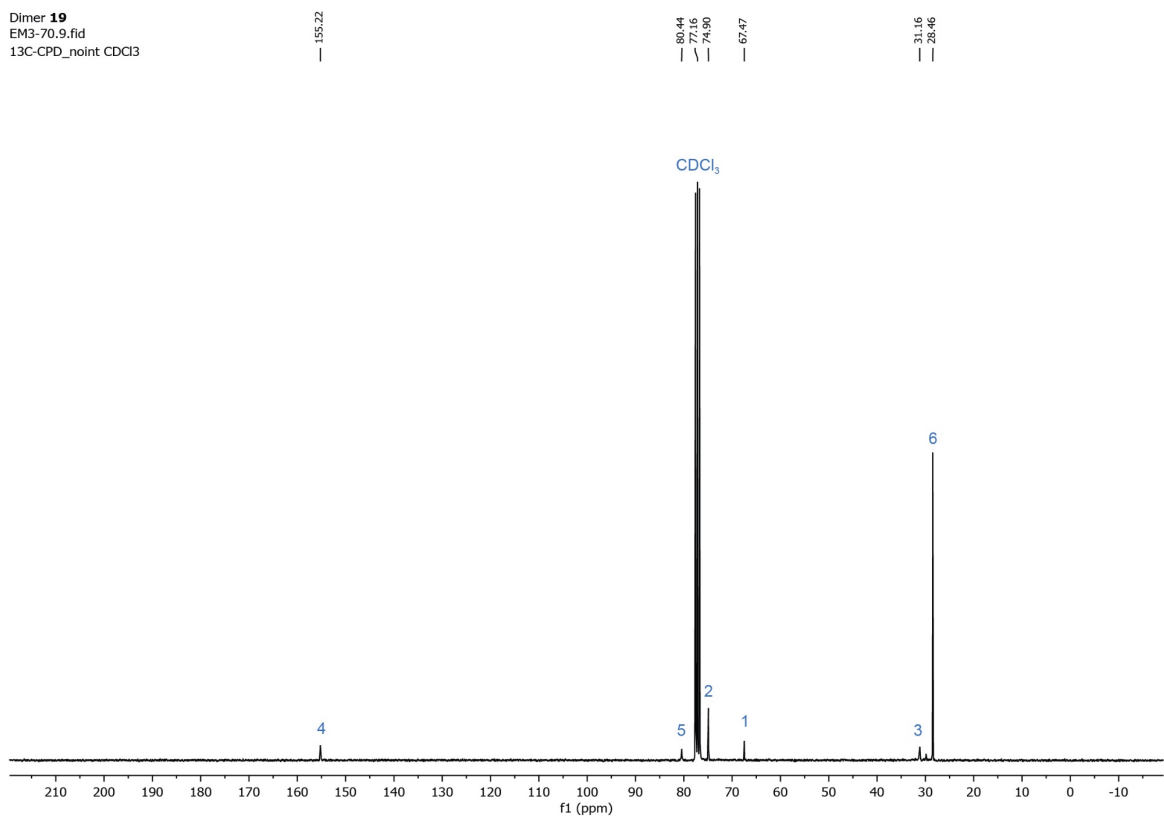


Figure S54. ¹H NMR + ¹³C NMR spectra of **19**.

References

1. El Oualid, F.; Merckx, R.; Ekkebus, R.; Hameed, D. S.; Smit, J. J.; de Jong, A.; Hilkmann, H.; Sixma, T. K.; Ovaa, H. Chemical Synthesis of Ubiquitin, Ubiquitin-Based Probes, and Diubiquitin. *Angew. Chem. Int. Ed.* **2010**, *49* (52), 10149-10153.
2. Ekkebus, R.; van Kasteren, S. I.; Kulathu, Y.; Scholten, A.; Berlin, I.; Geurink, P. P.; de Jong, A.; Goerdalay, S.; Neefjes, J.; Heck, A. J. R.; Komander, D.; Ovaa, H. On Terminal Alkynes That Can React with Active-Site Cysteine Nucleophiles in Proteases. *J. Am. Chem. Soc.* **2013**, *135* (8), 2867-2870.
3. Altun, M.; Kramer, H. B.; Willems, L. I.; McDermott, J. L.; Leach, C. A.; Goldenberg, S. J.; Kumar, K. G. S.; Konietzny, R.; Fischer, R.; Kogan, E.; Mackeen, M. M.; McGouran, J.; Khoronenkova, S. V.; Parsons, J. L.; Dianov, G. L.; Nicholson, B.; Kessler, B. M. Activity-Based Chemical Proteomics Accelerates Inhibitor Development for Deubiquitylating Enzymes. *Chem. Biol.* **2011**, *18* (11), 1401-1412.
4. Borodovsky, A.; Ovaa, H.; Kolli, N.; Gan-Erdene, T.; Wilkinson, K. D.; Ploegh, H. L.; Kessler, B. M. Chemistry-Based Functional Proteomics Reveals Novel Members of the Deubiquitinating Enzyme Family. *Chem. Biol.* **2002**, *9* (10), 1149-1159.
5. Gjonaj, L.; Sapmaz, A.; Flierman, D.; Janssen, G. M. C.; van Veelen, P. A.; Ovaa, H. Development of a DUB-selective fluorogenic substrate. *Chem. Sci.* **2019**, *10* (44), 10290-10296.
6. Tresse, C.; Guissart, C.; Schweizer, S.; Bouhoute, Y.; Chany, A.-C.; Goddard, M.-L.; Blanchard, N.; Evano, G. Practical Methods for the Synthesis of Trifluoromethylated Alkynes: Oxidative Trifluoromethylation of Copper Acetylides and Alkynes. *Adv. Synth. Catal.* **2014**, *356* (9), 2051-2060.
7. de Jong, A.; Merckx, R.; Berlin, I.; Rodenko, B.; Wijdeven, R. H. M.; El Atmioui, D.; Yalçin, Z.; Robson, C. N.; Neefjes, J. J.; Ovaa, H. Ubiquitin-Based Probes Prepared by Total Synthesis To Profile the Activity of Deubiquitinating Enzymes. *ChemBioChem* **2012**, *13* (15), 2251-2258.
8. Klepacz, A.; Zwierzak, A. New protocol for converting alcohols into amines. *Synth. Commun.* **2001**, *31* (11), 1683-1689.
9. Dharadhar, S.; Clerici, M.; van Dijk, W. J.; Fish, A.; Sixma, T. K. A conserved two-step binding for the UAF1 regulator to the USP12 deubiquitinating enzyme. *J. Struct. Biol.* **2016**, *196* (3), 437-447.
10. Gersch, M.; Wagstaff, J. L.; Toms, A. V.; Graves, B.; Freund, S. M. V.; Komander, D. Distinct USP25 and USP28 Oligomerization States Regulate Deubiquitinating Activity. *Mol. Cell* **2019**, *74* (3), 436-451.e7.
11. Sauer, F.; Klemm, T.; Kollampally, R. B.; Tessmer, I.; Nair, R. K.; Popov, N.; Kisker, C. Differential Oligomerization of the Deubiquitinases USP25 and USP28 Regulates Their Activities. *Mol. Cell* **2019**, *74* (3), 421-435.e10.
12. Gersch, M.; Gladkova, C.; Schubert, A. F.; Michel, M. A.; Maslen, S.; Komander, D. Mechanism and regulation of the Lys6-selective deubiquitinase USP30. *Nat. Struct. Mol. Biol.* **2017**, *24* (11), 920-930.
13. Sahtoe, D. D.; van Dijk, W. J.; El Oualid, F.; Ekkebus, R.; Ovaa, H.; Sixma, T. K. Mechanism of UCH-L5 Activation and Inhibition by DEUBAD Domains in RPN13 and INO80G. *Mol. Cell* **2015**, *57* (5), 887-900.
14. Mevissen, T. E. T.; Kulathu, Y.; Mulder, M. P. C.; Geurink, P. P.; Maslen, S. L.; Gersch, M.; Elliott, P. R.; Burke, J. E.; van Tol, B. D. M.; Akutsu, M.; El Oualid, F.; Kawasaki, M.; Freund, S. M. V.; Ovaa, H.; Komander, D. Molecular basis of Lys11-polyubiquitin specificity in the deubiquitinase Cezanne. *Nature* **2016**, *538* (7625), 402-405.
15. Hermanns, T.; Pichlo, C.; Woiwode, I.; Klopffleisch, K.; Witting, K. F.; Ovaa, H.; Baumann, U.; Hofmann, K. A family of unconventional deubiquitinases with modular chain specificity determinants. *Nat. Commun.* **2018**, *9* (1), 799.
16. Kwasna, D.; Abdul Rehman, S. A.; Natarajan, J.; Matthews, S.; Madden, R.; De Cesare, V.; Weidlich, S.; Virdee, S.; Ahel, I.; Gibbs-Seymour, I.; Kulathu, Y. Discovery and Characterization of ZUFSP/ZUP1, a Distinct Deubiquitinase Class Important for Genome Stability. *Mol. Cell* **2018**, *70* (1), 150-164.e6.
17. Abdul Rehman, S. A.; Kristariyanto, Y. A.; Choi, S.-Y.; Nkosi, P. J.; Weidlich, S.; Labib, K.; Hofmann, K.; Kulathu, Y. MINDY-1 Is a Member of an Evolutionarily Conserved and Structurally Distinct New Family of Deubiquitinating Enzymes. *Mol. Cell* **2016**, *63* (1), 146-155.
18. Basters, A.; Geurink, P. P.; Röcker, A.; Witting, K. F.; Tadayon, R.; Hess, S.; Semrau, M. S.; Storic, P.; Ovaa, H.; Knobloch, K.-P.; Fritz, G. Structural basis of the specificity of USP18 toward ISG15. *Nat. Struct. Mol. Biol.* **2017**, *24* (3), 270-278.
19. Békés, M.; van der Heden van Noort, G. J.; Ekkebus, R.; Ovaa, H.; Huang, T. T.; Lima, C. D. Recognition of Lys48-Linked Di-ubiquitin and Deubiquitinating Activities of the SARS Coronavirus Papain-like Protease. *Mol. Cell* **2016**, *62* (4), 572-585.
20. Dackowski, C. M.; Dzimianski, J. V.; Clasman, J. R.; Goodwin, O.; Mesecar, A. D.; Pegan, S. D. Structural Insights into the Interaction of Coronavirus Papain-Like Proteases and Interferon-Stimulated Gene Product 15 from Different Species. *J. Mol. Biol.* **2017**, *429* (11), 1661-1683.

21. Daczkowski, C. M.; Goodwin, O. Y.; Dzimianski, J. V.; Farhat, J. J.; Pegan, S. D. Structurally Guided Removal of DeISGylase Biochemical Activity from Papain-Like Protease Originating from Middle East Respiratory Syndrome Coronavirus. *J. Virol.* **2017**, *91* (23), e01067-17.
22. Clasman, J. R.; Everett, R. K.; Srinivasan, K.; Mesecar, A. D. Decoupling deISGylating and deubiquitinating activities of the MERS virus papain-like protease. *Antiviral Res.* **2020**, *174*, 104661.
23. Klemm, T.; Ebert, G.; Calleja, D. J.; Allison, C. C.; Richardson, L. W.; Bernardini, J. P.; Lu, B. G. C.; Kuchel, N. W.; Grohmann, C.; Shibata, Y.; Gan, Z. Y.; Cooney, J. P.; Doerflinger, M.; Au, A. E.; Blackmore, T. R.; van der Heden van Noort, G. J.; Geurink, P. P.; Ovaa, H.; Newman, J.; Riboldi-Tunncliffe, A.; Czabotar, P. E.; Mitchell, J. P.; Feltham, R.; Lechtenberg, B. C.; Lowes, K. N.; Dewson, G.; Pellegrini, M.; Lessene, G.; Komander, D. Mechanism and inhibition of the papain-like protease, PLpro, of SARS-CoV-2. *EMBO J.* **2020**, *39* (18), e106275.
24. Dzimianski, J. V.; Scholte, F. E. M.; Williams, I. L.; Langley, C.; Freitas, B. T.; Spengler, J. R.; Bergeron, É.; Pegan, S. D. Determining the molecular drivers of species-specific interferon-stimulated gene product 15 interactions with nairovirus ovarian tumor domain proteases. *PLoS One* **2019**, *14* (12), e0226415.
25. Swatek, K. N.; Aumayr, M.; Pruneda, J. N.; Visser, L. J.; Berryman, S.; Kueck, A. F.; Geurink, P. P.; Ovaa, H.; van Kuppeveld, F. J. M.; Tuthill, T. J.; Skern, T.; Komander, D. Irreversible inactivation of ISG15 by a viral leader protease enables alternative infection detection strategies. *Proc. Natl. Acad. Sci.* **2018**, *115* (10), 2371-2376.
26. Deaton, M. K.; Dzimianski, J. V.; Daczkowski, C. M.; Whitney, G. K.; Mank, N. J.; Parham, M. M.; Bergeron, E.; Pegan, S. D. Biochemical and Structural Insights into the Preference of Nairoviral DeISGylases for Interferon-Stimulated Gene Product 15 Originating from Certain Species. *J. Virol.* **2016**, *90* (18), 8314-8327.
27. Dzimianski, J. V.; Mace, S. L.; Williams, I. L.; Freitas, B. T.; Pegan, S. D. Flipping the substrate preference of Hazara virus ovarian tumour domain protease through structure-based mutagenesis. *Acta Crystallogr., Sect. D* **2020**, *76* (11), 1114-1123.
28. Pruneda, J. N.; Durkin, C. H.; Geurink, P. P.; Ovaa, H.; Santhanam, B.; Holden, D. W.; Komander, D. The Molecular Basis for Ubiquitin and Ubiquitin-like Specificities in Bacterial Effector Proteases. *Mol. Cell* **2016**, *63* (2), 261-276.
29. Liu, S.; Luo, J.; Zhen, X.; Qiu, J.; Ouyang, S.; Luo, Z.-Q. Interplay between bacterial deubiquitinase and ubiquitin E3 ligase regulates ubiquitin dynamics on Legionella phagosomes. *eLife* **2020**, *9*, e58114.
30. Ramirez, Y. A.; Adler, T. B.; Altmann, E.; Klemm, T.; Tiesmeyer, C.; Sauer, F.; Kathman, S. G.; Statsyuk, A. V.; Sotriffer, C.; Kisker, C. Structural Basis of Substrate Recognition and Covalent Inhibition of Cdu1 from Chlamydia trachomatis. *ChemMedChem* **2018**, *13* (19), 2014-2023.
31. Pruneda, J. N.; Bastidas, R. J.; Bertsoulaki, E.; Swatek, K. N.; Santhanam, B.; Clague, M. J.; Valdivia, R. H.; Urbé, S.; Komander, D. A Chlamydia effector combining deubiquitination and acetylation activities induces Golgi fragmentation. *Nat. Microbiol.* **2018**, *3* (12), 1377-1384.
32. Hausman, J. M.; Kenny, S.; Iyer, S.; Babar, A.; Qiu, J.; Fu, J.; Luo, Z.-Q.; Das, C. The Two Deubiquitinating Enzymes from Chlamydia trachomatis Have Distinct Ubiquitin Recognition Properties. *Biochemistry* **2020**, *59* (16), 1604-1617.
33. Mons, E.; Jansen, I. D. C.; Loboda, J.; van Doodewaerd, B. R.; Hermans, J.; Verdoes, M.; van Boeckel, C. A. A.; van Veelen, P. A.; Turk, B.; Turk, D.; Ovaa, H. The Alkyne Moiety as a Latent Electrophile in Irreversible Covalent Small Molecule Inhibitors of Cathepsin K. *J. Am. Chem. Soc.* **2019**, *141* (8), 3507-3514.
34. Wang, T.; Yin, L.; Cooper, E. M.; Lai, M.-Y.; Dickey, S.; Pickart, C. M.; Fushman, D.; Wilkinson, K. D.; Cohen, R. E.; Wolberger, C. Evidence for Bidentate Substrate Binding as the Basis for the K48 Linkage Specificity of Otubain 1. *J. Mol. Biol.* **2009**, *386* (4), 1011-1023.
35. Nanao, M. H.; Tcherniuk, S. O.; Chroboczek, J.; Dideberg, O.; Dessen, A.; Balakirev, M. Y. Crystal structure of human otubain 2. *EMBO Rep.* **2004**, *5* (8), 783-788.
36. Mevissen, T. E. T.; Hospenthal, M. K.; Geurink, P. P.; Elliott, P. R.; Akutsu, M.; Arnaudo, N.; Ekkebus, R.; Kulathu, Y.; Wauer, T.; El Oualid, F.; Freund, S. M. V.; Ovaa, H.; Komander, D. OTU Deubiquitinases Reveal Mechanisms of Linkage Specificity and Enable Ubiquitin Chain Restriction Analysis. *Cell* **2013**, *154* (1), 169-184.
37. Larsen, C. N.; Price, J. S.; Wilkinson, K. D. Substrate Binding and Catalysis by Ubiquitin C-Terminal Hydrolases: Identification of Two Active Site Residues. *Biochemistry* **1996**, *35* (21), 6735-6744.
38. García-Nafría, J.; Watson, J. F.; Greger, I. H. IVA cloning: A single-tube universal cloning system exploiting bacterial In Vivo Assembly. *Sci. Rep.* **2016**, *6* (1), 27459.
39. Liu, H.; Naismith, J. H. An efficient one-step site-directed deletion, insertion, single and multiple-site plasmid mutagenesis protocol. *BMC Biotechnol.* **2008**, *8* (1), 91.

40. Luna-Vargas, M. P. A.; Christodoulou, E.; Alfieri, A.; van Dijk, W. J.; Stadnik, M.; Hibbert, R. G.; Sahtoe, D. D.; Clerici, M.; Marco, V. D.; Littler, D.; Celie, P. H. N.; Sixma, T. K.; Perrakis, A. Enabling high-throughput ligation-independent cloning and protein expression for the family of ubiquitin specific proteases. *J. Struct. Biol.* **2011**, *175* (2), 113-119.
41. Kim, R. Q.; Geurink, P. P.; Mulder, M. P. C.; Fish, A.; Ekkebus, R.; El Oualid, F.; van Dijk, W. J.; van Dalen, D.; Ovaa, H.; van Ingen, H.; Sixma, T. K. Kinetic analysis of multistep USP7 mechanism shows critical role for target protein in activity. *Nat. Commun.* **2019**, *10* (1), 231.
42. Ward, S. J.; Gratton, H. E.; Indrayudha, P.; Michavila, C.; Mukhopadhyay, R.; Maurer, S. K.; Caulton, S. G.; Emsley, J.; Dreveny, I. The structure of the deubiquitinase USP15 reveals a misaligned catalytic triad and an open ubiquitin-binding channel. *J. Biol. Chem.* **2018**, *293* (45), 17362-17374.
43. Abramoff, M.; Magalhães, P.; Ram, S. J. Image Processing with ImageJ. *Biophotonics Intern.* **2003**, *11*, 36-42.
44. Rasband, W. S. *ImageJ*, U. S. National Institutes of Health, Bethesda, Maryland, USA: 1997-2018, <https://imagej.nih.gov/ij/>.
45. Schneider, C. A.; Rasband, W. S.; Eliceiri, K. W. NIH Image to ImageJ: 25 years of image analysis. *Nat. Methods* **2012**, *9* (7), 671-675.
46. Copeland, R. A. Chapter 9. Irreversible Enzyme Inactivators. In *Evaluation of Enzyme Inhibitors in Drug Discovery: A Guide for Medicinal Chemists and Pharmacologists*, 2nd ed.; John Wiley & Sons: Hoboken, NJ, 2013; pp 345-382.
47. Copeland, R. A. Chapter 2. Chemical Bonds and Reactions in Biochemistry. In *Enzymes; A Practical Introduction to Structure, Mechanism, and Data Analysis*, 2nd ed.; John Wiley & Sons: New York, NY, 2000; pp 11-41.
48. Copeland, R. A. Chapter 4. Protein–Ligand Binding Equilibria. In *Enzymes; A Practical Introduction to Structure, Mechanism, and Data Analysis*, 2nd ed.; John Wiley & Sons: New York, NY, 2000; pp 76-108.
49. Moerke, N. J. Fluorescence Polarization (FP) Assays for Monitoring Peptide-Protein or Nucleic Acid-Protein Binding. *Curr. Protoc. Chem. Biol.* **2009**, *1* (1), 1-15.
50. Hameed, D. S.; Sapmaz, A.; Burggraaff, L.; Amore, A.; Slingerland, C. J.; van Westen, G. J. P.; Ovaa, H. Development of Ubiquitin-Based Probe for Metalloprotease Deubiquitinases. *Angew. Chem. Int. Ed.* **2019**, *58* (41), 14477-14482.
51. Morrow, M. E.; Morgan, M. T.; Clerici, M.; Growkova, K.; Yan, M.; Komander, D.; Sixma, T. K.; Simicek, M.; Wolberger, C. Active site alanine mutations convert deubiquitinases into high-affinity ubiquitin-binding proteins. *EMBO Rep.* **2018**, *19* (10), e45680.
52. Crowe, S. O.; Rana, A. S. J. B.; Deol, K. K.; Ge, Y.; Strieter, E. R. Ubiquitin Chain Enrichment Middle-Down Mass Spectrometry Enables Characterization of Branched Ubiquitin Chains in Cellulo. *Anal. Chem.* **2017**, *89* (8), 4428-4434.
53. Xu, P.; Peng, J. Characterization of Polyubiquitin Chain Structure by Middle-down Mass Spectrometry. *Anal. Chem.* **2008**, *80* (9), 3438-3444.
54. Lonsdale, R.; Burgess, J.; Colclough, N.; Davies, N. L.; Lenz, E. M.; Orton, A. L.; Ward, R. A. Expanding the Armory: Predicting and Tuning Covalent Warhead Reactivity. *J. Chem. Inf. Model.* **2017**, *57* (12), 3124-3137.
55. Geurink, P. P.; van Tol, B. D. M.; van Dalen, D.; Brundel, P. J. G.; Mevissen, T. E. T.; Pruneda, J. N.; Elliott, P. R.; van Tilburg, G. B. A.; Komander, D.; Ovaa, H. Development of Diubiquitin-Based FRET Probes To Quantify Ubiquitin Linkage Specificity of Deubiquitinating Enzymes. *ChemBioChem* **2016**, *17* (9), 816-820.
56. Nishizawa, R.; Nishiyama, T.; Hisaichi, K.; Hirai, K.; Habashita, H.; Takaoka, Y.; Tada, H.; Sagawa, K.; Shibayama, S.; Maeda, K.; Mitsuya, H.; Nakai, H.; Fukushima, D.; Toda, M. Discovery of orally available spirodiketopiperazine-based CCR5 antagonists. *Bioorg. Med. Chem.* **2010**, *18* (14), 5208-5223.
57. Kathman, S. G.; Span, I.; Smith, A. T.; Xu, Z.; Zhan, J.; Rosenzweig, A. C.; Statsyuk, A. V. A Small Molecule That Switches a Ubiquitin Ligase From a Processive to a Distributive Enzymatic Mechanism. *J. Am. Chem. Soc.* **2015**, *137* (39), 12442-12445.
58. Moroder, L. Isosteric replacement of sulfur with other chalcogens in peptides and proteins. *J. Pept. Sci.* **2005**, *11* (4), 187-214.
59. Xin, B.-T.; van Tol, B. D. M.; Ovaa, H.; Geurink, P. P. Native chemical ligation at methionine bioisostere norleucine allows for N-terminal chemical protein ligation. *Org. Biomol. Chem.* **2018**, *16* (34), 6306-6315.
60. Roşca, D.-A.; Radkowski, K.; Wolf, L. M.; Wagh, M.; Goddard, R.; Thiel, W.; Fürstner, A. Ruthenium-Catalyzed Alkyne trans-Hydrometalation: Mechanistic Insights and Preparative Implications. *J. Am. Chem. Soc.* **2017**, *139* (6), 2443-2455.